DETECTION OF MODE-LOCKED LASER SIGNALS

Thesis by

Robert J. D'Orazio

In Partial Fulfillment of the Requirements

For the Degree of

Doctor of Philosophy

California Institute of Technology

Pasadena, California

1973

(Submitted July 13, 1972)

To my wife, Elizabeth....

the one person that made this dream come true

with her love,

understanding, and

encouragement.

ACKNOWLEDGMENTS

I wish to express my sincere thanks and gratitude to my advisor, Dr. Nicholas George, for the guidance, inspiration and friendship I received from him throughout all phases of this investigation. His invaluable comments and suggestions initiated and formed the contents of this work. His unceasing encouragement and support to all of his students was refreshing.

I would also like to acknowledge the support of Dr. Robert D. Middlebrook during the initial phases of my studies and Dr. Amnon Yariv for many interesting and helpful discussions. Special thanks are due to Mrs. Karen Current, Mrs. Kathy Ellison and Mrs. Ruth Stratton for their skillful typing of this work.

I am grateful for the generous support I received under the Doctoral Support Fellowship Program of the Bell Telephone Laboratories.

ABSTRACT

In this work we describe our approach to matched-filtering for mode-locked laser signals. Our optical receiver consists of a passive laser cavity controlled in length and a photodetector with its associated electronics. The length of the passive Fabry-Perot cavity is chosen roughly equal to the cavity length of the transmitting laser, but with provision for fine fractional wavelength control of its length. In addition to the selective filtering characteristics of the passive cavity (passbands of unity transmission matching the frequencies of the multi-mode laser), a readout of the vernier length control, peaking the output, provides for an extremely wide range of velocity measurements with either an active or passive vehicle moving relative to the receiver.

In studying the mode-locked laser we use the matched-filter criterion resulting from the optimization of the signal-to-noise ratio. This criterion specifies that the amplitude transmission function be $T_m(\omega) = AE^*(\omega)/S_n(\omega)$; where $E(\omega)$ is the Fourier transform of the laser signal $E_1(t)$; $S_n(\omega)$ is the power spectral density of the additive input noise; the asterisk denotes the complex conjugate; and A is any nonzero complex constant. For an actual laser signal, writing $E(\omega)$ for the multi-tone laser with finite linewidths $\Delta\omega_\ell$ yields an expression which is comparable on a mode by mode basis to the transmission function for a Fabry-Perot cavity. The resulting matching conditions are that $\Delta\omega_p = \Delta\omega_\ell$ and $h_o = h$ in which $\Delta\omega_p$ is the linewidth of the receiver cavity of length h_o, and h is the length of the transmitter cavity.

The Fabry-Perot cavity is probably as close a physical realization to a matched-filter for the multi-toned laser as can be attained in a passive system. Even so, gain narrowing invariably results in $\Delta\omega_\ell < \Delta\omega_p$, thereby limiting the observed improvement in signal-to-noise ratio from its optimal value. For high gain lasers with cavities of low finesse, the receiver can be made closer to the ideal, while greater departures are to be expected in the case of low gain.

Further study of the use of the passive cavity in contrast to no cavity shows that the signal-to-noise ratio improves approximately by the finesse of the cavity which is typically 150. Considering the improvement in signal-to-noise ratio as a function of the number of oscillating modes N we find that the peak value of the temporally varying detected output has a signal-to-noise ratio proportional to N^2, i.e., it varies as the peak power of the mode-locked laser.

Now, suppose that the mode-locked laser is moving toward our receiver with a velocity v. For TEM waves, an emitted frequency ω' will be observed shifted to ω given by $\omega = \gamma(1+v/c)\omega'$ in which $\gamma = [1-(v/c)^2]^{-1/2}$ and c is the speed of light. In this case where there is relative motion, we find that optimal detection of the mode-locked laser signal requires a receiver with a cavity length h_o given by $h_o = h/[\gamma(1+v/c)]$. Similarly, if the mode-locked laser and the passive cavity were on a common platform, then the echo from a vehicle moving toward this platform with velocity v would be shifted to $\omega = (1+2v/c)\omega'$, where we have set $\gamma = 1$. So by vernier adjustments of the passive cavity length we can read a large range of approach velocities with a resolution independent of the velocity.

TABLE OF CONTENTS

FIGURE CAPTIONS

Fig. [2-1] Periodically stratified multi-layer.

Fig. [2-2] Multi-layer reflection coefficient vs. wavelength.

Fig. [2-3] Transmissivity as a function of normalized frequency ($PA = 1 \Rightarrow \omega - \omega_o = 33$ MHz).

Fig. [3-1] Passive cavity receiver. The components are: (T) laser transmitter; (M_3,M_4) laser mirrors; (h) laser cavity length; (E) signal; (V) velocity of laser relative to receiver; (N_o) noise; (F) coarse bandpass filter; (M_1,M_2) passive cavity mirrors; (h_o) passive cavity length; (D) detector; (A) detector electronics; (C) mirror control.

Fig. [4-1] Bottom curve is diffraction losses for a confocal resonator for TEM_{oo} mode, Figure [4-1a] (after Reference 3); Top - Experimentally obtained diffraction loss, Fig. [4-1b].

Fig. [4-2] Scattering centers of a new Spectra-Physics laser reflector illuminated in transmission (500 X).

Fig. [5-1] Signal-to-noise vs. time (8 nsec between peaks) for various number of modes (top to bottom 11, 9, 7, 5, 3).

Fig. [5-2] Attenuation of signal due to mismatch in cavity lengths h_o/h for various number of modes oscillating.

Fig. [5-3] Signal-to-noise vs. time vs. h_o/h for 3 modes oscillating. h_o/h increment is 0.0001 between lines. Time interval between peaks is 8 ns. Peak value of signal-to-noise is 9.

Chapter 1

Introduction

1.1 Statement of the Problem

Multi-tone lasers of the mode-locked[1,2] and cavity dumped[3-5] types emit their energy in short pulses. Sensitive detection of these emissions for point-to-point communications, Doppler measurements, or echo-ranging systems can be accomplished by using appropriate filtering at the optical frequencies before detection and radio-frequency amplification. An optimal filter for the detection of the multi-tone signals described above is the matched-filter.[6-8] An excellent review paper by Turin[9] describes the properties, synthesis, and applications of matched-filters.

In the literature, related prior studies of laser detection include scanning Fabry-Perot cavities using a single pass-band of the passive cavity to analyze laser radiation.[10] Spatial filtering techniques have also been considered to reduce noise in laser amplifiers.[11] Various laser heterodyne techniques[12-16] have been considered which employ local oscillators to overcome the quantum efficiency limitations of the detector which are a problem in the IR but not in the visible. Barrett and Myers[17] used the Fabry-Perot interferometer to study periodic spectra using the equally spaced spectral lines of the interferometer to coincide with the spectral characteristics of N_2O.

They did not consider the degree of improvement or its applications to optical pre-detection filtering. Smiley[18] and Boersch et al.[19] have considered active filters for single tone amplification but did not extend their work to multi-tone filtering. The consideration herein appears to be the first study of the multiplex advantage of using a Fabry-Perot interferometer as a detection filter.

1.2 Matched-Filter for Mode-Locked Laser Signals

Our approach to the matched-filter optical receiver for mode-locked gas laser signals consists simply of a passive laser cavity controlled in length and a photodetector with its associated electronics. The length of the passive Fabry-Perot cavity is chosen roughly equal to the cavity length of the transmitting laser, but with provision for fine fractional wavelength control of its length. In addition to the selective filtering characteristics of the passive cavity (pass bands of unity transmission matching the frequencies of the multi-mode laser) a readout of the vernier length control, peaking the output, provides for an extremely wide range of velocity measurements with either an active or passive vehicle moving relative to the receiver.

To study the passive cavity we first develop a matrix formalism and apply it to the Fabry-Perot. This approach yields a cavity transmission function which is cast in the Laplace transform domain making it suitable for transient analysis. With this generalized transmission function the passive cavity is shown to be, in certain limiting conditions, the matched-filter for mode-locked gas laser

signals. Chapter 4 deals with an important factor in the detection of signals in noise using the passive laser cavity; that is the passive cavity finesse. With this understanding of the cavity characteristics we consider the signal-to-noise improvement with use of the passive cavity. We compare this improvement with that of the theoretical matched-filter and show the departure of the passive cavity from the matched-filter for various cavity parameters. If we are going to use the passive cavity for communication purposes it is important to consider the bandwidth and rise-time of the detection system. This is done using the Laplace transform representation of the passive cavity transmission function. Finally an interesting application of this detection filter to Doppler velocity measurements is considered. Several experiments are described which demonstrate the degree of improvement which is obtained in the pre-detection signal-to-noise ratio of a self mode-locked He-Ne laser signal with use of the passive Fabry-Perot resonant cavity.

Chapter 1

References

1. L.E. Hargrove, R.L. Fork, M.A. Pollack, Appl. Phys. Letters 5, p. 4 (1964).
2. M.H. Crowell, IEEE J. Quantum Electron. QE-1, p. 12 (1965).
3. K. Gürs, R. Müller, Phys. Letters 5, p. 179 (1963).
4. A.A. Vuylsteke, J. Appl. Phys. 34, p. 1615 (1963).
5. W.H. Steier, Proc. IEEE 54, p. 1604 (1966).
6. Y.W. Lee, T.P. Cheatham, Jr., J.B. Wiesner, Proc. IRE , p. 1165, October (1950).
7. S.F. George, A.S. Zamanakos, Proc. IRE , p. 1159, July (1954).
8. W.M. Brown, Analysis of Linear Time-Invariant Systems, (McGraw-Hill, New York, 1963), p. 245.
9. G.L. Turin, IRE Trans. on Information Theory , p. 311, June (1960).
10. R.L. Fork, D.R. Herriott, H. Kogelnik, Appl. Opt. 3, p. 1471, (1964).
11. H. Kogelnik, A. Yariv, Proc. IEEE 52, p. 165 (1964).
12. R.W. Uhlhorn, D.F. Holshouser, IEEE J. Quantum Electron. QE-6, p. 775 (1970).
13. C.M. Sonnenschien, F.A. Horrigan, Appl. Opt. 10, p. 1600 (1971).
14. M.J. Rudd, J. Phys. E: Sci. Instrum. 2, p. 55 (1969).
15. W.M. Hubbard, Bell Sys. Tech. J. 50, p. 1, January (1971).
16. W.L. Kuriger, Digest of Tech. papers of 1971 IEEE/OSA Conference on Laser Engineering and Applications, Wash. D.C., 2-4 June 1971 (New York, USA: IEEE 1971), p. 29-30.

17. J.J. Barrett, S.A. Myers, J. Opt. Soc. Amer. 61, p. 1246, September (1971).

18. V.N. Smiley, Proc. IEEE , p. 120, January (1963).

19. H. Boersch, G. Herziger, IEEE J. Quantum Electron. QE-2, p. 549, September (1966).

Chapter 2

The Passive Laser Cavity Idealized As A Periodically Stratified Medium

2.1 Introduction

In this chapter Maxwell's equations are expressed in the Laplace transform domain and the solutions are formulated in a standard matrix notation. This matrix formalism is then applied to a stratified dielectric medium. The expressions are then used to generate a novel representation of the passive Fabry-Perot resonant cavity. Standard expressions for transmissivity are developed which keep the free space reflection and transmission functions of the end reflectors completely general. These analyses are presented as a review of the standard multilayer theory, e.g., see Born and Wolf[1], although the direct application of the stratified media analysis to a laser cavity has not been explicitly presented in the literature and conceptually it provides an interesting complement to the bouncing wave point of view.[2,3] Also we present the transmissivity cast in the Laplace transform domain which makes it suitable for transient analysis. The general transmissivity function is then simplified in taking the transmission and reflection coefficients as standard multilayers by using the Chebyshev representation for unimodular matrices.

2.2 Maxwell's Equations and Their Solution for Dielectric Materials

We start with Maxwell's equations in the time domain and Laplace transform them assuming linear, isotropic, ohmic media, i.e.,

μ, ε, and σ are time independent scalars. Thus we have for the time domain where $\underline{E}_1$ and $\underline{H}_1$ are the intensities of the electric and magnetic fields respectively, $\underline{D}_1$ is the electric displacement, $\underline{B}_1$ is the magnetic induction, $\underline{J}_1$ is the current density, and μ, ε, and σ are the permeability, permittivity and conductance respectively:

$$\nabla \times \underline{E}_1 = - \frac{\partial \underline{B}_1}{\partial t} \tag{2-1}$$

$$\nabla \times \underline{H}_1 = \underline{J}_1 + \frac{\partial \underline{D}_1}{\partial t} \tag{2-2}$$

$$\underline{D}_1 = \varepsilon \, \underline{E}_1 \tag{2-3}$$

$$\underline{B}_1 = \mu \, \underline{H}_1 \tag{2-4}$$

$$\underline{J}_1 = \sigma \, \underline{E}_1 \tag{2-5}$$

where the subscript 1 is used to denote time variation, i.e., $\underline{E}_1 = \underline{E}_1(\underline{r},t)$ where $\underline{r}$ is the radius vector of a spherical coordinate system.

Now we take the Laplace transform of Eqs. (2-1)-(2-5), i.e.,

$$\underline{E}(\underline{r},s) = \int_0^\infty \underline{E}_1(\underline{r},t) e^{-st} dt \tag{2-6.1}$$

dropping the subscript 1 on all of the Laplace transformed fields. The inverse operation of the transform pair is given by:

$$\underline{E}_1(\underline{r},t) \, u(t) = \frac{1}{2\pi i} \int_{\alpha - i\infty}^{\alpha + i\infty} \underline{E}(\underline{r},s) e^{st} ds \tag{2-6.2}$$

where

$$u(x) = \begin{cases} 1 & x > 0 \\ 0 & x < 0 \end{cases}$$

where α is chosen greater than the real part of the poles of $\underline{E}(\underline{r},s)$[4]. Thus for this linear isotropic medium Eqs. (2-1) and (2-2) are

$$\nabla \times \underline{E} = - s\mu\underline{H} + \underline{B}_1(\underline{r},0) \tag{2-7.1}$$

$$\nabla \times \underline{H} = (\sigma + s\varepsilon)\underline{E} - \varepsilon\underline{E}_1(\underline{r},0) \tag{2-7.2}$$

Now we drop the initial fields, i.e., assume $\underline{E}_1(\underline{r},0)$ and $\underline{B}_1(\underline{r},0)$ are zero, assume that $\nabla\cdot\underline{E} = 0$ and with the standard vector manipulations derive the vector wave equation:

$$[\nabla^2 - (s^2\mu\varepsilon + s\mu\sigma)]\underline{E} = 0 \tag{2-8}$$

Now assuming that $\underline{E}$ is polarized in the x direction, i.e., $\underline{E} = (E_x, 0, 0)$ and $\underline{H} = (0, H_y, H_z)$ then by Eqs. (2-8), (2-7.1), and (2-7.2) we have:

$$[\nabla^2 - (s^2\mu\varepsilon + s\mu\sigma)]E_x = 0 \tag{2-9.1}$$

$$H_y = - \frac{1}{s\mu} \frac{\partial E_x}{\partial z} \tag{2-9.2}$$

Equations (2-9.1) and (2-9.2) are the equations presented in Born and Wolf[5], except in this case we have the Laplace transformed fields instead of the harmonic form. The general solutions to Eqs. (2-9.1) and (2-9.2) are outlined in Appendix C. Thus if we assume a normally incident x polarized electric field onto a dielectric homogeneous slab with parameters μ, ε, and σ all scalars, then the field at a point z in the

medium is related to the field at the input by Eq. (C-13)

$$\begin{bmatrix} E_x \\ H_y \end{bmatrix}_z = \begin{bmatrix} \cos\beta z & -\frac{s\mu}{\beta}\sin\beta z \\ \frac{\beta}{s\mu}\sin\beta z & \cos\beta z \end{bmatrix} \begin{bmatrix} E_x \\ H_y \end{bmatrix}_{z=o} \tag{2-10}$$

where the separation constant $\beta = \sqrt{-s^2\mu\varepsilon - s\mu\sigma}$.

The solution of the single slab Eq. (2-10) may be extended to the multilayer case (Appendix C) by expressing the input fields E_{x_1}, H_{y_1} in terms of the output fields E_{x_2}, H_{y_2} by the chain matrix as Eq. (C-16)

$$\begin{bmatrix} E_{x_1} \\ H_{y_1} \end{bmatrix} = \begin{bmatrix} A & B \\ C & D \end{bmatrix} \begin{bmatrix} E_{x_2} \\ H_{y_2} \end{bmatrix} \tag{2-11}$$

where the chain matrix is given by Eq. (C-17).

The general solution for the multilayer with N layers may be applied to various problems. In this thesis, in one case the N layers are taken to be the periodically stratified dielectric interference filter used as a laser mirror (see Section 2.4), and in a second case, the entire Fabry-Perot laser cavity is idealized as the multilayer. In the cavity case, the chain matrix is given by the product of the mirror matrices and the matrix describing the region between them (See Section 2.5).

2.3 The Transmission and Reflection Functions

In the application of the chain matrix representation of multilayers to the expression of the reflected and transmitted waves, it is convenient to express the fields entering and leaving the multilayer in a traveling wave notation. This wave notation is reviewed in Appendix C.

Considering a plane wave normally incident upon a multilayer that is bounded on each side by a homogeneous, semi-infinite medium, the input fields

$$\begin{bmatrix} E_{x_1} \\ H_{x_1} \end{bmatrix} = \begin{bmatrix} a_1 + b_1 \\ g_1(a_1 - b_1) \end{bmatrix} \tag{2-12.1}$$

and the output fields

$$\begin{bmatrix} E_{x_2} \\ H_{y_2} \end{bmatrix} = \begin{bmatrix} a_2 + b_2 \\ g_2(a_2 - b_2) \end{bmatrix} \tag{2-12.2}$$

may be assumed (Appendix C, Eq. (C-20)). g_1 is the complex wave admittance of the input medium and g_2 is the complex wave admittance of the output medium. The amplitude transmission function, defined by the ratio of the amplitude of the field propagated into region 2, at the output, to the amplitude of the field incident at the input in region 1, may be shown to be (Appendix C, Eq. (C-23))

$$T_{12} = \frac{2}{(A + \frac{g_2}{g_1} D) + (g_2 B + \frac{C}{g_1})} \tag{2-13}$$

where A, B, C, and D are the elements of the chain matrix of Eq. (2-11). (The 12 indicates transmission from region 1 to region 2 through the multilayer). Similarly the amplitude reflection function, defined by the ratio of the amplitude of the field propagated back from a surface to the amplitude of the field incident on the surface, may be shown to be (Appendix C, Eq. (C-25))

$$R_1 = \frac{(A - \frac{g_2}{g_1} D) + (g_2 B - \frac{C}{g_1})}{(A + \frac{g_2}{g_1} D) + (g_2 B + \frac{C}{g_1})} \tag{2-14}$$

where the subscript 1 denotes the reflection at the input surface in region 1. From Eq. (2-13) and Eq. (2-14) we define

$$\mathcal{R} = |R_1|^2 \qquad \text{and} \qquad \mathcal{T} = |T_{12}|^2 \tag{2-15}$$

as the reflectivity and transmissivity respectively.[6] One may note that if Eq. (2-11) is written for the field in region 2 in terms of the field in region 1, it may be shown that the transmission function $T_{21} \equiv b_1/b_2$ (transmission from region 2 through the multilayer into region 1) is related to Eq. (2-13) by

$$\text{for} \quad \begin{aligned} T_{21} &= T_{12} \\ g_1 &= g_2 = g. \end{aligned} \tag{2-16}$$

It may also be shown by writing the amplitude reflection function in region 2 $R_2 \equiv a_2/b_2$, similar to Eq. (2-14), that R_1 is related to R_2 by

$$\frac{R_1}{R_2} = \frac{A\text{-}D + g_o B - \frac{C}{g_o}}{D\text{-}A + g_o B - \frac{C}{g_o}} \tag{2-17}$$

for $g_1 = g_2 = g_o$.

For a laser mirror, which is fabricated by a quarter-wave-multilayer stack which will be described in more detail in the next section, at resonance $B = C = 0$ for which we obtain the familiar result $R_1 = -R_2$. More generally A and D are real and $g_o B$ and C/g_o are imaginary for which Eq. (2-17) becomes

$$R_1 = R_2 \, e^{i(\pi - 2\phi)} \tag{2-18}$$

where

$$\phi = \tan^{-1} \frac{B' - C'}{A-D}$$

with

$$iB' = g_o B \qquad iC' = \frac{C}{g_o}$$

Let us pause in our development of the transmission function for a passive laser cavity to consider the standard dielectric multilayer laser mirror.

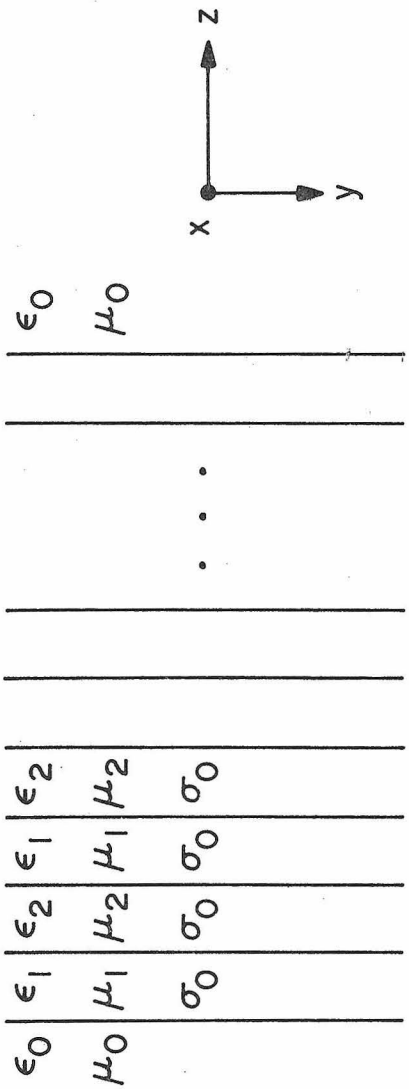
z
y
x
ϵ_0
μ_0
ϵ_0 μ_0
ϵ_1 μ_1 σ_0
ϵ_2 μ_2 σ_0
ϵ_1 μ_1 σ_0
ϵ_2 μ_2 σ_0

Fig. [2-1]

2.4 The Multilayer Laser Mirror

The standard multilayer laser mirror is fabricated to obtain a desired reflection which is constant around the frequencies of interest. This is accomplished by appropriate selection of the dielectric material's index of refraction and layer thickness. To see this let us consider a periodically stratified dielectric linear medium as shown in Fig. [2-1] for which the first two layers have indices n_1 and n_2 respectively. Now if we repeat these 2 layers N times the elements of the resulting matrix (Appendix D, Eq. (D-3.2)) may be introduced into Eq. (2-14) to obtain the reflection function. Now for quarter wavelength layers, $\beta h = \frac{2\pi}{\lambda} nh$ and $nh = \frac{\lambda_o}{4}$, the elements of the matrix which relates the input field in terms of the output field at the resonant frequency $f_o = \frac{c}{\lambda_o}$ as in Eq. (2-11) are given by Eq. (D-10)

$$A = \left(-\frac{n_2}{n_1}\right)^N \tag{2-19}$$

$$D = \left(-\frac{n_1}{n_2}\right)^N \tag{2-20}$$

and

$$B = C = 0 \tag{2-21}$$

Thus for $\lambda = \lambda_o$ the reflection function leads to the reflection coefficient r_1 introducing Eq. (2-19), (2-20) and (2-21) into Eq. (2-14)

$$r_1 = R_1(\lambda_o) = \frac{\left(-\frac{n_2}{n_1}\right)^N - \left(-\frac{n_1}{n_2}\right)^N}{\left(-\frac{n_2}{n_1}\right)^N + \left(-\frac{n_1}{n_2}\right)^N} \tag{2-22}$$

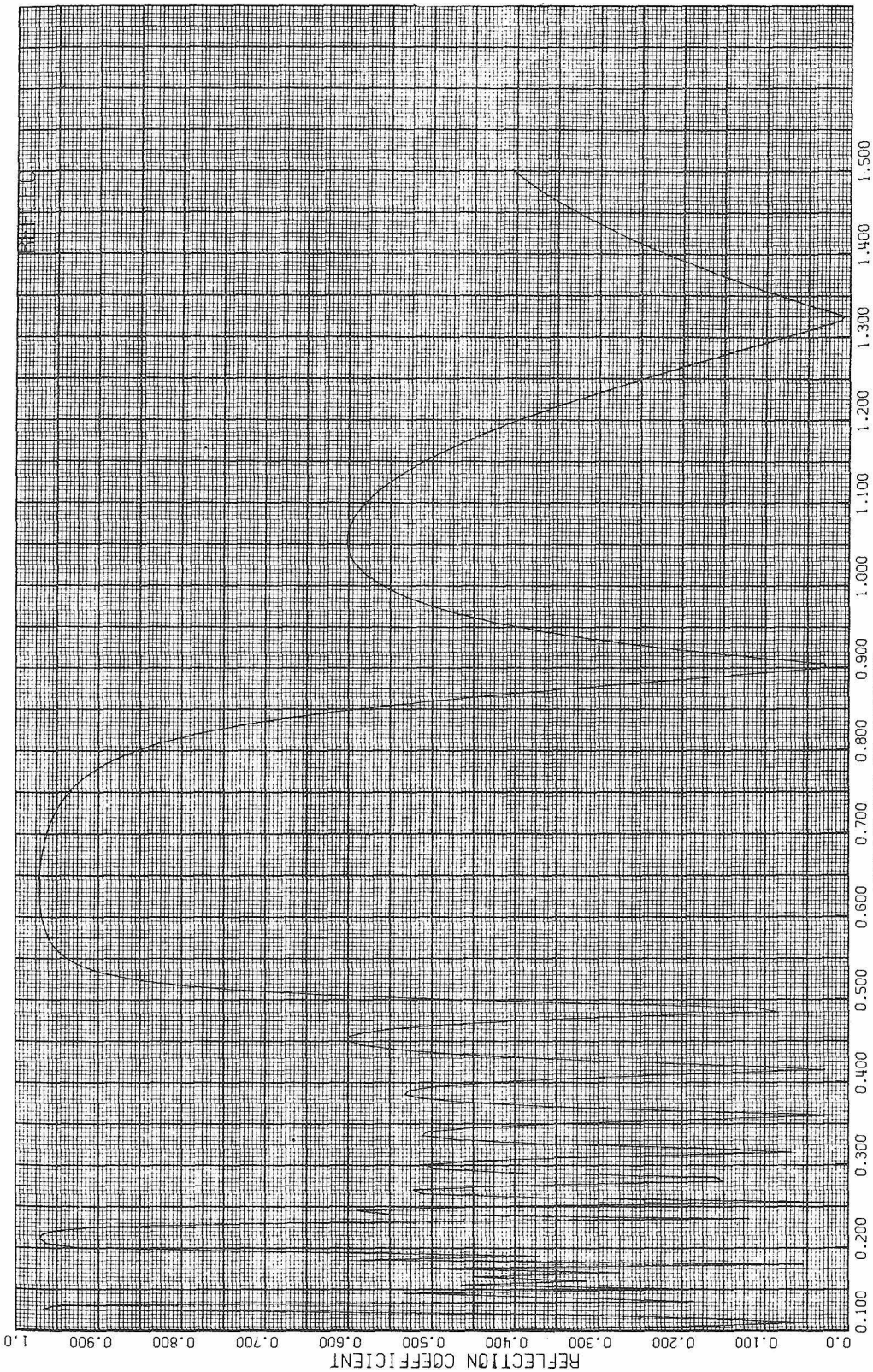
REFLECTION COEFFICIENT
0.0
0.100
0.200
0.300
0.400
0.500
0.600
0.700
0.800
0.900
1.0
WAVELENGTH IN MICRONS
0.100
0.200
0.300
0.400
0.500
0.600
0.700
0.800
0.900
1.000
1.100
1.200
1.300
1.400
1.500

Fig. [2-2]

Similarly the transmission function of Eq. (2-13) leads to the transmission coefficient t_1 when $\lambda = \lambda_o$

$$t_1 = T_{12}(\lambda_o) = \frac{2}{\left(-\frac{n_2}{n_1}\right)^N + \left(-\frac{n_1}{n_2}\right)^N} \qquad (2\text{-}23)$$

We may check our results by noting that in the case of no loss the intensity reflected and the intensity transmitted must satisfy a conservation of energy consideration and we see by putting Eq. (2-23) and (2-22) into Eqs. (2-15) that this is so.

$$\mathcal{R} + \mathcal{T} = 1 \qquad (2\text{-}24)$$

An important consequence of choosing the effective layer thickness as quarter wave in length may be illustrated in the plot of Eq. (2-14). Figure [2-2] was generated from Eq. (2-14) using the results of Appendix D according to which the elements of the N^{th} power of a unimodular matrix developed by the first two layers may be expressed by Chebyshev polynomials. From Fig. [2-2] we see that the $\lambda_o/4$ thick layers, with λ_o = 6328 Å and N = 4, give a very flat reflection coefficient curve in a 1,000 Å region around 6328 Å and the corresponding maximum phase shift on reflection (not shown) of $\pi/24$. This plot and the following illustrative example justify our later interpretation of a passive cavity having mirrors with reflection coefficients that are constant in amplitude and phase over a 5,000 MHz band around the center transmission peaks. Also it serves to solidify

the standard bouncing wave derivation of the transmission function for a passive Fabry-Perot resonant cavity.

In corroboration with the general result we may rewrite Eq. (2-14) as $R_1(\lambda) = V/W$ from which the percentage change of the reflection function with respect to wavelength is

$$\frac{1}{R_1}\frac{\partial R_1}{\partial \lambda} = \frac{1}{V}\frac{\partial V}{\partial \lambda} - \frac{1}{W}\frac{\partial W}{\partial \lambda} \quad . \tag{2-25}$$

Now recalling that $\beta h = \frac{\pi}{2}\frac{\lambda_o}{\lambda}$ for $nh = \frac{\lambda_o}{4}$ then evaluating Eq. (2-25) for $\lambda = \lambda_o$ we obtain

$$\frac{1}{R_1}\frac{\partial R_1}{\partial \lambda}\bigg|_{\lambda = \lambda_o} = \frac{2\left(D\frac{\partial g_o B}{\partial \lambda} - A\frac{\partial \frac{1}{g_o} C}{\partial \lambda}\right)}{A^2 - D^2}\bigg|_{\lambda = \lambda_o} \tag{2-26}$$

where the frequency dependence of A,B,C, and D is developed in Appendix D. And thus the change in reflection function around $\lambda = \lambda_o$ is given by introducing A,B,C, and D into Eq. (2-26)

$$\frac{1}{R_1}\frac{\partial R_1}{\partial \lambda} = \frac{\pi}{\lambda_o}\frac{-i\,U_{N-1}(a)}{\left(-\frac{n_2}{n_1}\right)^N}\frac{(n_1+n_2)\left[\frac{1}{n_1 n_2} - \left(-\frac{n_2}{n_1}\right)^{2N}\right]}{\left(-\frac{n_2}{n_1}\right)^{2N} - \left(-\frac{n_1}{n_2}\right)^{2N}}$$

$$\cong \frac{i\,U_{N-1}(a)}{\left(-\frac{n_2}{n_1}\right)^N}(n_1 + n_2) \tag{2-27}$$

where U_N is a Chebyshev polynomial of the second kind. Thus if we let $N = 4$, $n_1 = 1.5$, $n_2 = 2.5$ and $\lambda_o = 0.6328\ \mu$, then a 10% change in wavelength will yield approximately a 1% change in the reflectivity function around 6328 Å. With this example in mind we may consider R_1 constant and hence let $r_1 = R_1(\lambda_o)$ be the reflection coefficient, i.e., the reflection function evaluated at $\lambda = \lambda_o$.

2.5 Transmission Function of a Laser Cavity

We are now in a position to consider the laser cavity as a periodically stratified media. To do this we will develop a chain matrix involving three component matrices. The first will characterize the input medium, i.e., the laser input mirror I, the second will characterize the cavity region o, and the third will characterize the output medium, i.e., the laser output mirror II. The matrix which relates the input fields to the output fields as in Eq. (2-11) is given by

$$\begin{bmatrix} A & B \\ C & D \end{bmatrix} = \begin{bmatrix} A_1 & B_1 \\ C_1 & D_1 \end{bmatrix}_I \begin{bmatrix} A_0 & B_0 \\ C_0 & D_0 \end{bmatrix}_o \begin{bmatrix} A_2 & B_2 \\ C_2 & D_2 \end{bmatrix}_{II} \tag{2-28}$$

For the laser cavity, it is more convenient to renumber the layers as in Eq. (C-17) as follows:

Input region (1); Mirror I has m layers of thickness

$h_{11}, h_{12}, h_{13}, \ldots, h_{1m}$

Cavity region (o); has length h_o

Output region (2); Mirror II has n layers of thickness $h_{21}, h_{22}, h_{23}, \ldots, h_{2n}$. If one assumes the permeabilities of each layer are equal then the matrix relating the input fields in terms of the output fields of a laser cavity by Eq. (2-11), Eq. (C-17), and Eq. (2-28) is

$$\begin{bmatrix} A & B \\ C & D \end{bmatrix} = \prod_{p=1}^{m} \begin{bmatrix} \cos \beta_{1p} h_{1p} & \frac{s\mu}{\beta_{1p}} \sin \beta_{1p} h_{1p} \\ -\frac{\beta_{1p}}{s\mu} \sin \beta_{1p} h_{1p} & \cos \beta_{1p} h_{1p} \end{bmatrix} \cdot \begin{bmatrix} \cos \beta_o h_o & \frac{s\mu}{\beta_o} \sin \beta_o h_o \\ -\frac{\beta_o}{s\mu} \sin \beta_o h_o & \cos \beta_o h_o \end{bmatrix} \cdot \prod_{q=1}^{n} \begin{bmatrix} \cos \beta_{2q} h_{2q} & \frac{s\mu}{\beta_{2q}} \sin \beta_{2q} h_{2q} \\ -\frac{\beta_{2q}}{s\mu} \sin \beta_{2q} h_{2q} & \cos \beta_{2q} h_{2q} \end{bmatrix} \tag{2-29}$$

One can generate the transmission function by substituting the elements of Eq. (2-28) into the transmission function of Eq. (2-13). But before this is done, we associate with mirror I, the amplitude transmission coefficient t_1.

As was described in Section 2.4, frequency variations in the optical field do not effect the mirror transmission as may be seen by the fact that for a 99% reflecting mirror a 1% change in the transmission is caused by a 10% change in wavelength. So if frequency variations are unimportant then Eq. (2-23) is suitable for t_1; however for the general case Eq. (2-13) is appropriate, i.e., $t_1 = T_{12}$. Similarly one may associate with mirror I, the amplitude reflection coefficient r_{12} (where 12 means first mirror right side incidence). Again we note that r_{12} may be considered constant for certain geometries as in Eq. (2-22), but we will keep it for this derivation completely arbitrary, i.e., $r_1 = R_1$ from Eq. (2-14). In a similar fashion one may associate with mirror II, t_2 and r_{21} (where 21 means second mirror left side incident), which are the amplitude transmission and reflection coefficients respectively. Rewriting Eqs. (2-13) and (2-16) for the entire Fabry-Perot resonant cavity gives

$$T = \frac{2}{A + gB + \frac{C}{g} + D} \tag{2-30.1}$$

where the composite elements of the cavity matrix are obtained by expanding the triple product of Eq. (2-28) leading to:

$$\begin{aligned} A &= A_2(A_1A_0 + B_1C_0) + C_2(A_1B_0 + B_1D_0) \\ gB &= gB_2(A_1A_0 + B_1C_0) + gD_2(A_1B_0 + B_1D_0) \\ \frac{1}{g}C &= \frac{1}{g}A_2(C_1A_0 + D_1C_0) + \frac{1}{g}C_2(C_1B_0 + D_1D_0) \\ D &= B_2(C_1A_0 + D_1C_0) + D_2(C_1B_0 + D_1D_0) \end{aligned} \tag{2-30.2}$$

and by rearranging Eq. (2-30) and noting the association for t_1, t_2,

r_{12}, r_{21} one obtains

$$T = \frac{t_1 t_2 e^{-i\beta_o h_o}}{1 - r_{12} r_{21} e^{-2i\beta_o h_o}} \tag{2-31}$$

or

$$T = \frac{t_1 t_2}{1 - r_{12} r_{21} e^{-2\alpha h_o}} \quad \frac{e^{i\psi(\beta_o)}}{\sqrt{1 + P \sin^2(\beta h_o)}} \tag{2-32}$$

where

$$P = \frac{4 r_{12} r_{21} e^{-2\alpha h_o}}{(1 - r_{12} r_{21} e^{-2\alpha h_o})^2} \tag{2-33}$$

and

$$\beta_o = \beta - i\alpha$$

with

$$\psi(\beta_o) = -(\beta - i\alpha) h_o - \tan^{-1} \frac{r_{12} r_{21} \sin(2\beta h_o)}{1 - r_{12} r_{21} \cos(2\beta h_o)} \tag{2-34}$$

We note that $\alpha < 0$ implies gain per unit length in the cavity and $\alpha > 0$ implies loss per unit length in the cavity. An equivalent result to Eq. (2-31) is obtained by consideration of a multiple bounce argument, e.g., Born and Wolf, page 324.[2] Without an outline of this method, we will compare the result of Eq. (2-31) to the result of the bouncing mode method. Overall, the transmission function of Eq. (2-31) differs from the multiple bounce results in the following ways:

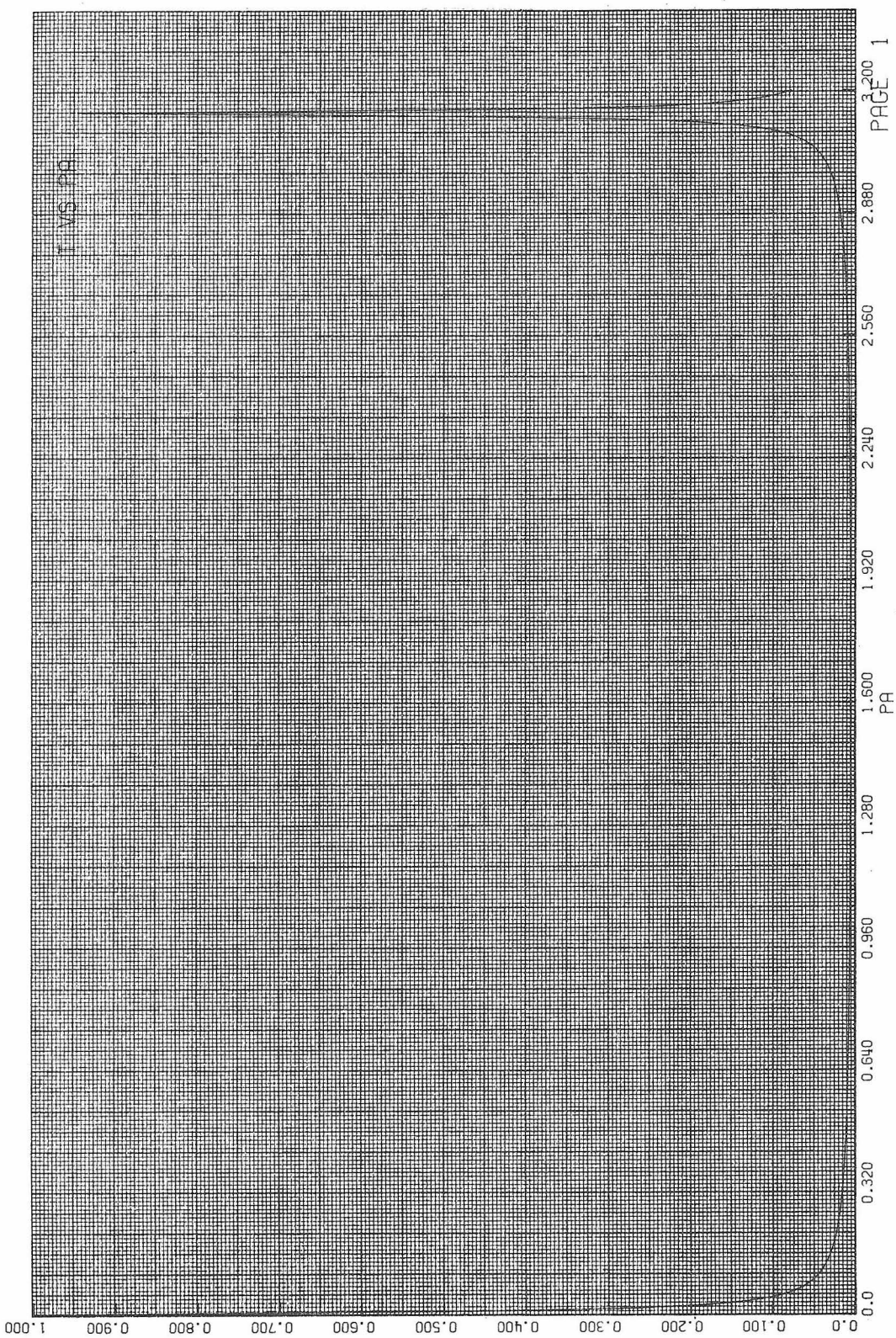
1 VS PA
0.0
0.320
0.640
0.960
1.280
1.600
1.920
2.240
2.560
2.880
3.200
PA
0.0
0.100
0.200
0.300
0.400
0.500
0.600
0.700
0.800
0.900
1.000
PAGE 1

Fig. [2-3]

1. The end reflectors are generalized in Eq. (2-31) to include any stratified multilayer or linear medium.

2. The transmission function is generalized in the Laplace transform domain to allow for transient analysis of the cavity in later chapters.

3. The loss factor is included to allow for analysis of finesse and to generalize the transmission function to employ an active linear medium in the cavity.

Before we go on to consider the passive cavity as a matched-filter for mode-locked laser signals, let us express Eq. (2-31) in the transmissivity expression of Eq. (2-15). Assuming $r_{12}r_{21}$ is real, which it generally is and may be seen by considering Eq. (2-14) and Eq. (2-17), we take TT* of Eq. (2-32) to obtain

$$T = |T|^2 = \frac{|t_1 t_2|^2 e^{-2\alpha h_o}}{(1 - r_{12}r_{21}e^{-2\alpha h_o})^2} \frac{1}{1 + P\sin^2(\beta h_o)} \qquad (2\text{-}35)$$

which may also be compared with the bouncing mode method as per Born and Wolf page 325. We plot Eq. (2-35) for $\beta = \omega/c$ where c is the speed of light and ω is the radian frequency, $r_{12}r_{21} = .991$ and $\alpha = 0$ Eq. (2-35) is plotted in Fig. [2-3] as a function of normalized radian frequency so that when PA = 1, $\omega - \omega_o = 33$ MHz where ω_o is a resonant frequency. This plot demonstrates the fact that a laser cavity has periodically spaced resonant peaks which we will see coincide with certain types of input signals. Before going into a more detailed discussion of

the finesse, loss factors, and other characteristics of the transmission function, we will consider the passive laser cavity characterized by Eq. (2-31) or Eq. (2-32) as the matched-filter for mode-locked laser signals.

Chapter 2

References

1. M. Born, E. Wolf, Principles of Optics, 4th edition, (Pergamon Press, 1970), p. 67-69.

2. Ibid., p. 323-329.

3. A. Yariv, Introduction to Optical Electronics, (Holt, Rinehart, Winston, 1971), p. 99-100.

4. G. F. Carrier, M. Krook, C. E. Pearson, Functions of A Complex Variable, (McGraw-Hill, 1966), p. 347-348.

5. M. Born, E. Wolf, op. cit., p. 52-53.

6. M. Born, E. Wolf, op. cit., p. 60.

Chapter 3

The Passive Cavity: A Matched-Filter for Mode-Locked Laser Radiation

3.1 Introduction

With use of the generalized transmission function developed in Section 2.5, our approach to the matched-filter optical receiver for mode-locked gas laser signals will be considered. Before we consider the passive cavity as a matched-filter we will review the applicable linear system theory and present the matched-filter criteria. We will then discuss the signal for which the passive cavity is a matched-filter. By approximating the transmission function of the passive cavity we observe the form of the types of signals for which the cavity is an optimal filter. Finally we consider the matched-filter for the mode-locked laser signal with zero and finite linewidth and connect it to the passive cavity results.

3.2 Linear System Theory and the Matched-Filter

Consider the linear system with impulse response function $h(t)$, input signal $f(t)$ and additive input noise $n(t)$. The system output $g(t)$ is given by

$$g(t) = f(t) \otimes h(t) + n(t) \otimes h(t) \qquad (3\text{-}1)$$

where $\otimes$ indicates convolution (see Appendix A for more details). The problem is to find $h(t)$ which maximizes the signal-to-noise ratio defined by

$$SNR \equiv \frac{|f \otimes h|^2}{\langle |n \otimes h|^2 \rangle} \qquad (3\text{-}2)$$

where < > indicates the average value.

To do this we assume the existence of the following transform pairs:

$$F(\omega) = \int_{-\infty}^{\infty} f(t)e^{-i\omega t}dt \tag{3-3}$$

$$f(t) = \frac{1}{2\pi}\int_{-\infty}^{\infty} F(\omega)e^{i\omega t}d\omega \tag{3-4}$$

$$H(\omega)=\int_{-\infty}^{\infty} h(t)e^{-i\omega t}dt \tag{3-5}$$

$$h(t) = \frac{1}{2\pi}\int_{-\infty}^{\infty} H(\omega)e^{i\omega t}d\omega \tag{3-6}$$

Since the Fourier transform of the additive input noise n(t) does not exist we will develop some formalism which will allow us to express the denominator of Eq. (3-2). We define the autocorrelation function of the additive input noise by

$$R_n(\tau) \equiv <n(t + \tau)\ n^*(t)> \tag{3-7}$$

Then the power spectral density of the input noise is

$$S_n(\omega) = \int_{-\infty}^{\infty} R_n(t)e^{-i\omega t}dt \tag{3-8}$$

which forms one element of the transform pair since

$$R_n(t) = \frac{1}{2\pi}\int_{-\infty}^{\infty} S_n(\omega)e^{i\omega t}d\omega \qquad (3\text{-}9)$$

Thus using Eq. (3-7) and Eq. (3-9) the denominator of Eq. (3-2) becomes

$$\langle |n \otimes h|^2 \rangle = R_{n\otimes h}(0) = \frac{1}{2\pi}\int_{-\infty}^{\infty} S_{n\otimes h}(\omega)\, d\omega \qquad (3\text{-}10)$$

It may be shown that the power spectral density of the output noise is related to the power spectral density of the input by (Appendix A, Eq. (A-15)).

$$S_{n\otimes h}(\omega) = |H(\omega)|^2 S_n(\omega) \qquad (3\text{-}11)$$

As outlined in Appendix A (Eqs. (A-19) - (A-22)), Eq. (3-2) becomes, using Schwartz's inequality,

$$SNR = \frac{\left|\frac{1}{2\pi}\int_{-\infty}^{\infty} F(\omega)H(\omega)e^{i\omega t}d\omega\right|^2}{\frac{1}{2\pi}\int_{-\infty}^{\infty} |H(\omega)|^2 S_n(\omega)\, d\omega} \leq \frac{1}{2\pi}\int_{-\infty}^{\infty} \frac{|F(\omega)|^2}{S_n(\omega)}\, d\omega \qquad (3\text{-}12)$$

The equality of Eq. (3-12) will be satisfied if and only if

$$H_m(\omega) = \frac{A\, F^*(\omega)}{S_n(\omega)} \qquad (3\text{-}13)$$

where A is any non-zero complex constant. This is the definition of the matched-filter for the input signal $f(t)$ with Fourier transform $F(\omega)$ and the additive input noise whose power spectral density is $S_n(\omega)$. Then Eq. (3-12) using Eq. (3-13) becomes

$$SNR(t) = \frac{\left|\frac{1}{2\pi}\int_{-\infty}^{\infty}\frac{|F(\omega)|^2}{S_n(\omega)}e^{i\omega t}d\omega\right|^2}{\frac{1}{2\pi}\int_{-\infty}^{\infty}\frac{|F(\omega)|^2}{S_n(\omega)}d\omega} \tag{3-14}$$

where we see the maximum occurs at t = 0. An alternative representation for Eq. (3-13) is

$$h_m \circledast R_n = A\, f^*(-t) \tag{3-15}$$

Eq. (3-15) is a valid expression for the matched-filter even if the Fourier transform of f(t) does not exist as long as some realizability constraint is used for h(t), i.e., h(t) acts on the input for only some finite time (Appendix A). With this criteria we will now consider the signal for which the passive cavity is a matched-filter.

3.3 Passive Cavity as a Matched-Filter

From our analysis in Chapter 2 we developed a generalized transmission function for the passive laser cavity which we repeat here for convenience, Eq. (2-32).

$$T = K\,\frac{e^{i\phi(\beta)}}{\sqrt{1 + P\sin^2(\beta h_o)}} \tag{3-16}$$

where

$$K = \frac{t_1 t_2\, e^{-\alpha h_o}}{1 - r_{12}r_{21}e^{-2\alpha h_o}} \tag{3-17}$$

$$P = \frac{4r_{12}r_{21}e^{-2\alpha h_o}}{(1 - r_{12}r_{21}e^{-2\alpha h_o})^2} \tag{3-18}$$

$$\phi(\beta) = -\beta h_o - \tan^{-1} \frac{r_{12}r_{21}\sin(2\beta h_o)}{1 - r_{12}r_{21}\cos(2\beta h_o)} \tag{3-19}$$

for $$\beta_o = \beta - i\alpha \tag{3-20}$$

We note that for the passive region $\beta = \omega\sqrt{\mu_o \varepsilon_o} = \omega/c$. Thus if we wish to determine the signal for which the passive laser cavity is a matched-filter we set Eq. (3-13) equal to Eq. (3-16), $T(\omega) = H(\omega)$, to obtain

$$F(\omega) = \frac{S_n(\omega)}{A^*} H^*(\omega) = \frac{S_n(\omega)}{A^*} T^*(\omega) \tag{3-21}$$

Since the signals we will be considering in the next section have a finite number of frequency peaks (band limited signal) and negligible linewidth, we will approximate $T(\omega)$ expanding around the zeroes ω_p of $\sin^2(\beta h_o) = \sin^2(\omega h_o/c)$ for a finite number of peaks centered around ω_o and dropping $\phi(\beta)$ so that Eq. (3-16) becomes

$$T(\omega)_A = K \sum_{p=-N}^{N} \frac{1}{\sqrt{1 + \left(\frac{2\Delta\omega}{\Delta\omega_p}\right)^2}} \tag{3-22}$$

where $\Delta\omega = \omega - \omega_p = \omega - (\omega_o + p\omega_c)$, $\omega_c = \pi c/h_o$, and $\Delta\omega_p = 2c/(h_o\sqrt{P})$. We note that $\Delta\omega_p$ is the full width at half power of each Lorentzian lineshape function generated by Eq. (3-22). With this approximation

Eq. (3-21) becomes

$$F(\omega) = C_1 \sum_{p=-N}^{N} \frac{1}{\sqrt{1 + \left(\frac{2\Delta\omega}{\Delta\omega_p}\right)^2}} \qquad (3\text{-}23)$$

where $C_1 = S_n(\omega)K^*/A^*$.

Generally we will assume white noise so that $S_n(\omega) = N_o$ is uniform over the frequencies of interest. Also from Section 2.4 we could assume r_{12}, r_{21}, t_1, and t_2 are constant so that K is constant over the frequencies of interest. Thus we may assume C_1 is constant. In the case of no loss $t_1t_2 + r_{12}r_{21} = 1$ for $r_{12} = r_{21}$ and if we allow $\Delta\omega_p \to o$, i.e., $P \to \infty$ then Eq. (3-23) becomes

$$F(\omega) = C_2 \sum_{p=-N}^{N} \delta(\omega - (\omega_o + p\omega_c)) \qquad (3\text{-}24)$$

where $\delta(\omega)$ is the Dirac delta function.

Another way of considering the case of the linewidth of the passive cavity going to zero is to take the inverse Fourier transform of $T(\omega)_A$ to obtain the impulse response function for the approximate band-limited transmission function of Eq. (3-22):

$$\tau_A(t) = e^{-\frac{\Delta\omega_p}{2}|t|} \sum_{p=-N}^{N} e^{i(\omega_o + p\omega_c)t} \qquad (3\text{-}25)$$

This result is developed in Appendix A, Example 2. Then from Eq. (3-15) with $\tau_A = h_m$, one can obtain the signal which matches the impulse response of Eq. (3-25) by the following convolution:

$$\tau_A \circledast R_n = A\, f^*(-t) \tag{3-26}$$

For $R_n = N_o\delta(t)$, which implies uniform white noise, i.e., $S_n(\omega) = N_o$ we obtain

$$f = C_3 e^{-\frac{\Delta\omega_p}{2}|t|} \sum_{p=-N}^{N} e^{i(\omega_o + p\omega_c)t} \tag{3-27}$$

and as $\Delta\omega_p \to 0$ we obtain the signal for which the idealized passive cavity with zero linewidth is a matched-filter.

3.4 Matched-Filter for Mode-Locked Laser Signals

From Appendix B we obtain the idealized field amplitude at the output of the mode-locked laser with 2N+1 modes as

$$E_1(t) = \sum_{p=-N}^{N} \exp\, i(\omega_o + p\omega_c)t = \exp\,(i\omega_o t)\, \frac{\sin(2N+1)\frac{\omega_c}{2}t}{\sin\frac{\omega_c}{2}t} \tag{3-28}$$

where ω_o is the center frequency of the laser output, $\omega_c = 2\pi f_c$, $f_c = c/2h$ is the spacing between modes, and h is the effective cavity length. Then the Fourier transform of Eq. (3-28) is

$$E(\omega) = 2\pi \sum_{p=-N}^{N} \delta(\omega - (\omega_o + p\omega_c)) \tag{3-29}$$

One may notice that the same term ω_c has been used to express the mode spacing of the passive laser cavity, $\omega_c = \pi c/h_o$, and to express the mode spacing of the mode-locked laser signal $\omega_c = \pi c/h$. We see that Eq. (3-28) and Eq. (3-27) are identical for $h = h_o$, i.e., if the lengths of the passive cavity and laser are equal. To see this more clearly since

$$\int_{-\infty}^{\infty} |E_1|^2 dt \quad \text{does not exist}$$

we express the matched-filter criteria by Eq. (A-36) as

$$(h_m \otimes R_n)_T = A\, E_1^* (-t) \quad . \tag{3-30}$$

If we assume $R_n(t) = N_o \delta(t)$ which implies $S_n(\omega) = N_o$ then from Eq. (3-28)

$$h_m(t) = \frac{A}{N_o} \sum_{p=-N}^{N} \exp i(\omega_o + p\omega_c)t \tag{3-31}$$

which exactly matches Eq. (3-25) for $\Delta\omega_p \to 0$ and $h = h_o$.

For an actual laser signal, writing $E(\omega)$ for a multi-tone laser with finite linewidths will yield an expression as an alternative to the monochromatic idealization of Eq. (3-29). We will assume that the actual multi-tone laser lineshape is given by a Lorentzian lineshape factor such that

$$E(\omega) = \frac{2}{\Delta\omega_\ell} \sum_{p=-N}^{N} \frac{1}{\sqrt{1+\left(\frac{2\Delta\omega}{\Delta\omega_\ell}\right)^2}} \tag{3-32}$$

where $\Delta\omega_\ell$ is the full bandwidth at half power of each mode and where $\Delta\omega = \omega-\omega_p = \omega-(\omega_o+ p\omega_c)$, $\omega_c = \pi c/h$, and h is the effective length of the mode-locked laser cavity.

This Lorentzian lineshape is consistent with our mathematical idealization of Eq. (3-16) by Eq. (3-22) and it should not be considered as a physical hypothesis of the lineshape which occurs in a helium-neon gas laser. As is discussed in Chapter 5, the functional form of an oscillator lineshape is closely related to the appropriate transmission function for the system. More specifically, lumped circuit oscillators have approximately Lorentzian lineshapes while cavity and transmission line systems will have lineshapes as determined by gain narrowing arguments based on equations of the form of Eq. (3-16). The matched-filter for the mode-locked laser signal modeled by Eq. (3-32) is given by Eq. (3-13) as

$$H_m(\omega) = \frac{A\, E^*(\omega)}{S_n(\omega)} = \frac{A}{S_n(\omega)} \sum_{p=-N}^{N} \frac{2}{\Delta\omega_\ell} \frac{1}{\sqrt{1+\left(\frac{2\Delta\omega}{\Delta\omega_\ell}\right)^2}} \tag{3-33}$$

If we compare Eq. (3-22) to Eq. (3-33) we see that for $S_n(\omega)$ constant over the frequencies of interest; and $\Delta\omega_\ell = \Delta\omega_p$, i.e., the linewidths of the signal and the passive cavity are the same; and $h = h_o$, then this passive cavity is a matched-filter for the mode-locked signal.

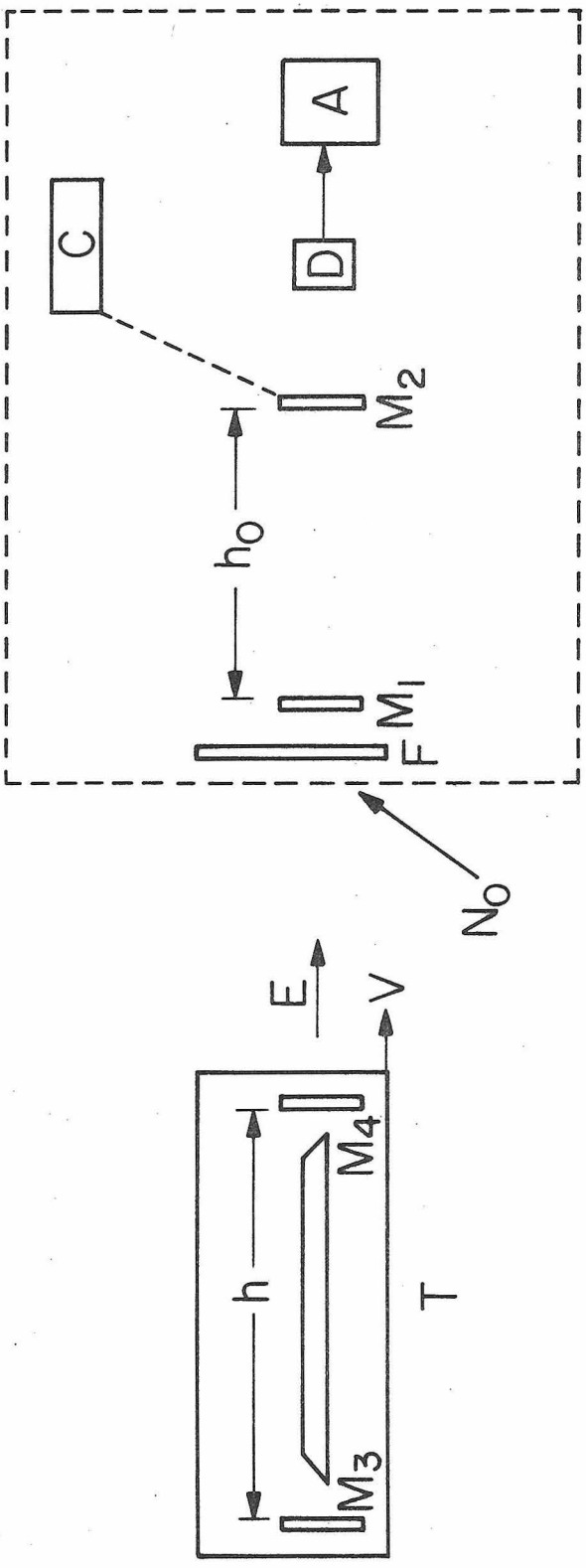

Fig. [3-1]

Thus we propose the following communication system shown in Fig. [3-1]. The transmitter T is a mode-locked laser of length h with mirrors M_3 and M_4 emitting a signal E and traveling at a velocity V. The output of the transmitter is detected by our matched-filter detection system. The system consists of a coarse bandpass filter F, chosen to pass those frequencies for which the mirrors M_1 and M_2 are constant with frequency. In the case where $V = 0$ the control C will set $h_o = h$ so that the passive cavity is matched to the incident mode-locked laser signal. We note that if $V \neq 0$ then the passive cavity provides a means of measuring the velocity by vernier adjustments of the cavity length. This property will be discussed in Chapter 7. The output of the passive cavity is detected and processed by the detector electronics.

The Fabry-Perot cavity is probably as close a physical realization to a matched-filter for the multi-toned laser as can be attained in a passive system. Even so, gain narrowing invariably results in $\Delta\omega_\ell < \Delta\omega_p$ [(1)], thereby limiting the observed improvement in the signal-to-noise ratio from its optimum value. For high gain lasers with cavities of low finesse, the receiver can be made closer to ideal, while greater departures are to be expected in the case of low gain. We note, too, that larger bandwidths, $\Delta\omega_p$, are called for with information modulated lasers and cavity-dumped lasers where mode-locking may not have been employed.

Before we go on to consider the signal-to-noise improvement of the passive cavity and the departure from the matched-filter condition for $\Delta\omega_\ell < \Delta\omega_p$ and $h \neq h_o$ (Chapter 5), we will consider the factors which control the finesse of the passive Fabry-Perot resonant cavity.

Chapter 3

Reference

1. A. Yariv, Quantum Electronics, (John Wiley, New York, 1967), p. 409.

Chapter 4

Finesse

4.1 Introduction

One of the more important characteristics which influences the performance of a passive resonant cavity is the finesse, defined as the ratio of the separation of the resonant frequencies, called the free spectral range, and the full width, $\Delta\omega_p$, at half power of one of the resonances. Thus we may write

$$F = \frac{\omega_n - \omega_{n-1}}{\Delta\omega_p} \tag{4-1}$$

where $\omega_n = n\pi c/h_o$, h_o is the length of the cavity, c is the speed of light, and n is some large integer.

This chapter deals with the factors that control the finesse of a passive cavity. The ideal situation is first discussed and we find that the finesse is controlled by the reflectivity of the end mirrors of the passive cavity. Then losses are introduced and their causes are discussed and quantified for the actual case used in the experiment.

4.2 The General Case

Before we begin it is of interest to relate the finesse of the cavity to the quality factor Q of a resonant cavity defined by

$$Q = \omega_o \cdot \frac{\text{energy stored}}{\text{power lost}} \approx \frac{\omega_o}{\Delta\omega_p} \tag{4-2}$$

Thus from Eq. (4-1) using Eq. (4-2) we have

$$F = Q \cdot \frac{\omega_n - \omega_{n-1}}{\omega_o} \tag{4-3}$$

We see from Eq. (2-35) that if t_1, t_2, r_{21}, r_{12} are constant, i.e., the end mirrors of the cavity are periodically stratified quarter-wave stacks as was considered in Section 2.4, and the loss per unit length $\alpha = 0$, then the transmissivity of the passive laser cavity is given by

$$T = \frac{1}{1 + P \sin^2 \omega \frac{h_o}{c}} \tag{4-4}$$

where for convenience we choose $r_{12} = r_{21} = r$

$$P = \frac{4r^2}{(1-r^2)^2} \tag{4-5}$$

Now to determine the finesse for this idealized case we must consider the values of ω for which T attains one half of its peak value. Thus from Eq. (4-4) we have

$$1 + P \sin^2 \omega \frac{h_o}{c} = 2 \tag{4-6}$$

and for $P >> 1$, i.e. $\sin\theta = \theta$, we have

$$\Delta\omega_P = \frac{2c}{h_o\sqrt{P}} \tag{4-7}$$

Thus since $\omega_n - \omega_{n-1} = \pi c/h_o$ we have from Eq. (4-1)

$$F = \frac{\pi\sqrt{P}}{2} = \frac{\pi\sqrt{R}}{1-R} \tag{4-8}$$

where $R = r^2$ from Eq. (2-15). This is the well known finesse formula [1] which ideally is only limited by the end mirror reflectivity. For a reflectivity of $R = .991$, $P \simeq 50{,}000$ and $F \simeq 350$. But unfortunately there are losses involved with the transmission function which reduce the finesse from this ideal case.

4.3 The Loss Case

Again we consider Eq. (2-35) with $\alpha \neq o$ repeated here for convenience with $\beta = \omega/c$

$$T = \frac{|t_1 t_2|^2 e^{-2\alpha h_o}}{(1-r_{12}r_{21}e^{-2\alpha h_o})^2} \quad \frac{1}{1 + P\sin^2(\omega h_o/c)} \tag{4-9}$$

$$P = \frac{4r_{12}r_{21}e^{-2\alpha h_o}}{(1-r_{12}r_{21}e^{-2\alpha h_o})^2} \tag{4-10}$$

Since the multiplier term of Eq. (4-9) is independent of frequency the derivation leading to the finesse is the same as above so that from Eq. (4-8)

$$F = \frac{\pi\sqrt{P(\alpha)}}{2} \tag{4-11}$$

Introducing Eq. (4-10) into Eq. (4-11) and letting $R = r_{12}r_{21}$ we have

$$F = \frac{\pi\sqrt{R}e^{-\alpha h_o}}{1-Re^{-2\alpha h_o}} \tag{4-12}$$

At this point we wish to expand Eq. (4-12) to relate it to the no loss case of Eq. (4-8). So we have dividing by $e^{\alpha h_o}$ and expanding

$$F = \frac{\pi\sqrt{R}}{(1-R) + (1+R)\sinh(\alpha h_o) + 2(1-R)\sinh^2(\frac{\alpha h_o}{2})} \tag{4-13}$$

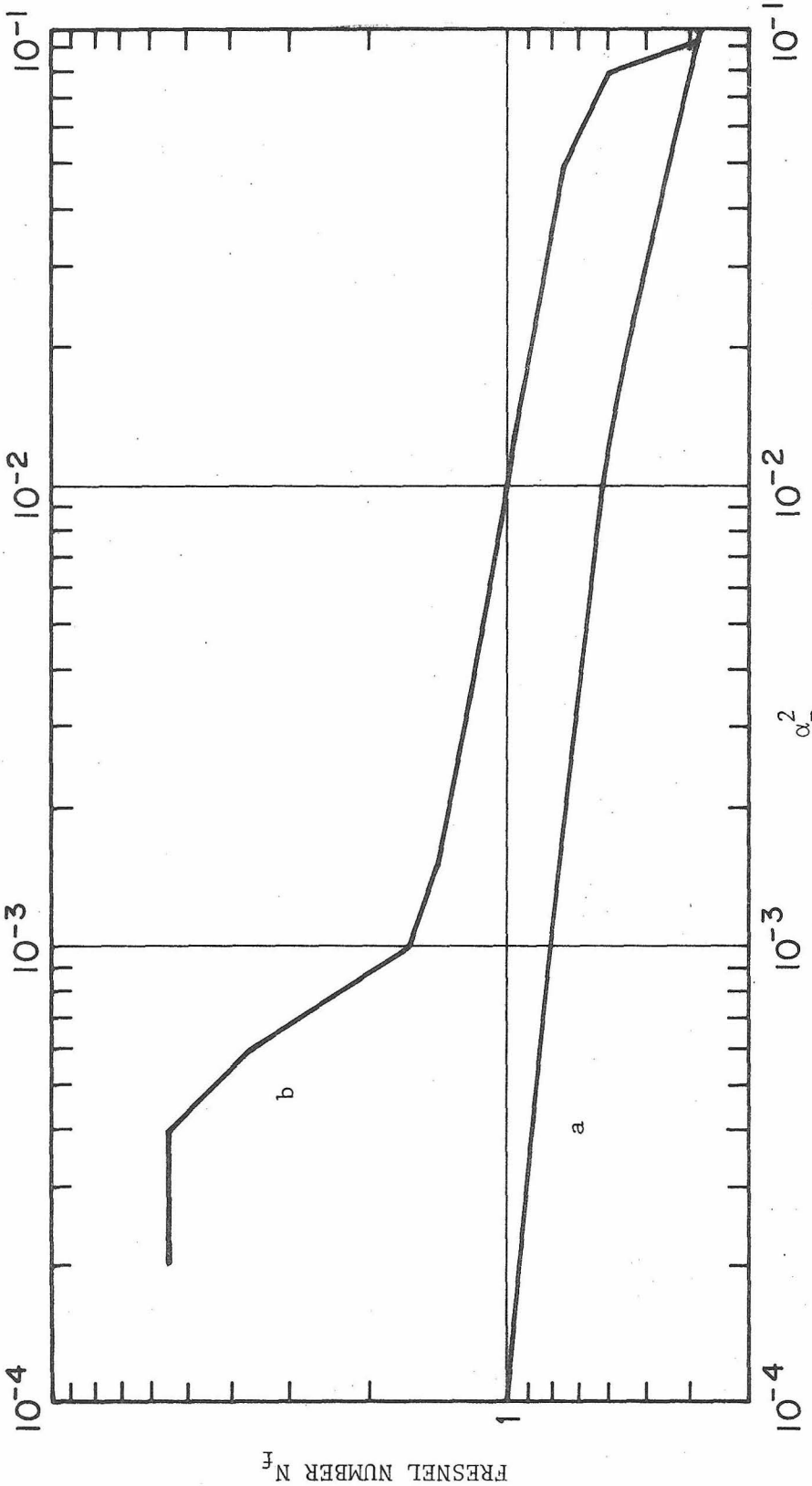

Fig. [4-1]

Thus Eq. (4-13) shows us the additive nature of the distributed loss term. We know that the (1-$\mathcal{R}$) term of Eq. (4-8), if we include loss, corresponds to the total intensity which is transmitted and/or absorbed as is indicated by Eq. (4-13). Thus by conservation of energy we write for $r_{12} = r_{21} = r$, $t_1 = t_2 = t$

$$1-\mathcal{R} = 1-r^2 = t^2 + \alpha^2 \tag{4-14}$$

α^2 is the total loss and may be broken down as $\alpha^2 = \alpha_D^2 + \alpha_S^2 + \alpha_R^2$ where α_D^2 is the loss due to diffraction, α_S^2 is the loss due to scattering centers in the end mirrors, and α_R^2 is the loss due to other irregularities of the end mirrors. Thus Eq. (4-13) becomes

$$\mathcal{F} = \frac{\pi\sqrt{r^2}}{t^2 + \alpha_D^2 + \alpha_S^2 + \alpha_R^2} \tag{4-15}$$

We will now consider the various losses in more detail.

4.4 Diffraction Losses

Diffraction loss in a plane-parallel Fabry-Perot cavity has been considered previously[2]. However we will consider the spherical mirror resonator since it has been shown to yield much lower loss[3,4]. Since any beam of light spreads as it propagates due to diffraction and since one can think of a set of mirrors folding the wave back on itself, then we see that with finite mirrors energy will be lost each time the beam is reflected by the end mirrors of the cavity. This diffraction loss per reflection is shown in Fig. [4-1a][3]. This curve was calculated for the confocal resonator but can readily be used for the non-confocal case by the conversion formula

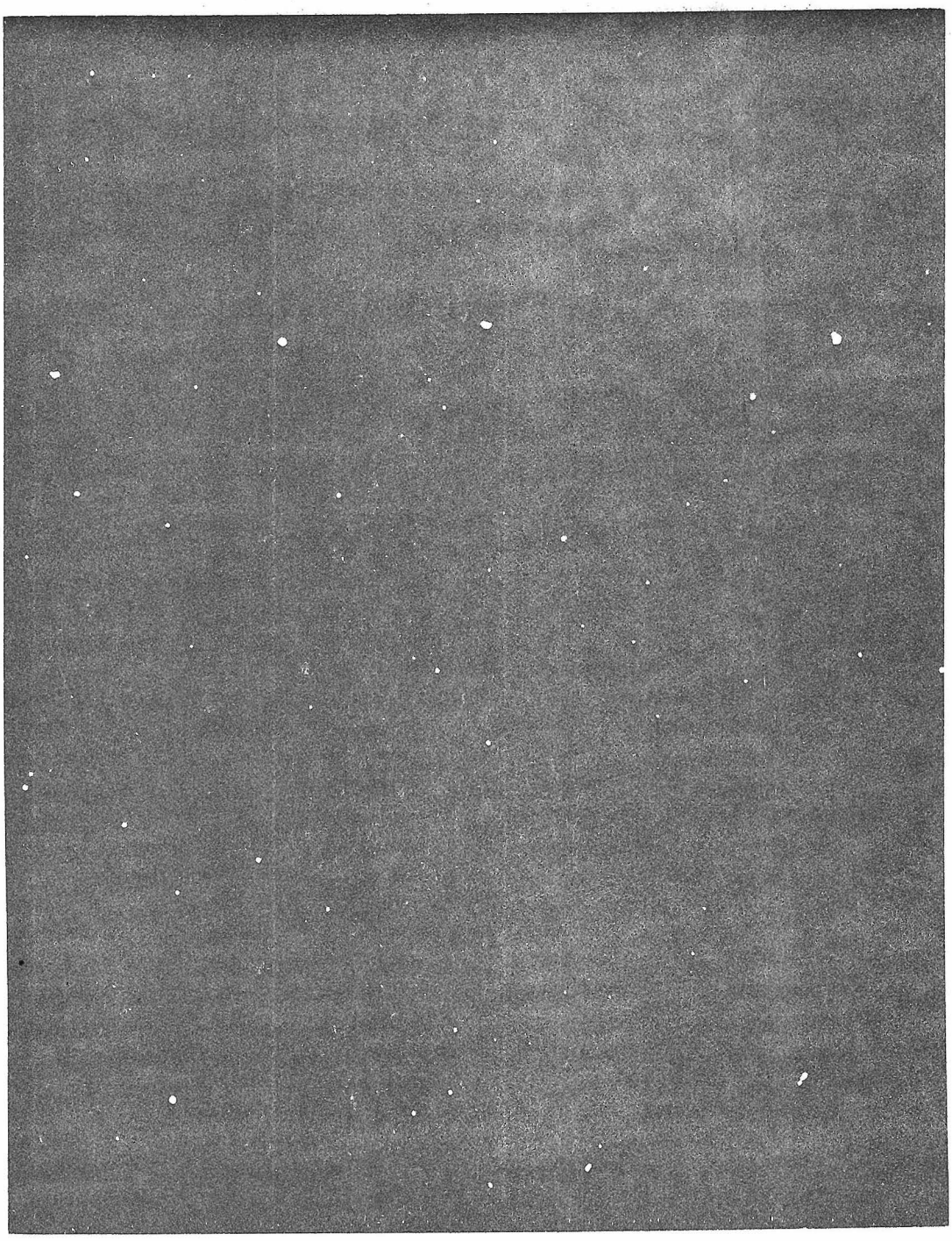

Fig. [4-2]

$$N_f = \frac{a^2}{b\lambda} = \frac{a'^2}{L\lambda}\left[\frac{L}{R} - \left[\frac{L}{R}\right]^2\right]^{\frac{1}{2}} \qquad (4\text{-}16)$$

where N_f is called the Fresnel number, λ is the wave length, a' is the radius of the mirror, b is the confocal spacing, L is the length between a flat mirror and a curved mirror of radius R, and a is the corresponding confocal mirror radius. Thus one sees that by controlling the aperture size and length of the cavity one can experimentally verify the Boyd and Gordon curve of Fig. [4-1a]. A curve was experimentally generated on an apparatus which will be described later in Chapter 8. It was plotted along with the calculated curve as Fig. [4-1b]. The general slope of the curves are the same for loss greater than 10^{-3} with the experimental curve having a constant displacement above the calculated curve. This constant displacement and the knee in the curve at 10^{-3} will be better understood after we consider the other loss mechanisms.

4.5 Scattering Loss at the End Mirrors

In this work the scattering losses that will be considered are due to small imperfections in the multilayer coating. These occlusions cause incident light to scatter at the multilayer surface. A photo taken at 500x magnification of these scattering centers is shown in Fig. [4-2]. Less than ten scatterers per 1/4 mm^2 were observed in the Spectra-Physics standard laser reflectors. Each scatterer averaged 5 μm in diameter which leads to a calculated loss factor, assuming all scattered light is lost, of $\alpha_S^2 = 10^{-3}$. This loss is independent of Fresnel number in that the area of the surface illuminated does not effect the constant loss per unit

area. Thus the scattering centers contribute to part of the constant shift in the experimental curve of Fig. [4-1b]. Notice also that the knee in the curve occurs around 10^{-3} indicating that the diffraction losses are becoming negligible for higher Fresnel numbers.

4.6 Other Losses

Other loss mechanisms in the optical resonator may include surface roughness of the end mirrors. These surface irregularities will introduce an uncertainty in the resonant frequency and/or cause scattering of light out of the passive cavity.

The loss due to scattering and other irregularities experimentally was obtained in the following way. Firstly, the free space transmission t^2 of the end mirrors was measured. Secondly, the finesse, as in Eq. (4-15) was measured for $\alpha_D^2 << t^2 + \alpha_s^2 + \alpha_R^2$ by setting the Fresnel number $N_f > 25$. Finally, the finesse was measured again with a known diffraction loss by choosing an N_f and taking the data off Fig. [4-1a]. Using the data to form two independent equations one could determine the non-diffraction losses as

$$\alpha_s^2 + \alpha_R^2 = \alpha_D^2 - t^2 \qquad (4\text{-}17)$$

The non-diffraction losses were found to be 3×10^{-3} which, in conjunction with the results of Section 4.5, led to the conclusion that the loss due to surface roughness was 2×10^{-3}.

Thus it may be concluded from this study that the finesse will

not be limited by diffraction losses for large Fresnel numbers ($N_f > 10$). The scattering centers and other irregularities play approximately an equal part in limiting the finesse below its theoretical maximum determined by the mirror transmissivity.

Chapter 4

References

1. Born, M., Wolf E., Principles of Applied Optics, 4th Edition, (Pergamon Press, 1970), p. 328.
2. Fox, A.G., Li, Tingye, Bell System Tech. J., Vol. 40, p. 453 (1961).
3. Boyd, G.D., Gordon, J.P., Bell System Tech. J., Vol. 40, p. 489 (1961).
4. Boyd, G.D., Kogelnik, H., Bell System Tech. J., Vol. 41, p. 1347 (1962).

Chapter 5

Signal-to-Noise Ratio

5.1 Introduction

The signal-to-noise ratio developed in Appendix A is defined by the ratio of the signal power, as a function of time, to the average noise power. We will, in this chapter, first consider the signal-to-noise ratio improvement with use of the passive cavity for mode-locked laser signals. Then the signal-to-noise ratio as a function of time and as a function of relative cavity length for various numbers of modes oscillating will be shown. Once having developed the improvement factor we will consider in more detail the degree to which the passive cavity approximates a matched-filter for actual multi-tone gas laser signals.

5.2 Signal-to-Noise Improvement

We are now in a position to consider the signal-to-noise ratio that is associated with the output of the passive Fabry-Perot cavity for a mode-locked laser input.

First consider that no passive cavity is present, then the modulus-squared value of the mode-locked laser signal is given from Eq. (B-1) by

$$|E_1|^2 = \left| \sum_{p=-N}^{N} e^{i(\omega_o + p\omega_c)t} \right|^2 \tag{5-1}$$

where we have $2N+1$ modes oscillating separated by $\omega_c = \pi c/h_o$ and centered around ω_o. The mean-squared value of the additive output

noise is given by the input correlation function evaluated at $t = 0$ from Eq. (3-7)

$$\langle |n|^2 \rangle = \frac{1}{2\pi} \int_{m\frac{\pi c}{h}} S_n(\omega)\, d\omega = \frac{N_o}{2\pi}\, m\, \frac{\pi c}{h} \tag{5-2}$$

where $S_n(\omega)$ is the power spectral density of the additive input noise, N_o is the constant value of the Gaussian white noise, and m is the number of free spectral ranges of the passive cavity over which the integration is taken. Thus the ratio of Eq. (5-1) to Eq. (5-2) yields the signal-to-noise ratio for (2N+1) modes without the passive cavity.

Now if we assume that we have a normally incident TEM wave of a (2N+1) mode mode-locked laser as the input to the passive cavity of length h_o then the modulus-squared value of the signal portion at the output of the cavity will be from Eq. (2-31) and the Fourier transform of Eq. (B-1) as in Eq. (A-17)

$$|E_1 \circledast \tau|^2 = \left| \int_{-\infty}^{\infty} \sum_{p=-N}^{N} \delta(\omega - (\omega_o + p\omega_c)) \frac{t_1 t_2\, e^{-i\omega\frac{h_o}{c} - \alpha h_o}}{1 - r_{12} r_{21}\, e^{-2i\omega\frac{h_o}{c} - 2\alpha h_o}} e^{i\omega t} d\omega \right|^2$$

where τ is the inverse Fourier transform of Eq. (2-31) (5-3)

Since we have shown that the matching condition occurs when $h = h_o$ then Eq. (5-3) becomes

$$|E_1 \circledast \tau|^2 = \left| K \sum_{p=-N}^{N} e^{i(\omega_o + p\omega_c)t} \right|^2 \tag{5-4}$$

where

$$K \equiv \frac{t_1 t_2 e^{-\alpha h_o}}{1 - r_{12} r_{21} e^{-2\alpha h_o}}$$

The mean-squared value of the additive output noise with the use of the passive cavity is given by Eq. (A-18) and Eq. (2-35)

$$\langle |n \otimes \tau|^2 \rangle = \frac{K^2}{2\pi} \int_{m\frac{\pi c}{h_o}} \frac{S_n(\omega)\, d\omega}{1 + P \sin^2(\omega \frac{h_o}{c})} \tag{5-5}$$

Now if we assume Gaussian white noise where $S_n(\omega) = N_o$ then we have

$$\langle |n \otimes \tau|^2 \rangle = \frac{K^2 N_o m}{2\pi} \int_{-\frac{\pi c}{2h_o}}^{\frac{\pi c}{2h_o}} \frac{d\omega}{1 + P \sin^2 \omega \frac{h_o}{c}} = \frac{K^2 N_o mc}{2\pi h_o} \int_{-\frac{\pi}{2}}^{\frac{\pi}{2}} \frac{du}{1 + P \sin^2 u} \tag{5-6}$$

If we use two trigonometric substitutions we see that

$$\int_{-\frac{\pi}{2}}^{\frac{\pi}{2}} \frac{du}{1 + P \sin^2 u} = \frac{\pi}{\sqrt{1+P}}$$

Hence the mean-squared value of the additive noise with the passive cavity from Eq. (5-6) becomes

$$\langle |n \otimes \tau|^2 \rangle = \frac{K^2 N_o}{2\pi} m \frac{\pi c}{h_o} \frac{1}{\sqrt{1+P}} \tag{5-7}$$

So the signal-to-noise ratio is given by the ratio of Eq. (5-4) to Eq. (5-7).

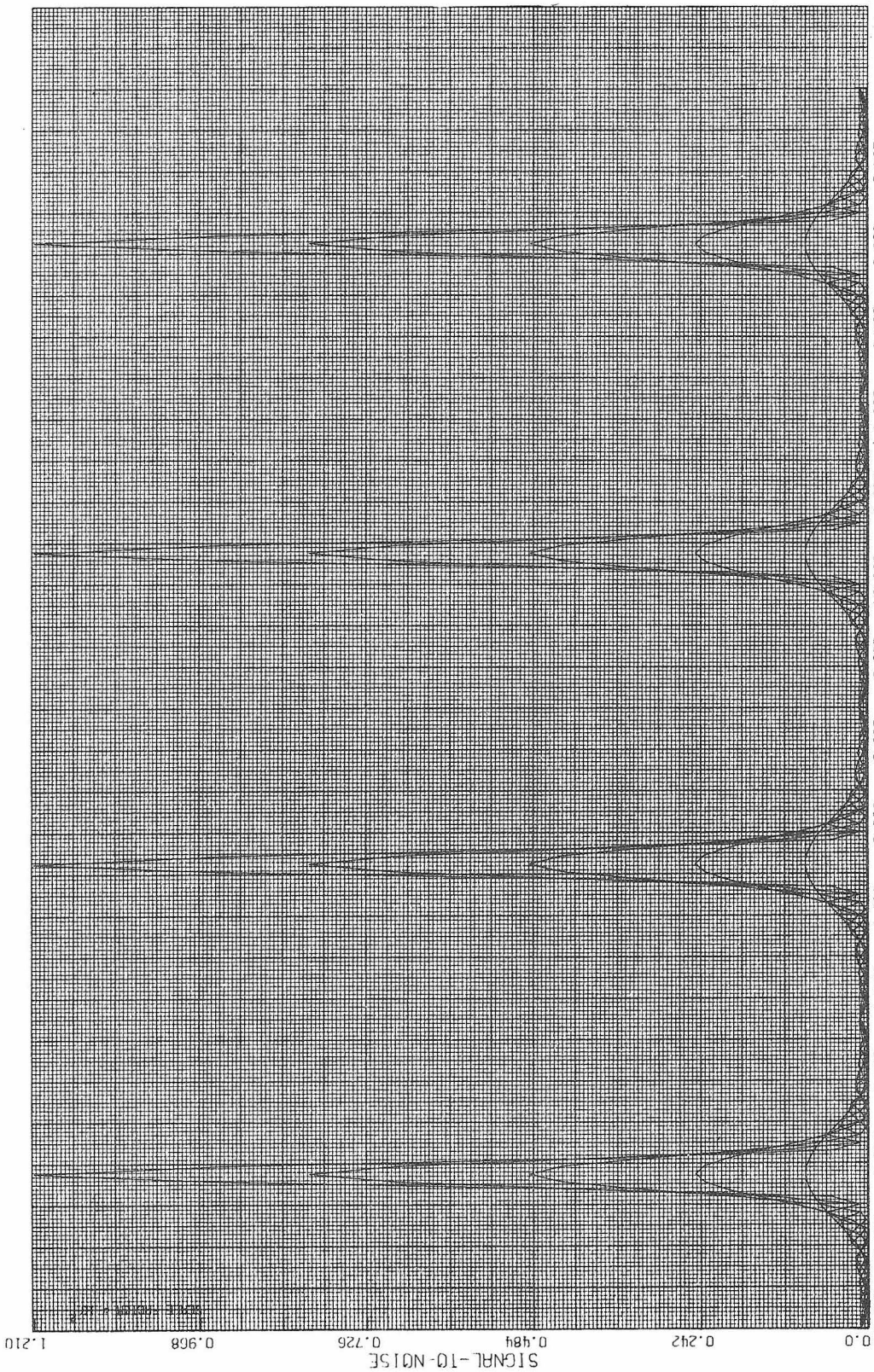
SIGNAL-10-NOISE
0.0
0.242
0.484
0.726
0.968
1.210
-4.000
-3.467
-2.933
-2.400
-1.867
-1.333
-0.800
-0.267
0.267
0.800
1.333
1.867
2.400
2.933
3.467
TIME

Fig. [5-1]

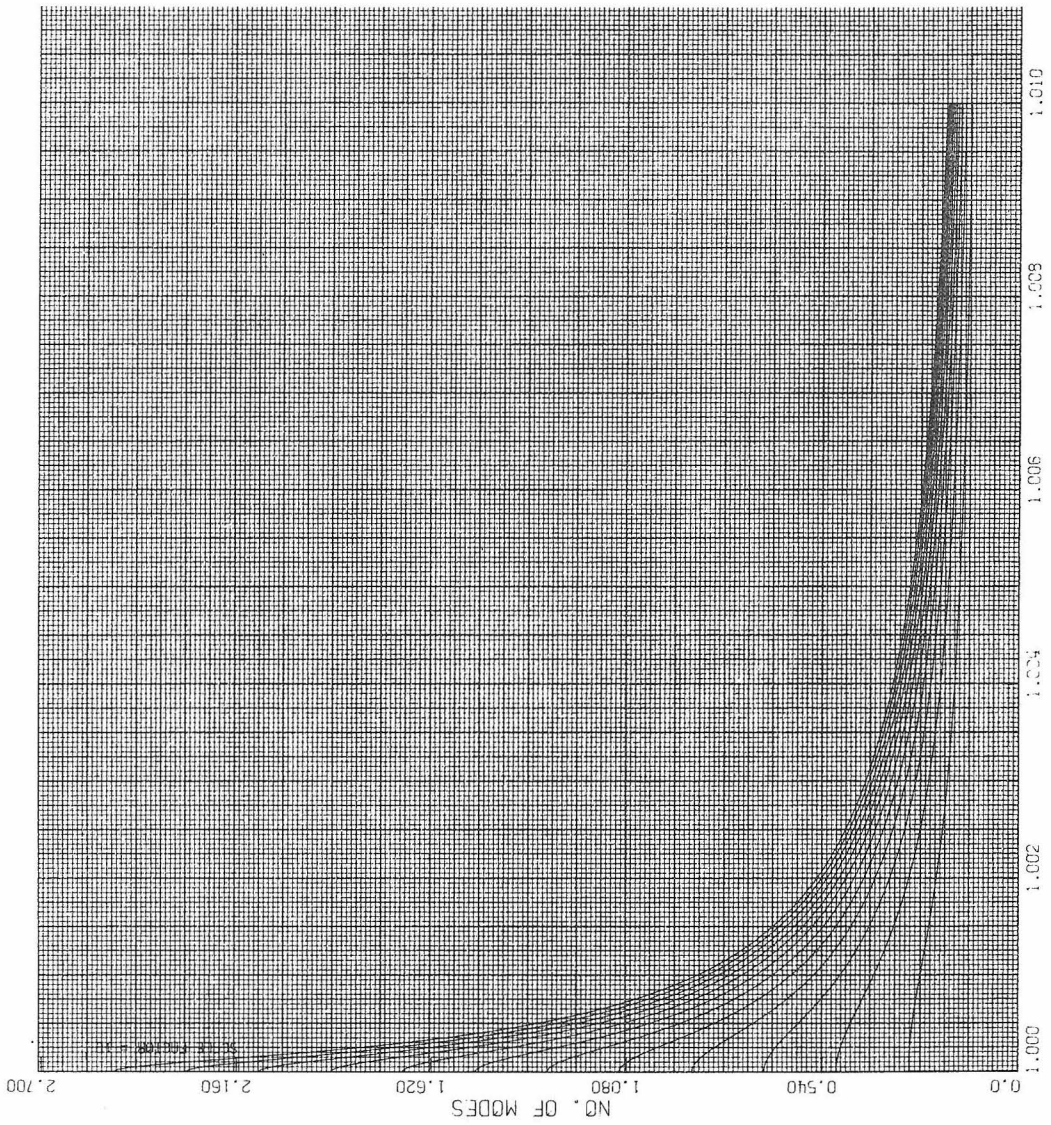
NO. OF MODES
0.0
0.540
1.080
1.620
2.160
2.700
1.000
1.002
1.006
1.008
1.010
h_o/h

Fig. [5-2]

It is now clear that the signal-to-noise improvement of passive cavity with respect to no cavity is given from Eqs. (5-1, 5-2, 5-4, and 5-7) by

$$\frac{SNR_{with}}{SNR_{without}} = \sqrt{1+P} \tag{5-8}$$

If we now refer back to Eq. (5-3) we can consider the sensitivity of the matched-filter for a small deviation of relative cavity lengths. Variation of the cavity length on the order of a wavelength will take the cavity in and out of resonance; however, we will concern ourselves with the larger mismatches in cavity length which, contrary to the matched condition, leads to the failure of all the modes to be transmitted simultaneously. We saw previously that the signal-to-noise with the passive cavity as a function of time is the ratio of Eq. (5-4) and Eq. (5-7). This is illustrated in Fig. [5-1] as a function of the number of modes oscillating in the mode-locked laser signal. Also by considering Eq. (5-3) for small variations in relative cavity lengths $x = h_o/h$ we obtain an attentuation factor A as a function of the number of modes given by

$$A = \sum_{p=-N}^{N} \frac{1}{\sqrt{1 + P \sin^2 p\pi x}}$$

# of modes = 3
peak SNR = 9
period = 8 nsec

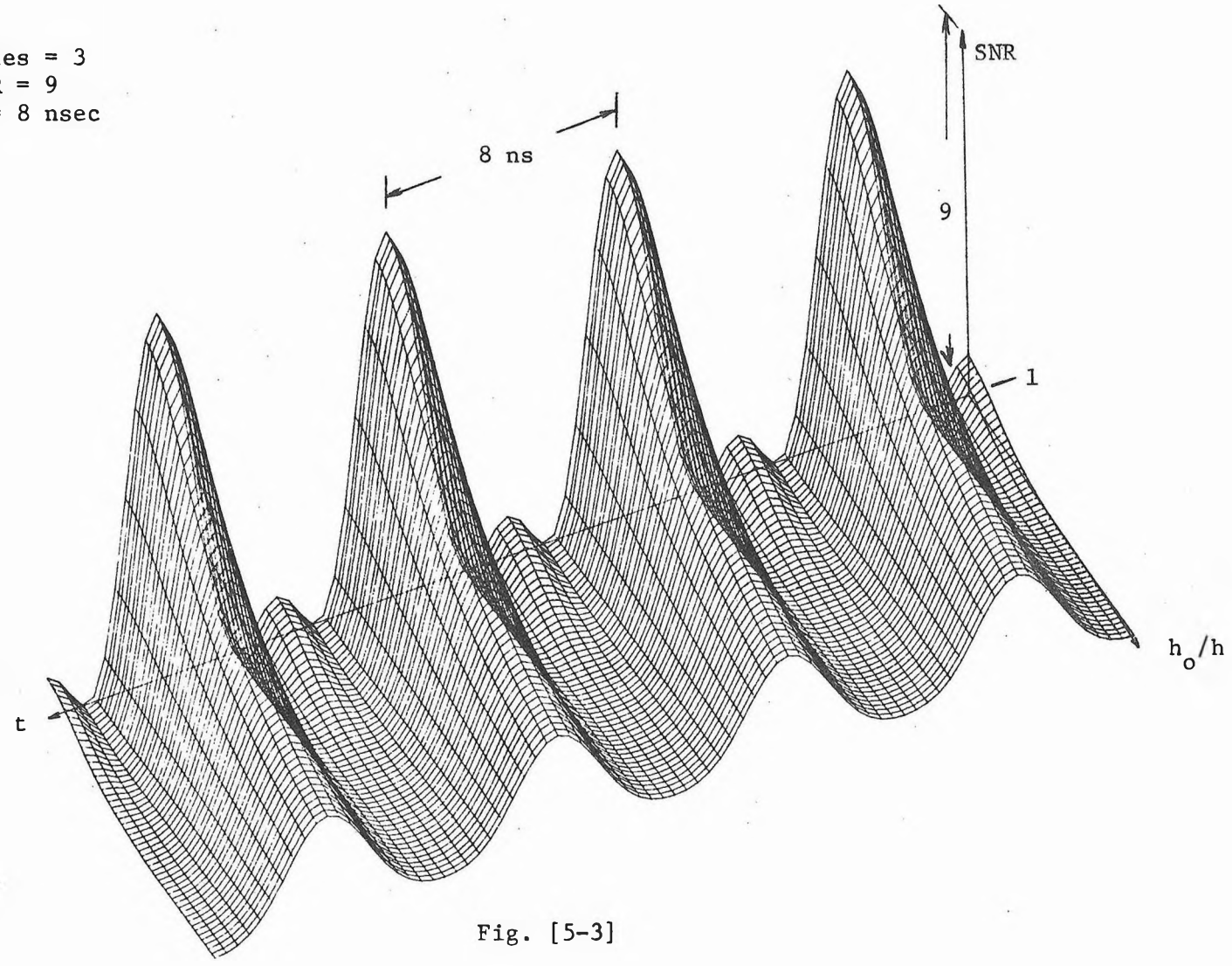

Fig. [5-3]

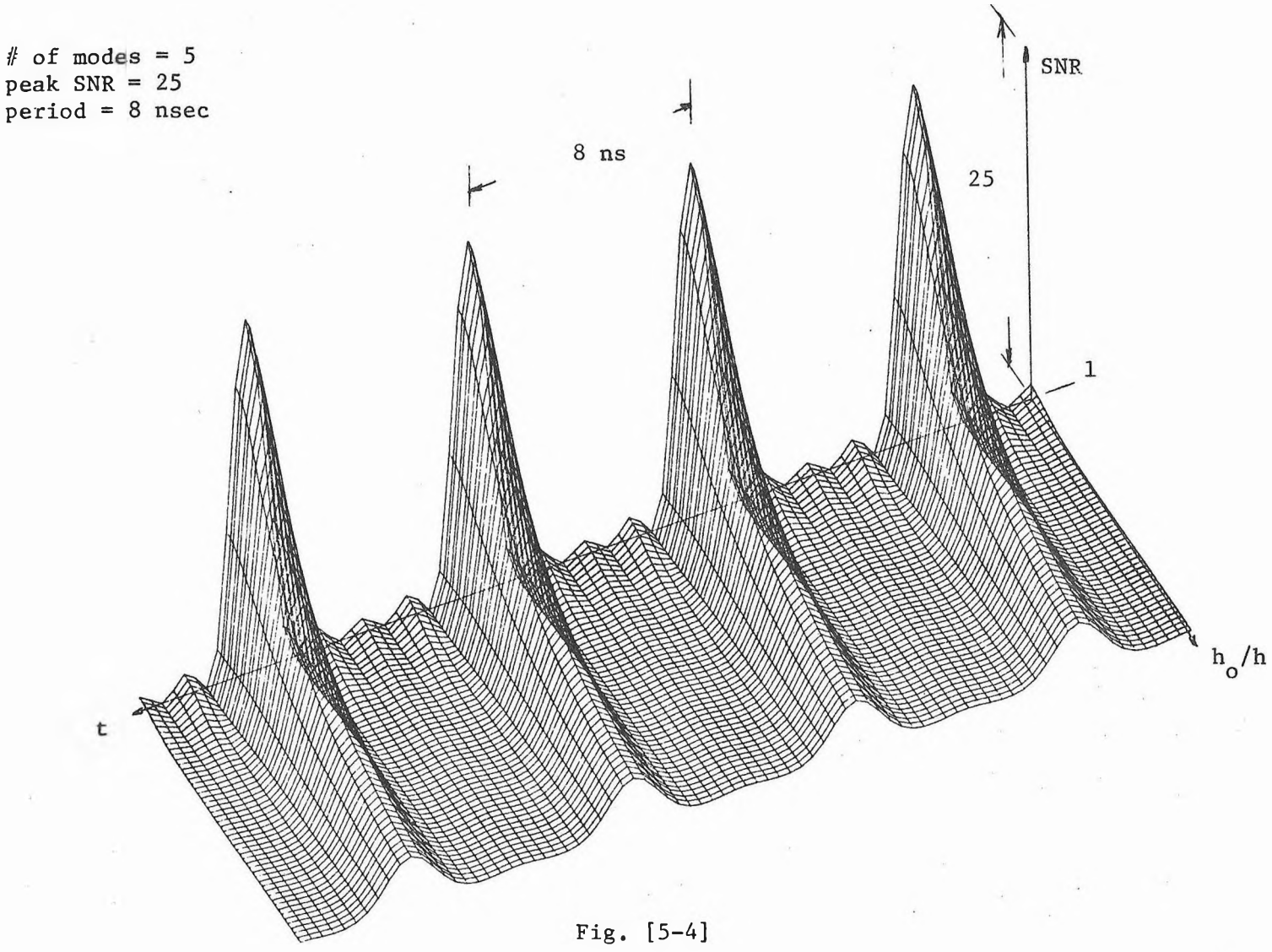

Fig. [5-4]

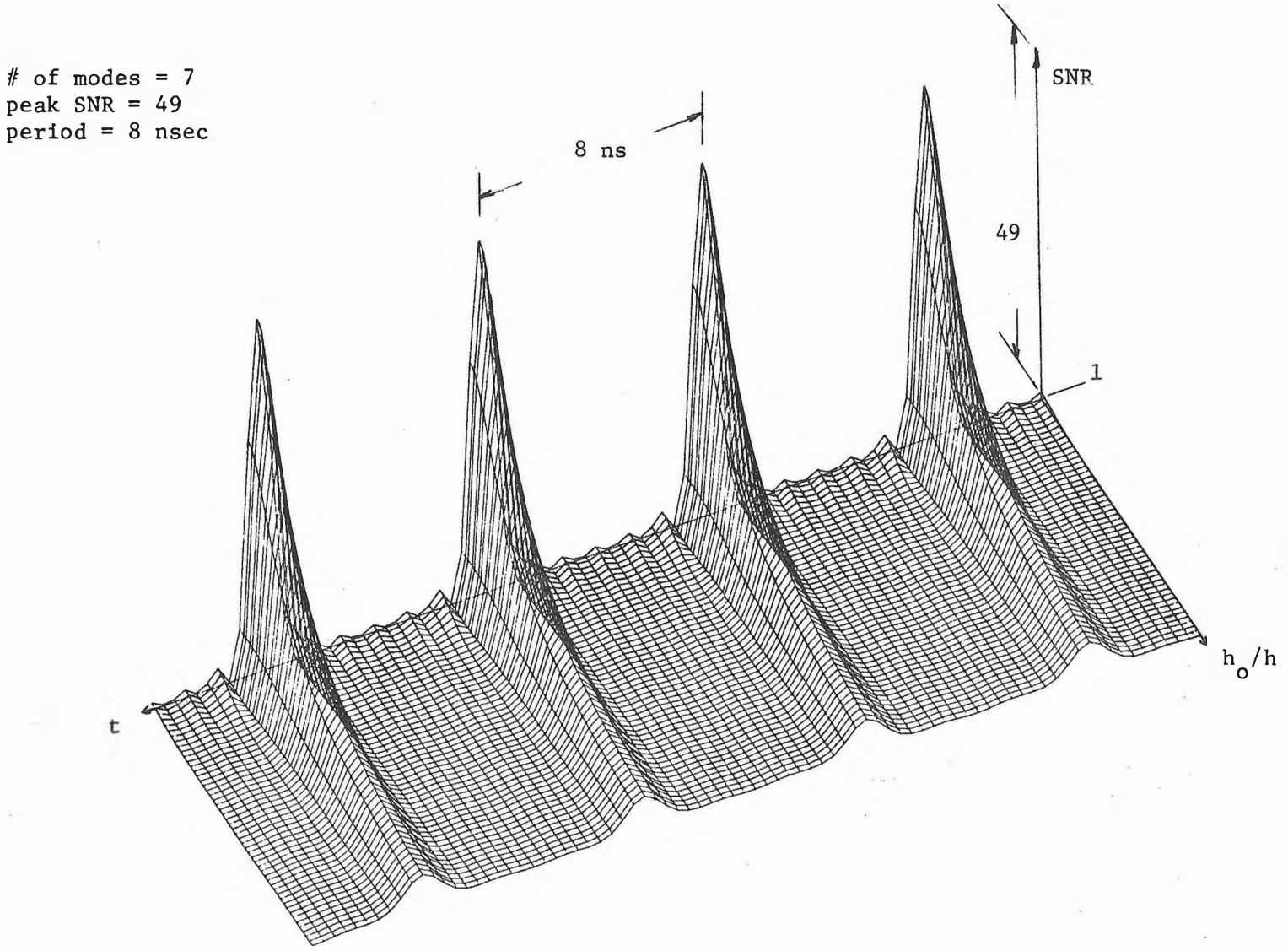

Fig. [5-5]

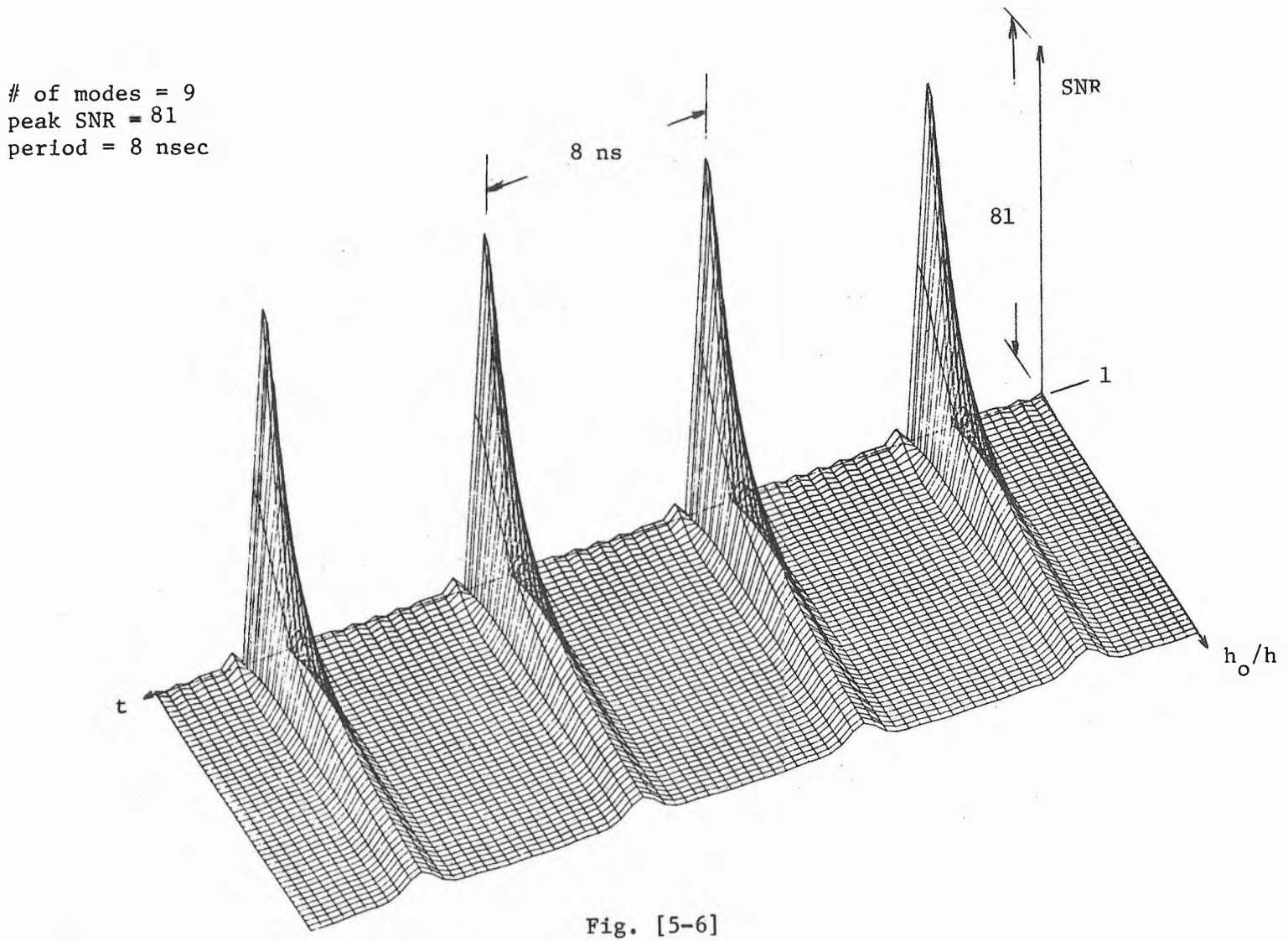

Fig. [5-6]

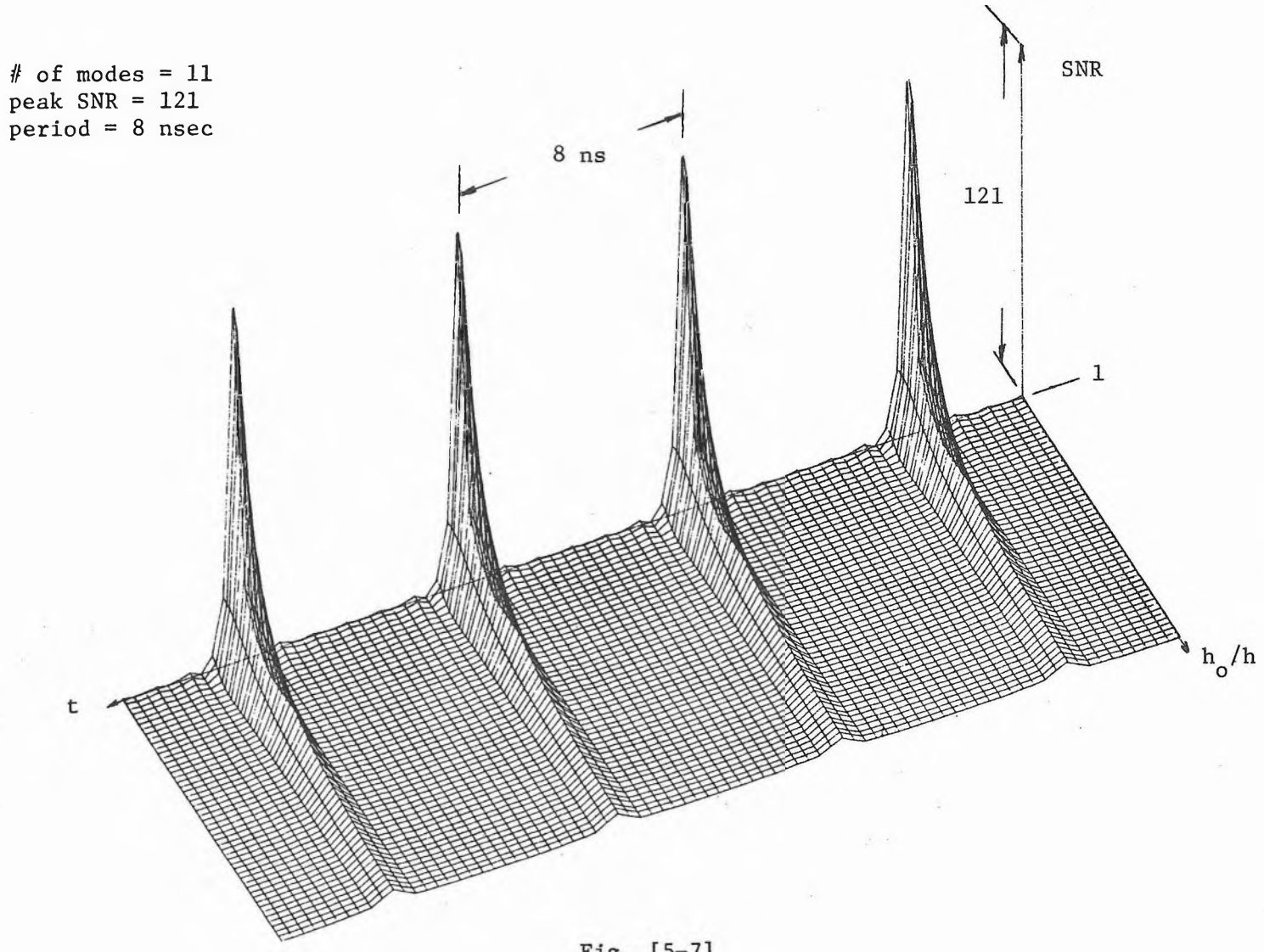

Fig. [5-7]

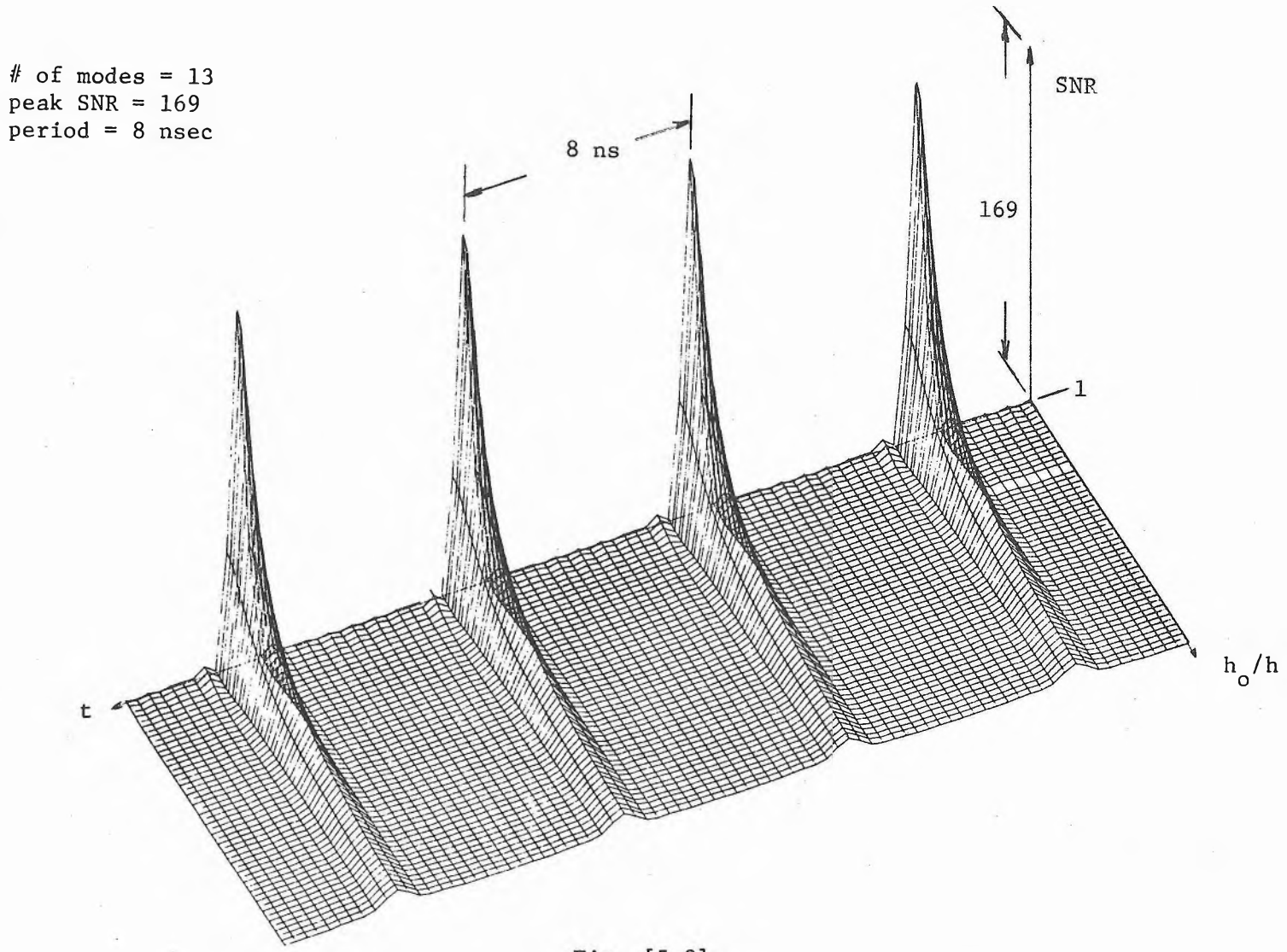

Fig. [5-8]

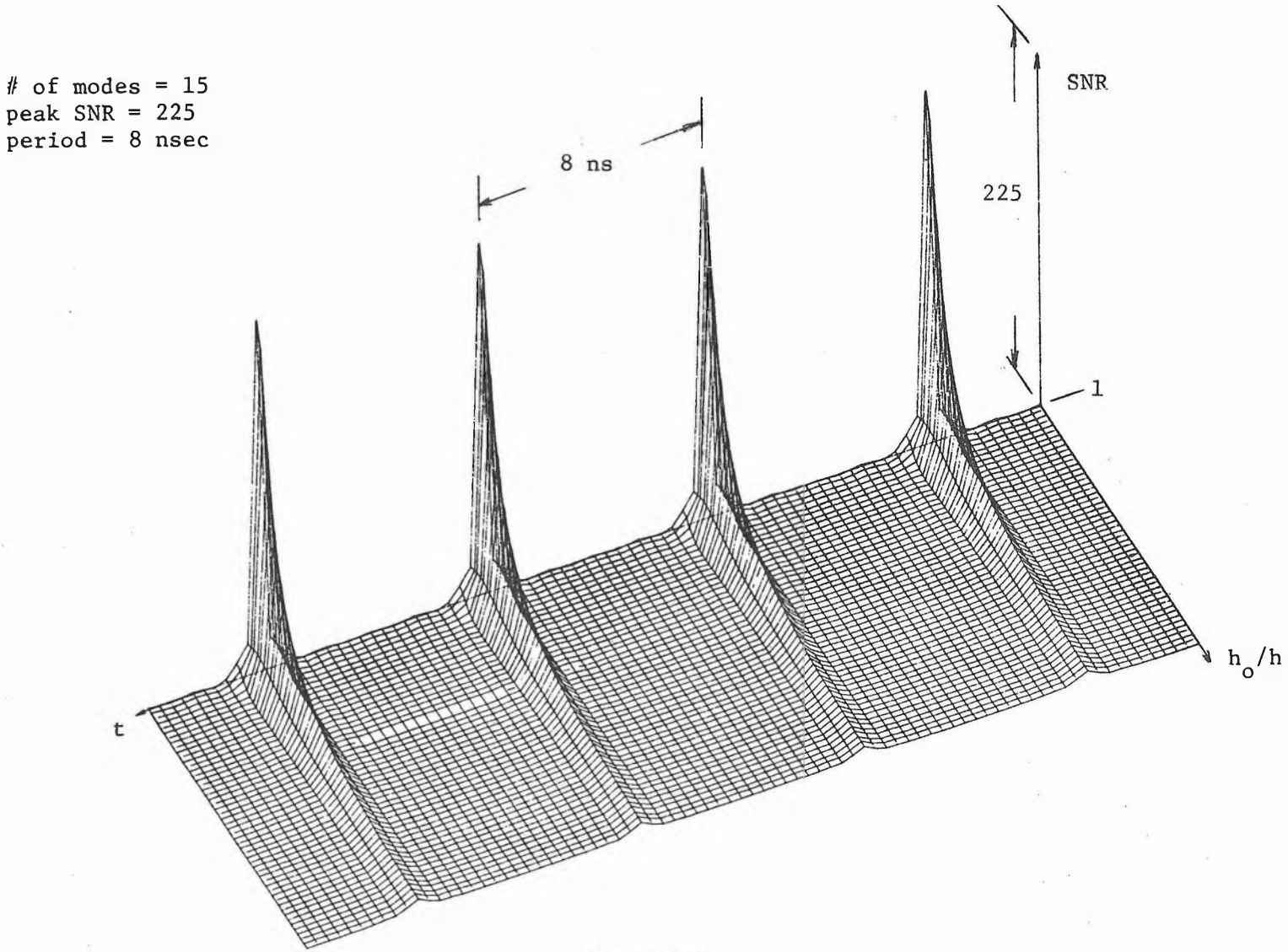

Fig. [5-9]

This fall-off from maximum improvement as a function of h_o/h is illustrated in Fig. [5-2]. To see how the signal-to-noise ratio varies as a function of time and relative cavity lengths we plot the three-dimensional illustrations for various number of modes oscillating. Figure [5-3] illustrates three modes oscillating with peak signal-to-noise of nine units occurring eight nanoseconds apart. Figure [5-4] illustrates five modes oscillating with peak signal-to-noise of 25 units, and so on for Fig. [5-5], Fig. [5-6], Fig. [5-7], Fig. [5-8], and Fig. [5-9]. In Figs. [5-3] - [5-9] the increment $\Delta h_o/h$ is 0.0001.

5.3 Laser Lineshape

Since an actual mode-locked laser has a finite linewidth $\Delta\omega_\ell$, before we can compare the signal-to-noise improvement of the passive cavity to the signal-to-noise improvement of the matched-filter, we must model the frequency spectrum of the laser signal. To do this we start with the amplitude transmission function of Eq. (2-32) and write it as

$$T = \frac{t_1 t_2}{2\sqrt{r_{12} r_{21}}} \sqrt{P} \frac{e^{i\phi(\beta)}}{\sqrt{1 + P \sin^2(\beta h_o)}} \tag{5-9}$$

where

$$P = \frac{4 r_{12} r_{21} e^{-2\alpha h_o}}{(1 - r_{12} r_{21} e^{-2\alpha h_o})^2}$$

where $\phi(\beta)$ is given by Eq. (3-19). As was mentioned in Chapter 2,

$\alpha < 0$ implies a gain per unit length for which T may become very large at the resonant frequencies.

In linear system theory, the criterion for oscillation is to find if a transfer function has poles in the right half portion of the complex s-plane (Nyquist stability criterion). For our purposes we note that the poles of $T(s)$ will occur on the imaginary axis when $\alpha = \ell n(r_{12}r_{21})/(2h_o)$ at the resonant radian frequencies $n\pi c/h_o$, where n is some large integer.

An actual laser, as discussed in Appendix B, consists of an active gain medium and a resonant cavity. One may consider Eq. (5-9) with α containing the unsaturated Doppler broadened gain and β including the unsaturated dispersion profile such that the peak gain is not sufficient to induce oscillation. Now as the peak gain is increased above that which is needed for oscillation, a single tone will burn a Lorentzian shaped hole into the center of the Doppler broadened gain curve. The width of this hole is inversely proportional to the decay time of the stimulated atoms. Since this width for He-Ne gas lasers is typically eight times broader than the mode-width of the passive cavity and up to 10^6 times broader than the laser linewidth we will assume that the frequency variations of P and β are negligible around the resonance. Thus as the α approaches the oscillation value the spectrum of the output signal will be controlled by a gain narrowed version of Eq. (5-9).

As the gain curve saturates, the right half-plane poles of Eq. (5-9) will migrate to the $i\omega$ axis. We select the value of α which is an amount ε from the saturated pole so that Eq. (5-10) becomes

$$P_1 = \frac{4e^{-2\varepsilon h_o}}{(1 - e^{-2\varepsilon h_o})^2} \tag{5-11}$$

Then from Eq. (5-9) and Eq. (5-11) we may write the spectrum of the laser signal dropping $\phi(\beta)$ as

$$E(\omega) = \frac{t_1 t_2}{2\sqrt{r_{12} r_{21}}} \sqrt{P_1} \frac{1}{\sqrt{1 + P_1 \sin^2 \beta h_o}} \tag{5-12}$$

In the literature related prior studies of the laser lineshape include lumped element LGC circuit models[1,2]. Freed and Haus[3] used the results to the solution of the nonlinear Van der Pol oscillator equation to describe the spectrum of the laser output. The basic result of using a lumped circuit model, even with complicated nonlinear conductances[4], is that the lineshape function is Lorentzian. An interesting point is that if one started with the transmission function for a cavity or a transmission line, the lineshape would be controlled by equations similar to Eq. (5-9). It is our contention that the passive cavity transmission function will control the lineshape of the laser output if the gain α and the dispersion β are independent of frequency around a resonant peak.

Both the lumped circuit and passive cavity approaches to the laser spectrum assume that the random cavity mirror vibrations and effective cavity length fluctuations are negligible. If one dropped these assumptions the lineshape could be considered Gaussian or some other lineshape function.

With the characterization as in Eq. (5-12) we may now compare the passive cavity to the matched-filter.

5.4 Matched-Filter vs. Passive Cavity

To see the signal-to-noise improvement of the passive cavity in comparison with the signal-to-noise improvement of a matched-filter for mode-locked laser signals with finite linewidth, the following analysis is presented. Given Eq. (5-12) as the spectrum of a mode-locked laser with finite linewidth $\Delta\omega_\ell$, the signal portion of the output of a passive cavity with mode-width $\Delta\omega_p$ is given by the inverse Fourier transform of the product of Eq. (5-12) and Eq. (3-16) dropping the phase term $\phi(\beta)$ as

$$\tau \circledast E_1 = \frac{K}{2\pi} \frac{t_1 t_2}{2\sqrt{r_{12} r_{21}}} \sqrt{P_1} \int_{-\infty}^{\infty} \frac{e^{i\omega t}\, d\omega}{\sqrt{1 + P_1 \sin^2 \omega \frac{h_o}{c}} \sqrt{1 + P_2 \sin^2 \omega \frac{h_o}{c}}} \tag{5-13}$$

Since the signal has only m modes we may write

$$\tau \circledast E_1 = \frac{K}{2\pi} \frac{t_1 t_2}{2\sqrt{r_{12} r_{21}}} \sqrt{P_1} \; m \int_{\omega_o - \frac{\pi c}{2h_o}}^{\omega_o + \frac{\pi c}{2h_o}} \frac{e^{i\omega t}\, d\omega}{\sqrt{(1 + P_1 \sin^2 \omega \frac{h_o}{c})(1 + P_2 \sin^2 \omega \frac{h_o}{c})}} \tag{5-14}$$

With the substitutions $\omega = \omega_o - \frac{c}{h_o} x$, $t = \frac{h_o}{c}$, $\omega_o = \frac{n\pi c}{h_o}$, where n is some large integer, and $e^{-ix} = \cos x - i \sin x$ and noting the sine integral vanishes over symmetric limits, we write

$$\tau \otimes E_1 = \frac{m}{2\pi} K \frac{t_1 t_2}{2\sqrt{r_{12} r_{21}}} \frac{2}{\sqrt{P_2}} \frac{c}{h_o} \int_0^{\pi/2} \frac{\cos x \, dx}{\sqrt{\frac{1}{P_1} + \sin^2 x} \sqrt{\frac{1}{P_2} + \sin^2 x}} \tag{5-15}$$

Consider $F(\phi,k)$ [5], the elliptic integral of the first kind, since

$$\int_0^x \frac{du}{\sqrt{a^2 + u^2} \sqrt{b^2 + u^2}} = \frac{1}{a} F(\phi,k) \quad (a > b > 0) \tag{5-16}$$

where

$$F(\phi,k) = \int_0^{\phi} \frac{d\delta}{\sqrt{1 - k^2 \sin^2 \delta}} \tag{5-17}$$

$$\phi = \tan^{-1}\left(\frac{x}{b}\right) \tag{5-18}$$

and

$$k = \frac{\sqrt{a^2 - b^2}}{a} \qquad (k^2 < 1) \tag{5-19}$$

Then for $a^2 = \frac{1}{P_2}$, $b^2 = \frac{1}{P_1}$, $\frac{1}{P_2} > \frac{1}{P_1} > 0$, $u = \sin x$

$$\phi = \tan^{-1}(\sqrt{P_1}) \quad , \quad k = \frac{\sqrt{\frac{1}{P_2} - \frac{1}{P_1}}}{\sqrt{1/P_2}}$$

Eq. (5-15) becomes

$$\tau \otimes E_1 = \frac{m}{2\pi} K \frac{t_1 t_2}{2\sqrt{r_{12} r_{21}}} \frac{2c}{h_o} F(\phi,k) \tag{5-20}$$

Then from Eq. (5-7) the peak signal-to-noise ratio for the passive

cavity taking the modulus-squared value of Eq. (5-20) is

$$SNR_p = \frac{4\,\frac{m}{2\pi}\left(\frac{t_1 t_2}{2\sqrt{r_{12}r_{21}}}\right)^2 \frac{c}{h_o}\sqrt{1+P_2}\,F^2(\phi,k)}{\pi N_o} \tag{5-21}$$

In a similar fashion we may write the signal portion of the output to the matched-filter for Eq. (5-12) integrating over the same limits as in Eq. (5-14) as

$$(E_1 \otimes E_1^*) = \left(\frac{t_1 t_2}{2\sqrt{r_{12}r_{21}}}\right)^2 \frac{m}{2\pi} P_1 \int_{\omega_o - \frac{\pi c}{2h_o}}^{\omega_o + \frac{\pi c}{2h_o}} \frac{e^{i\omega t}\,d\omega}{1+P_1 \sin^2 \omega \frac{h_o}{c}} \tag{5-22}$$

Again with the substitutions $\omega = \omega_o - \frac{c}{h_o}x$, $t = \frac{h_o}{c}$, $\omega_o = \frac{n\pi c}{h_o}$, and $e^{-ix} = \cos x - i \sin x$ we have

$$E_1 \otimes E_1^* = 2\left(\frac{t_1 t_2}{2\sqrt{r_{12}r_{21}}}\right)^2 \frac{m}{2\pi} P_1 \frac{c}{h_o} \int_0^{\pi/2} \frac{\cos x\,dx}{1+P_1 \sin^2 x} \tag{5-23}$$

Noting that with one trigonometric substitution

$$\int_0^y \frac{du}{cu^2+1} = \frac{1}{\sqrt{c}} \tan^{-1}(y\sqrt{c}), \qquad (c > 0) \tag{5-24}$$

we may write Eq. (5-23) for $c = P_1$ and $u = \sin x$ from Eq. (5-24) as

$$E_1 \otimes E_1^* = 2\left(\frac{t_1 t_2}{2\sqrt{r_{12}r_{21}}}\right)^2 \frac{m}{2\pi} \sqrt{P_1}\ \frac{c}{h_o} \tan^{-1}(\sqrt{P_1}) \tag{5-25}$$

Now in a similar fashion to Eq. (5-7) the mean-squared value of the additive noise at the output of a matched-filter for Eq. (5-12) is

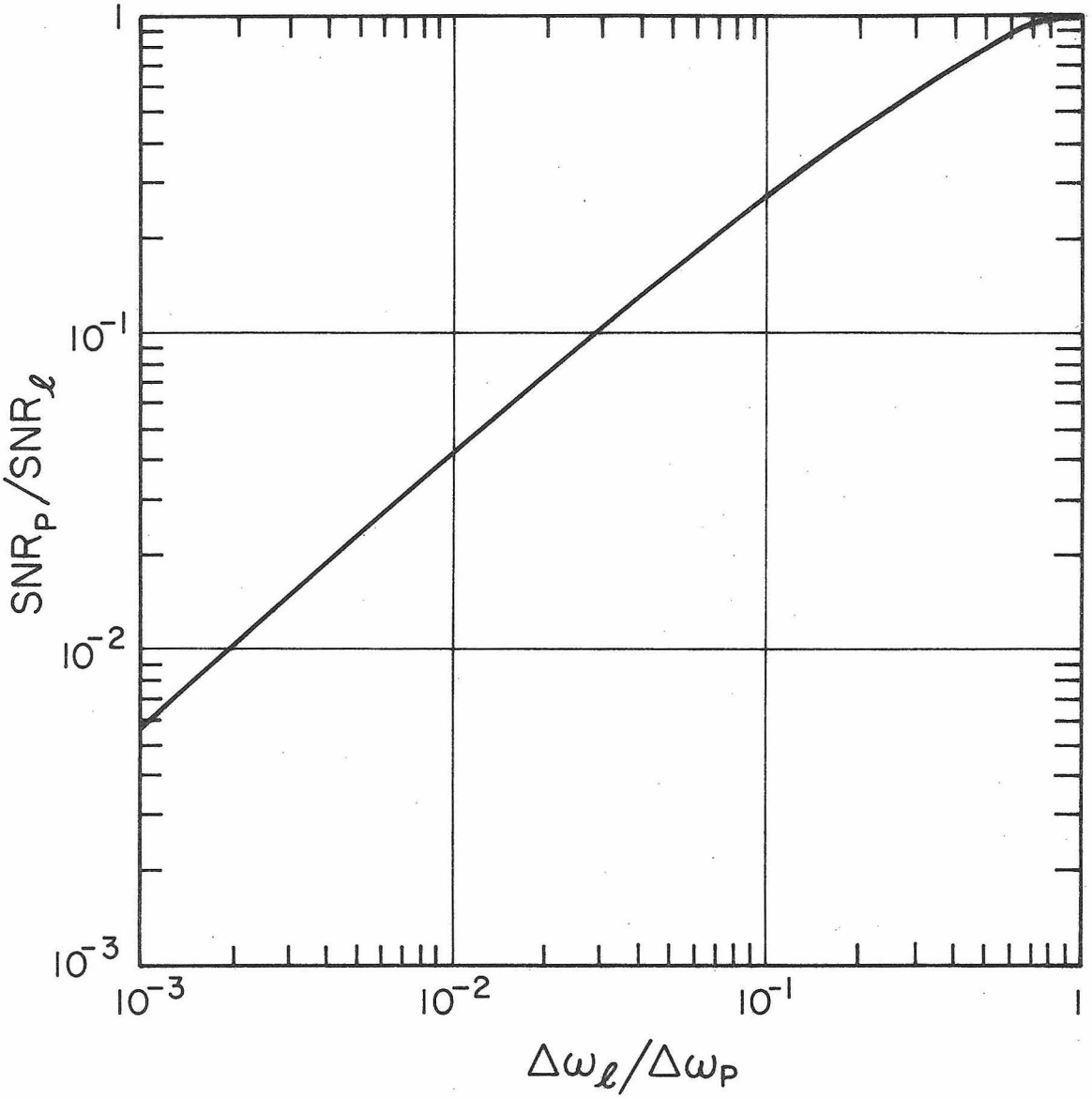
1
10^{-1}
10^{-2}
10^{-3}
SNR_p/SNR_ℓ
10^{-3}
10^{-2}
10^{-1}
1
$\Delta\omega_\ell/\Delta\omega_p$

Fig. [5-10]

$$\langle |n \otimes E_1|^2 \rangle = \left(\frac{t_1 t_2}{2\sqrt{r_{12} r_{21}}}\right)^2 P_1 N_o \frac{m}{2\pi} \frac{c}{h_o} \frac{\pi}{\sqrt{1+P_1}} \tag{5-26}$$

Taking the ratio of the modulus-squared value of Eq. (5-25) to Eq. (5-26) the peak signal-to-noise improvement of the matched-filter is

$$SNR_\ell = \frac{4 \frac{m}{2\pi} \left(\frac{t_1 t_2}{2\sqrt{r_{12} r_{21}}}\right)^2 \frac{c}{h_o} \left(\tan^{-1}(\sqrt{P_1})\right)^2 \sqrt{1+P_1}}{\pi N_o} \tag{5-27}$$

Thus taking the ratio of Eq. (5-21) to (5-27), the departure of the passive cavity to the matched-filter is

$$\frac{SNR_p}{SNR_\ell} = \frac{\sqrt{1+P_2}}{\sqrt{1+P_1}} \frac{F^2(\phi,k)}{[\tan^{-1}(\sqrt{P_1})]^2} \tag{5-28}$$

Now since $P_1 >> 1$, $\phi = \pi/2$ and since from Eq. (4-7) $\Delta\omega_p = 2c/(h_o\sqrt{P_2})$, $\Delta\omega_\ell = 2c/(h_o\sqrt{P_1})$ we may write Eq. (5-28) as

$$\frac{SNR_p}{SNR_\ell} = \left(\frac{2}{\pi}\right)^2 \frac{\Delta\omega_\ell}{\Delta\omega_p} F^2\left(\frac{\pi}{2},k\right) \tag{5-29}$$

where Eq. (5-29) is true only for $\Delta\omega_p > \Delta\omega_\ell > 0$. Note that $F^2(\pi/2,k) = (\pi/2)^2$ for $\Delta\omega_\ell = \Delta\omega_p$. Hence the signal-to-noise ratio approaches that of the matched-filter when $\Delta\omega_\ell \tilde{=} \Delta\omega_p$. Equation (5-29) is illustrated in Fig. [5-10].

Similar analyses have been performed for the cases where the mode-locked laser spectra are taken as a Gaussian and Lorentzian. The results of these analyses are similar to Eq. (5-29).

We note that a very good approximation to Eq. (5-12) may be obtained by expanding around the zeroes ω_p of the $\sin^2\omega\frac{h_o}{c}$ for 2N+1 tones so that

$$E(\omega) = \frac{2}{\Delta\omega_\ell} \sum_{p=-N}^{N} \frac{1}{\sqrt{1 + (\frac{2\Delta\omega}{\Delta\omega_\ell})^2}} \tag{5-30}$$

where $\Delta\omega = \omega - \omega_p = \omega - (\omega_o + p\omega_c)$. This approximate characterization is used in Chapter 3 to illustrate the dependency of the matched-filter criterion on the cavity and signal linewidths.

Chapter 5

References

1. A. Blaquiere, "Effect du bruit de fond sur la fréquence des auto-oscillateurs," Ann. Radio Elec. Vol. 8, p. 36-80, January (1953).

2. J. P. Gordon, H. J. Zeiger, C. H. Townes, Phys. Rev. 99, #4, p. 1264 (1955).

3. C. Freed, H. A. Haus, Appl. Phys. Lett. 6, p. 85 (1965).

4. P. Grivet and A. Blaquiere, Symposium on Optical Masers, (Polytechnic Institute of Brooklyn, 1963), p. 69.

5. I. S. Gradshteyn, I. M. Ryzhik, Table of Integrals Series and Products, (Academic Press, 1965), p. 245.

Chapter 6

Rise-Time of a Passive Cavity

6.1 Introduction

In this chapter the Laplace transform representation of the passive Fabry-Perot resonant cavity which was developed in Chapter 2 is used to analyze the rise-time of the passive cavity. Two methods are used to obtain a rise-time-bandwidth product. The first method is developed by expanding the amplitude transmission function in powers of the exponential. This is analogous to the standard multiple bounce approach. The second method involves an infinite partial fraction expansion in the poles of the amplitude transmission function. This leads to an approximated output which depends on the reflectivity of the passive cavity end mirrors.

6.2 Laplace Transform Representation: Multiple Bounce

In the consideration of the rise-time, τ , of a passive Fabry-Perot resonant cavity, we start with the Laplace transform representation of the amplitude transmission function for the cavity; assuming that $\beta^2 = -s^2\mu_o\varepsilon_o$ and $\beta_o = \beta - i\alpha$ we have from Eq. (2-31) that

$$\underline{T}(s) = \frac{T_\alpha e^{-as}}{1 - R_\alpha e^{-2as}} \tag{6-1}$$

where

$$T_\alpha = t_1 t_2 e^{-\alpha h_o} \quad , \quad R_\alpha = r_{12} r_{21} e^{-2\alpha h_o}$$

and $a = h_o/c$. If we assume an input signal $E_1(t)$ into our

linear system, whose Laplace transform of the impulse response function is $\underline{T}(s)$, such that the Laplace transform given by Eq. (2-6.1) of $E_1(t)$ is $L[E_1(t)] = \underline{E}(s)$, then the output $g(t)$ with Laplace transform $L[g(t)] = \underline{G}(s)$ is given by

$$\underline{G}(s) = \underline{T}(s)\ \underline{E}(s) \tag{6-2}$$

Before we continue we need to recall one general relationship of inverse Laplace transforms. Given a function $f(t)$ with $L[f(t)] = \underline{F}(s)$, the inverse Laplace transform of $\underline{F}(s)e^{-as}$ where a is any non-negative real number is given by

$$L^{-1}[\underline{F}(s)e^{-as}] = f(t-a)\ u(t-a) \tag{6-3}$$

where $\begin{cases} u(x) = 0 & x < 0 \\ u(x) = 1 & x > 0 \end{cases}$

Thus since Eq. (6-1) may be written

$$\underline{T}(s) = T_\alpha \sum_{n=0}^{\infty} R_\alpha^n\, e^{-(2n+1)as} \tag{6-4}$$

then the inverse Laplace transform of Eq. (6-2) using Eq. (6-3) becomes

$$g(t) = T_\alpha \sum_{n=0}^{\infty} R_\alpha^n\, E_1(t-(2n+1)a)\ u(t-(2n+1)a) \tag{6-5}$$

Rather than considering an arbitrary input we will consider the idealized mode-locked laser signal. Thus taking the real part of Eq. (B-1) we have

$$E_1(t) = \sum_{p=-N}^{N} \cos(\omega_o + p\omega_c)t = \cos\ \omega_o t\ \frac{\sin(2N+1)\frac{\omega_c}{2}t}{\sin\ \frac{\omega_c}{2}\ t} \tag{6-6}$$

where the Laplace transform is given by

$$L[E_1(t)] = \underline{E}(s) = \sum_{p=-N}^{N} \frac{s}{s^2 + (\omega_o + p\omega_c)^2} \tag{6-7}$$

We note that from Eq. (6-6)

$$\begin{aligned} E_1(t-(2n+1)a) &= \text{Real}\left[\sum_{p=-N}^{N} \exp(i(\omega_o+p\omega_c)(t-(2n+1)a))\right] \\ &= \text{Real}\left[\sum_{p=-N}^{N} \exp(i(\omega_o+p\omega_c)(t-a))\right] \\ &= E_1(t-a) \end{aligned} \tag{6-8}$$

since $\omega_o = m\pi/a$, $\omega_c = \pi/a$, $a = h_o/c$, where for optical frequencies, m is an integer on the order of 10^6, i.e., $(\omega_o + p\omega_c)2na = 2n\pi(m+p)$. Thus Eq. (6-5) using Eq. (6-8) becomes

$$g(t) = T_\alpha\, E_1(t-a) \sum_{n=0}^{\infty} R_\alpha^n\, u(t-(2n+1)a) \tag{6-9}$$

Now since

$$\sum_{n=0}^{M} R_\alpha^n = \frac{1 - R_\alpha^{M+1}}{1 - R_\alpha} \tag{6-10}$$

and since the maximum output of the system is $T_\alpha E_1(t-a) / (1-R_\alpha)$, which is obtained for $M \to \infty$, then the fraction of the final output which is obtained after M bounces is given by

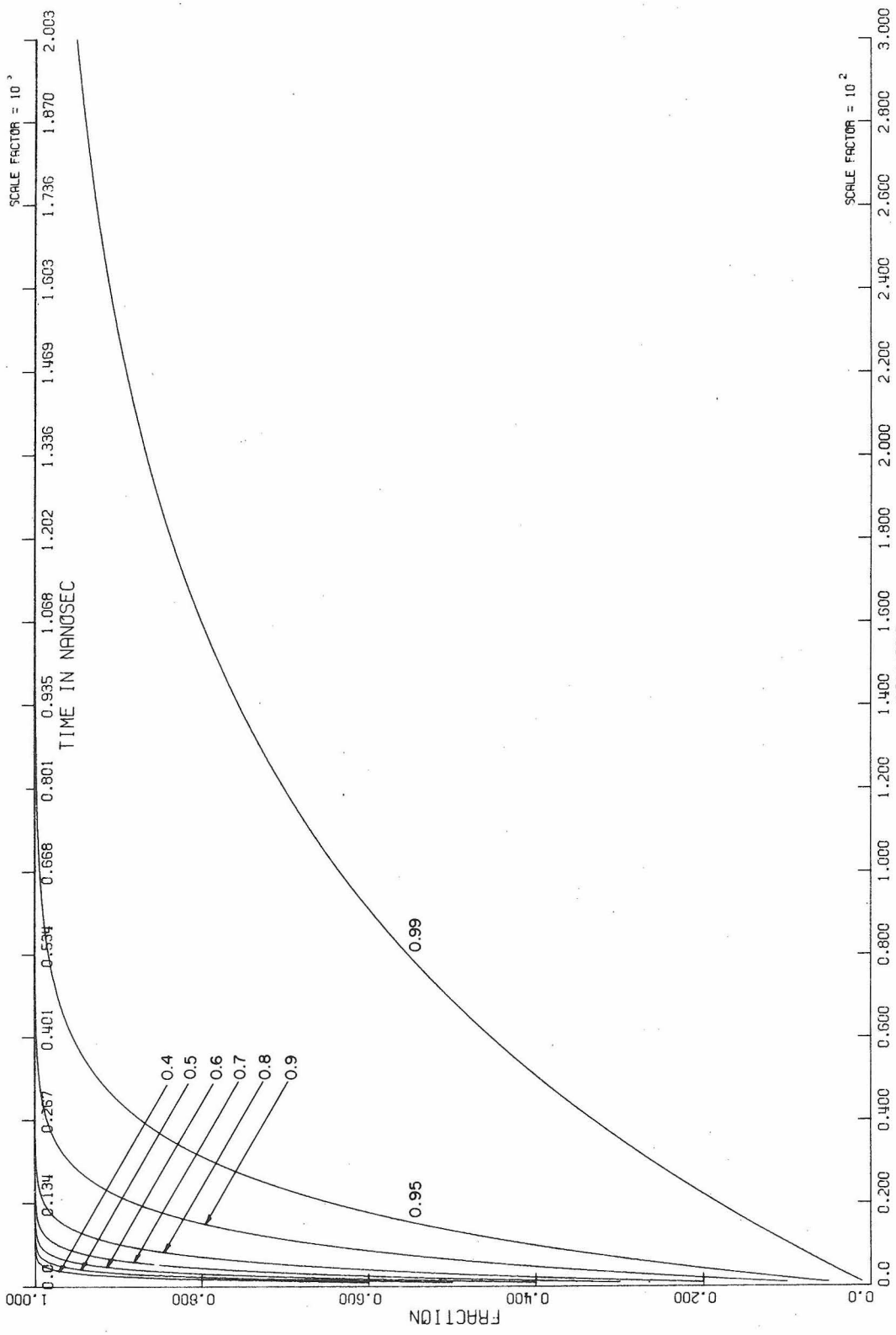
SCALE FACTOR = 10 ³
0.134
0.267
0.401
0.534
0.668
0.801
0.935
1.068
1.202
1.336
1.469
1.603
1.736
1.870
2.003
TIME IN NANOSEC
0.4
0.5
0.6
0.7
0.8
0.9
0.95
0.99
1.000
0.800
0.600
0.400
0.200
0.0
FRACTION
SCALE FACTOR = 10 ²
0.0
0.200
0.400
0.600
0.800
1.000
1.200
1.400
1.600
1.800
2.000
2.200
2.400
2.600
2.800
3.000
BOUNCES

Fig. [6-1]

$$\bar{P}_1 = 1 - R_\alpha^{M+1} \tag{6-11}$$

The time it takes to the M^{th} bounce is $\tau = (2M+1)h_o/c$ which indicates that $M = c\tau/2h_o - 1/2$ so Eq. (6-11) may be written

$$\bar{P}_1 = 1 - R_\alpha^{(\frac{c\tau}{2h_o} - \frac{1}{2})} \tag{6-12}$$

We note that in the plot of Eqs. (6-11) and (6-12) shown in Fig. [6-1] the rise-time and number of bounces increase as $R_\alpha \to 1$. This indicates the longer time for energy build up in the cavity due to the decreasing fraction of input energy allowed to interact at each bounce.

Solving Eq. (6-12) for the time to reach a particular fraction of the input gives

$$\tau = \left(\frac{\ell n(1-\bar{P})}{\ell n\ R_\alpha} + \frac{1}{2}\right) \frac{2h_o}{c} \tag{6-13}$$

Before we go further let us consider the partial fraction expansion approach to the rise-time analysis.

6.3 The Direct Laplace Transform Method

In this direct method we start with Eq. (6-1) and we suppress the e^{-as} in the numerator. Equation (6-3) will allow us to introduce this term later as a time shift. Thus we write $\underline{T}(s) = e^{-as}\ \underline{T}'(s)$ so

$$\underline{T}'(s) = \frac{T_\alpha}{1 - R_\alpha\ e^{-2as}} \tag{6-14}$$

If we take a partial fraction expansion of the poles of Eq. (6-14)

grouping the complex conjugate poles we may write

$$\underline{T}'(s) = \sum_{m=0}^{\infty} \left(\frac{b_m}{s - s_m} + \frac{b_{-m}}{s - s_m^*} \right) \tag{6-15}$$

where the asterisk indicates complex conjugate. Since the complex conjugate poles lead to real-valued functions we see that $b_m = b_{-m}^*$.

Since all the poles of Eq. (6-14) are of first order, we may determine the residue of the m^{th} pole by

$$b_m = \frac{T_\alpha}{\frac{d}{ds}\left(1 - R_\alpha e^{-2as}\right)_{s=s_m}} \tag{6-16}$$

And if we assume that the real and imaginary part of each pole is given by $s_m = \sigma_m + i\omega_m$ then Eq. (6-16) becomes

$$b_m = \frac{T_\alpha}{2aR_\alpha} e^{2a\sigma_m} (\cos 2a\omega_m + i \sin 2a\omega_m) \tag{6-17}$$

To determine the poles of the amplitude transmission function in Eq. (6-14) we set the denominator to zero so that

$$R_\alpha e^{-2as_m} = e^{\pm i2\pi m} \tag{6-18}$$

or

$$s_m = \frac{1}{2a} \ln R_\alpha \pm i\, 2\pi m/2a$$

Thus we have

$$\sigma = \sigma_m = \frac{1}{2a} \ln R_\alpha \tag{6-19.1}$$

$$\omega_m = 2\pi m/2a = m\pi \frac{c}{h_o} \tag{6-19.2}$$

Putting Eqs. (6-19.1) and (6-19.2) into Eq. (6-17) and into Eq. (6-15), Eq. (6-15) becomes

$$\underline{T}'(s) = \frac{T\alpha}{2a} \sum_{m=0}^{\infty} \left(\frac{1}{s - \sigma - i\omega_m} + \frac{1}{s - \sigma + i\omega_m} \right) \tag{6-20}$$

or

$$\underline{T}'(s) = \frac{T\alpha}{a} \sum_{m=0}^{\infty} \left(\frac{s - \sigma}{(s-\sigma)^2 + \omega_m^2} \right) \tag{6-21}$$

Thus Eq. (6-2) becomes

$$\underline{G}(s) = e^{-as}\, \underline{G}'(s) = e^{-as}\, \underline{E}(s)\, \underline{T}'(s) \tag{6-22}$$

So using Eq. (6-7) and Eq. (6-21), Eq. (6-22) becomes

$$\underline{G}(s) = \frac{T\alpha}{a} e^{-as} \sum_{p=-N}^{N} \left(\frac{s}{s^2 + \omega_p^2} \right) \sum_{m=0}^{\infty} \left(\frac{s-\sigma}{(s-\sigma)^2 + \omega_m^2} \right) \tag{6-23}$$

The inverse Laplace transform of a general term of $\underline{G}'(s)$ may be found on page 345 of Gardner and Barnes[1] as

$$L^{-1}\left[\frac{s}{s^2 + \omega_p^2} \cdot \frac{s-\sigma}{(s-\sigma)^2 + \omega_m^2} \right] =$$

$$\left[\frac{1 + \sigma^2}{(\sigma^2 + \omega_m^2 - \omega_p^2)^2 + 4\sigma^2\omega_p^2} \right]^{1/2} \left[\omega_p \sin(\omega_p t + \psi_1) + \omega_m e^{\sigma t} \sin(\omega_m t + \psi_2) \right] \tag{6-24}$$

where

$$\psi_1 \equiv \tan^{-1} \frac{\sigma}{\omega_p} + \tan^{-1} \left(\frac{2\sigma\omega_p}{\sigma^2 + \omega_m^2 - \omega_p^2} \right) \tag{6-25.1}$$

$$\psi_2 \equiv -\tan^{-1}\frac{\sigma}{\omega_p} - \tan^{-1}\left(\frac{2\sigma\omega_p}{\sigma^2 - \omega_p^2 + \omega_m^2}\right) \qquad (6\text{-}25.2)$$

We will now consider two cases: $\omega_p = \omega_m$ and $\omega_p \neq \omega_m$.

For $\omega_p = \omega_m >> \sigma$ and $\sigma >> 1$ since $\omega_p = p\pi/a$, $\omega_m = m\pi/a$, $\sigma = \frac{1}{2a}\ln R_\alpha$ where p and m are on the order of 10^6 and $a = h_o/c = 3.3$ nsec, the inverse Laplace transform of $\underline{G}(s)$ reduces to

$$g(t) = \frac{T_\alpha}{a}(1 - e^{\sigma(t-a)})\, u(t-a) \sum_{p=-N}^{N} \cos\, \omega_p(t-a) \qquad (6\text{-}26)$$

Thus the fraction of the final output reached after t seconds is

$$\overline{P}_2 = (1 - e^{\sigma(t-a)}) \qquad (6\text{-}27)$$

From Eq. (6-19.1) we may write putting in for σ

$$\overline{P}_2 = (1 - e^{\frac{1}{2a}\ln R_\alpha (t-a)}) = (1 - R_\alpha^{(\frac{t-a}{2a})}) \qquad (6\text{-}28)$$

We see that Eq. (6-28) and Eq. (6-12) are identical, since $a = h_o/c$.

For $\omega_p \neq \omega_m$, $\omega_p >> \sigma$, $\omega_m >> \sigma$ and in the case that ω_p and ω_m differ by one free spectral range, i.e., $\omega_m - \omega_p = \pi/a$, the coefficient multiplying the sine terms of Eq. (6-24) is on the order of $\ln R_\alpha$. Thus for $R_\alpha \simeq 1$, $\ln R_\alpha$ is very small and may be neglected in comparison to the terms in Eq. (6-26). As R_α becomes smaller the poles migrate into the left-half space and then we cannot neglect the response due to the neighboring poles. To see how good the approximation for the Laplace transform is, we tabulated the magnitude and phase

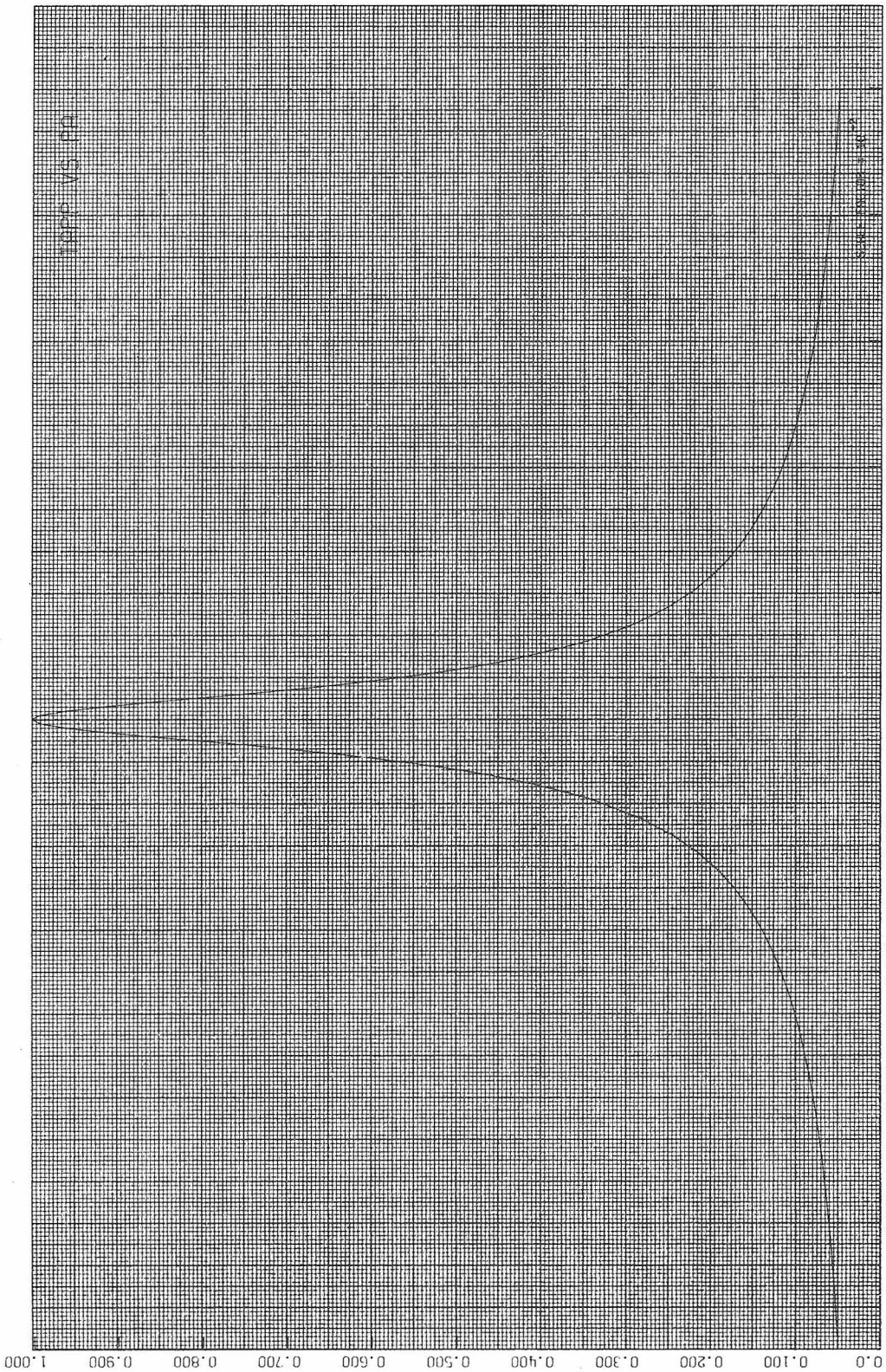
Ripple vs PA
8.000
6.000
4.000
2.000
-0.000
-2.000
-4.000
-6.000
-8.000
PA
0.0
0.100
0.200
0.300
0.400
0.500
0.600
0.700
0.800
0.900
1.000

Fig. [6-2]

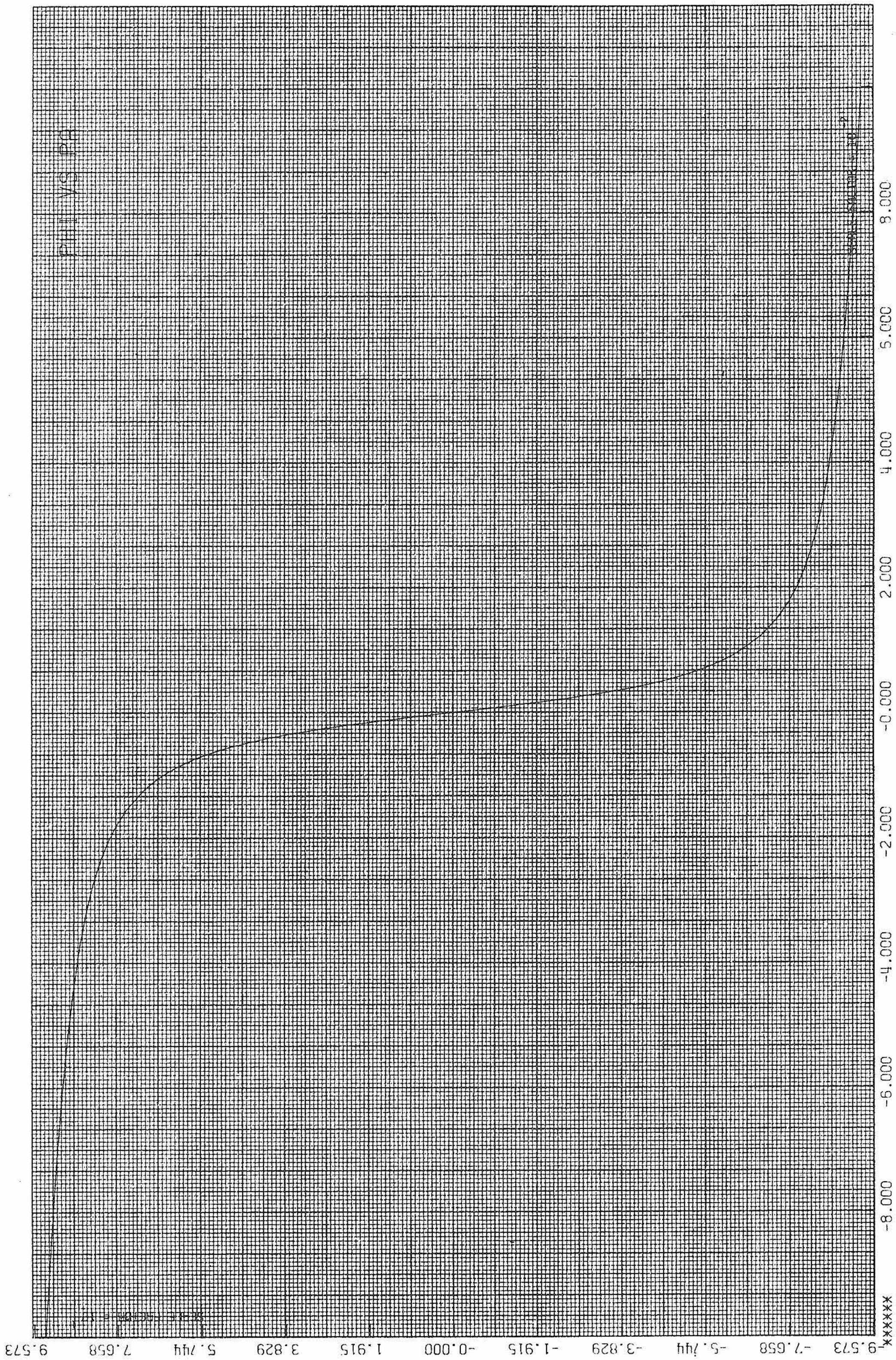
PHI VS PA
PA
-8.000
-6.000
-4.000
-2.000
-0.000
2.000
4.000
6.000
8.000
9.573
7.658
5.744
3.829
1.915
-0.000
-1.915
-3.829
-5.744
-7.658
-9.573

Fig. [6-3]

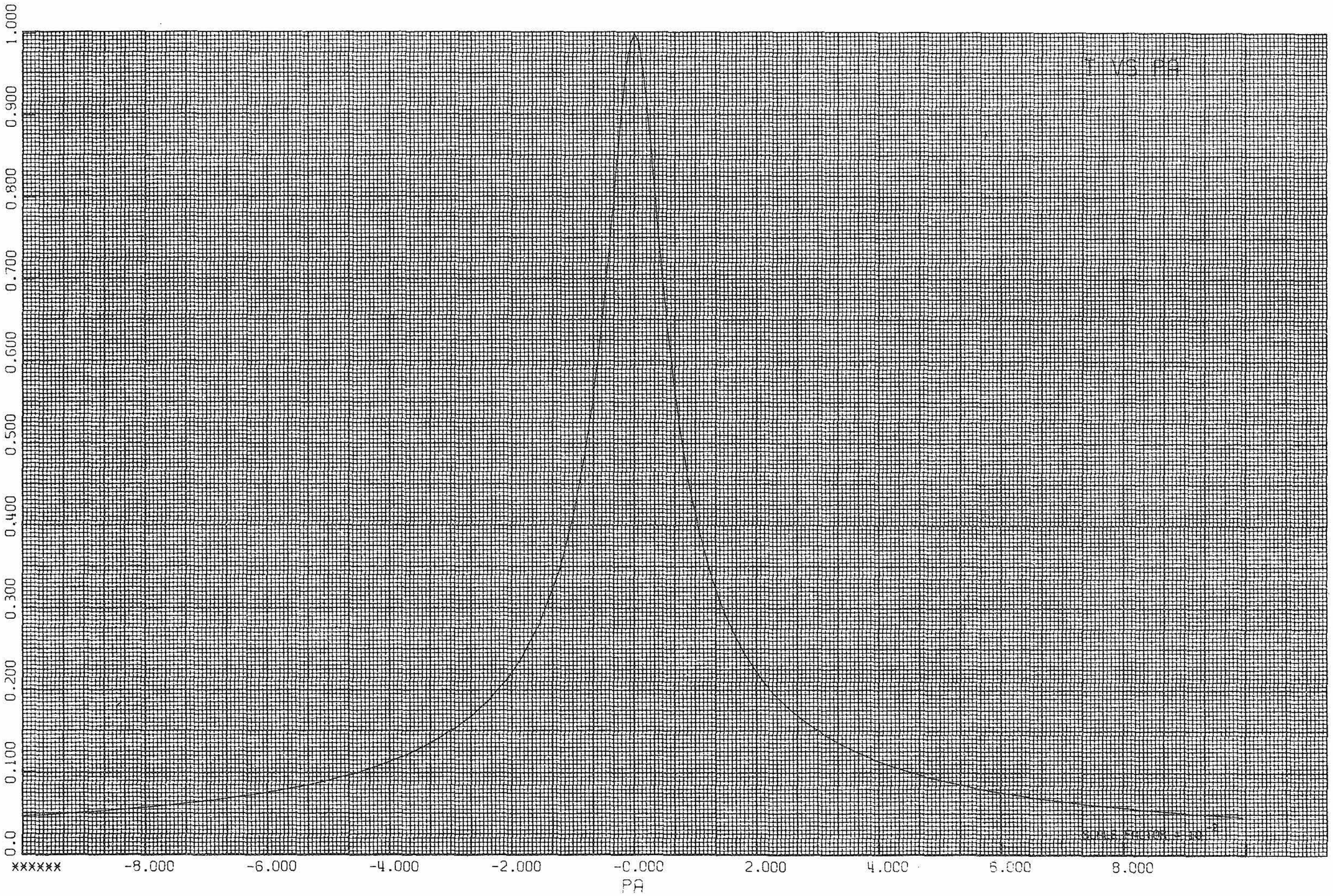
T VS PA
1.000
0.900
0.800
0.700
0.600
0.500
0.400
0.300
0.200
0.100
0.0
xxxxxx
-8.000
-6.000
-4.000
-2.000
-0.000
2.000
4.000
8.000
PA

Fig. [6-4]

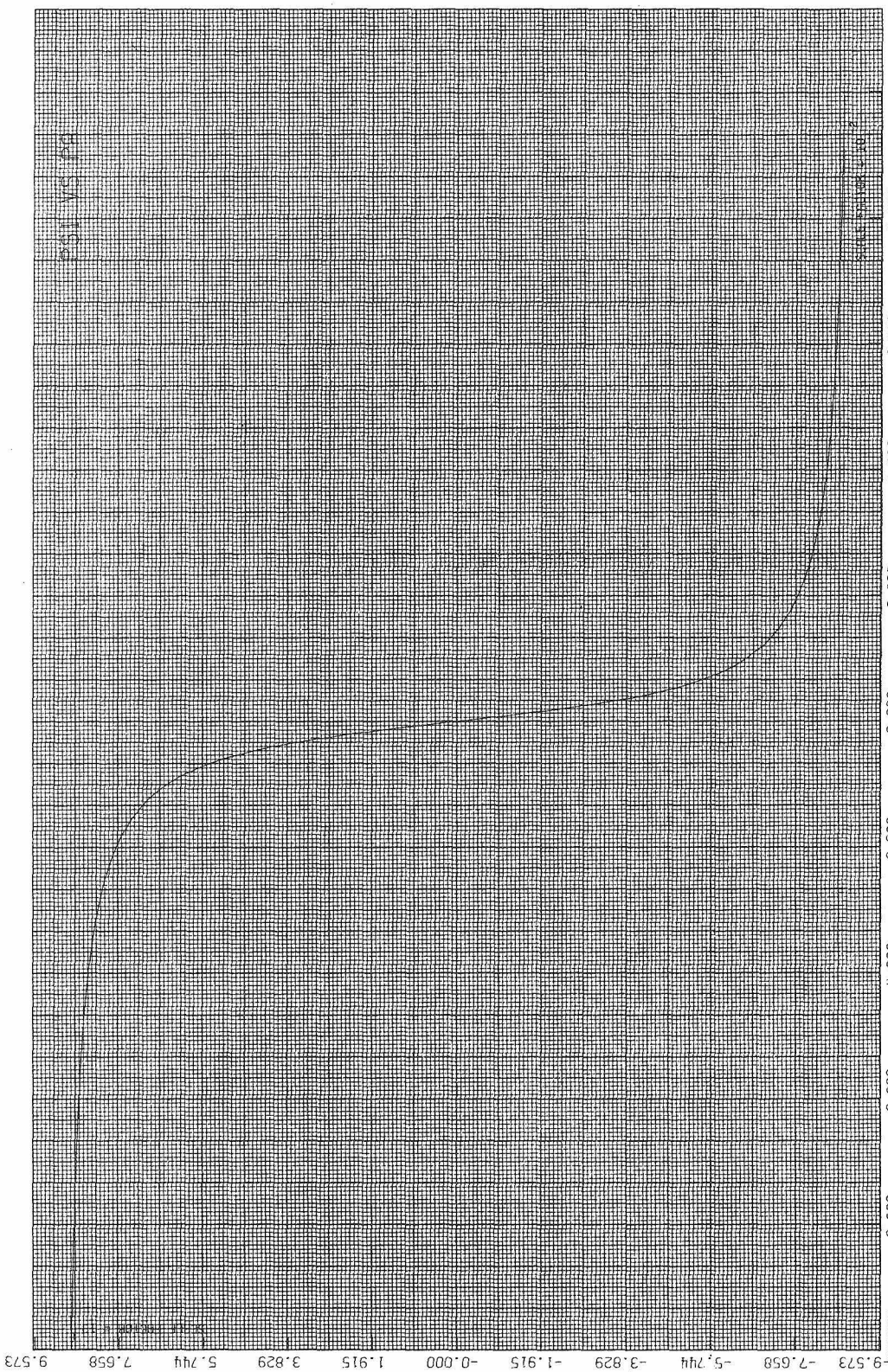
Psi VS Cp
PA
8.000
5.000
4.000
2.000
-0.000
-2.000
-4.000
-5.000
-8.000
*****
-9.573
-7.658
-5.744
-3.829
-1.915
-0.000
1.915
3.829
5.744
7.658
9.573

Fig. [6-5]

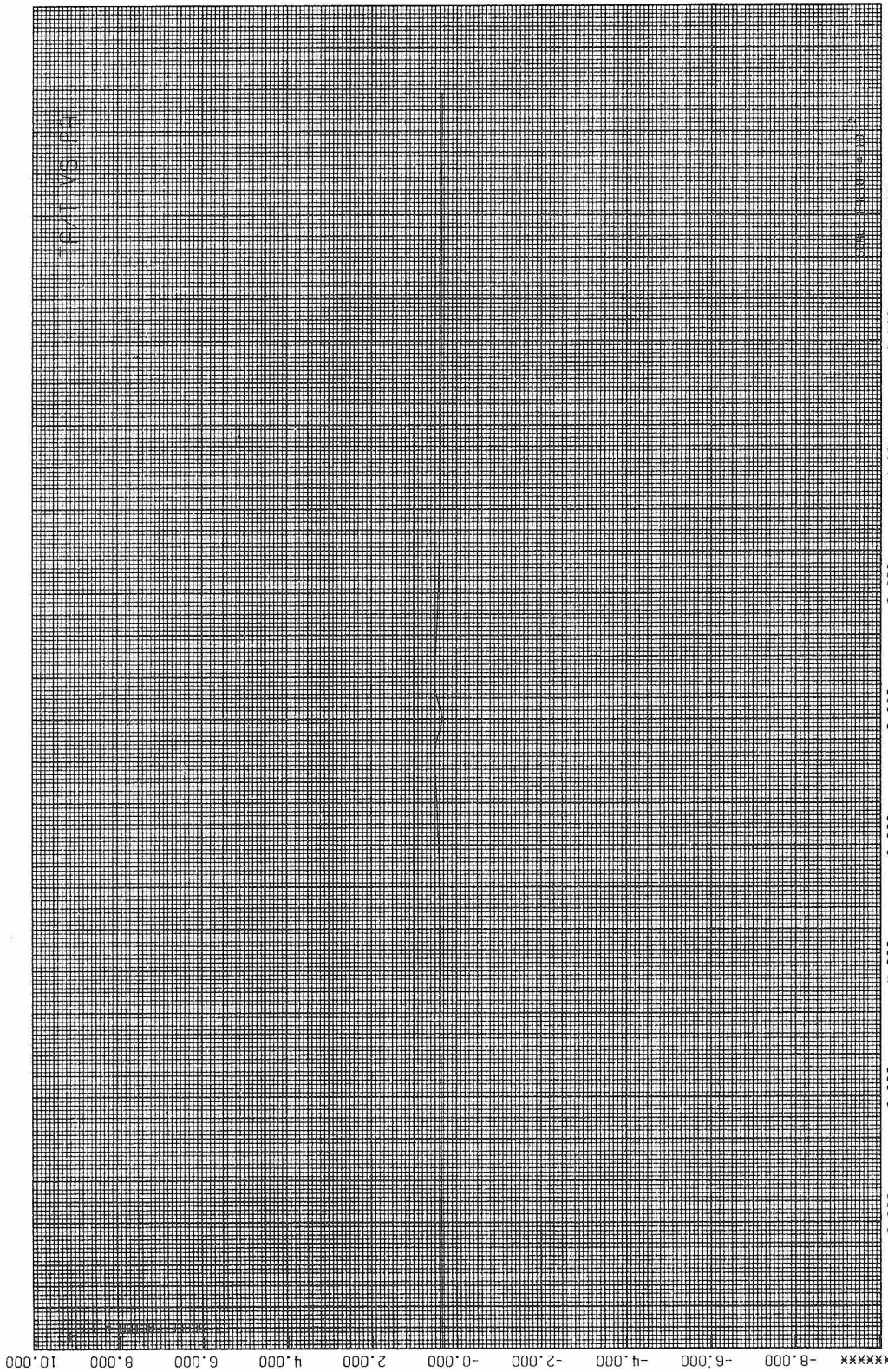

Fig. [6-6]

of Eq. (6-21) for the $2N+1$ modes coincident with the input as a function of the normalized frequency variable PA (PA = 1 $\longrightarrow$ $\omega - \omega_o = 33$ MHz where ω_o is the resonant frequency) and plotted them in Fig. [6-2] and Fig. [6-3] respectively. The magnitude and phase of Eq. (6-1) is also shown in Fig. [6-4] and Fig. [6-5] respectively. The similarity of Fig. [6-2] and Fig. [6-4] may best be shown by the difference of the magnitudes $|T_A| - |T|$ which is shown in Fig. [6-6]. The magnitude of the approximating function deviates from the exact function by less than 0.0005 in magnitude for all frequencies and is independent of the number of modes oscillating. The phase, however, is only a good approximation in a 3 MHz band around the resonant frequency. With Eq. (6-12) and Eq. (6-28) identical we are in a position to determine the rise-time-bandwidth product.

6.4 Rise-Time-Bandwidth Product

Now if the time τ_2 it takes to obtain P_2 of the output is subtracted from the time τ_1 to obtain P_1 of the output, then Eq. (6-13) becomes

$$\tau_c = \tau_2 - \tau_1 = \frac{1}{\nu_c} \frac{\ell n[(1-P_2)/(1-P_1)]}{\ell n\, R_\alpha} \tag{6-29}$$

where $\nu_c = c/2h_o$. We may expand the $\ell n R_\alpha$ for $R_\alpha \simeq 1$ so Eq. (6-29) becomes

$$\tau_c = -\ell n[(1-P_2)/(1-P_1)] \frac{R_\alpha}{\nu_c(1-R_\alpha)} \tag{6-30}$$

But since from Eq. (4-12), noting the change in R notation, $F = \pi\sqrt{R_\alpha}\,/\,(1-R_\alpha)$ and from Eq. (4-7) $\nu_c = F\Delta\nu_c$ with $\Delta\nu_c = c/(2h_oF)$,

we may write Eq. (6-30) as

$$\tau_c \Delta\nu_c = -\ell n[(1-P_2)/(1-P_1)] \frac{\sqrt{R_\alpha}}{\pi} \tag{6-31}$$

The rise-time of a pulsed system may be defined as the time from 10% to 90% of the final output. So for $P_2 = 0.9$ and $P_1 = 0.1$ we have

$$\tau_c \Delta\nu_c = 0.954 \frac{\sqrt{R_\alpha}}{\pi} \tag{6-32}$$

and for $R_\alpha = 0.991$ we obtain

$$\tau_c \Delta\nu_c = 0.304 \tag{6-33}$$

If we wish we may define the time constant as $P_2 = 1 - \frac{1}{e}$ and $P_1 = 0$ so Eq. (6-31) becomes

$$\tau_c \Delta\nu_c = \frac{\sqrt{R_\alpha}}{\pi} \tag{6-34}$$

and again for $R_\alpha = 0.991$ we obtain $\tau_c \Delta\nu_c = 0.3175$.

Chapter 6

References

1. M. F. Gardner, J. L. Barnes, Transients in Linear Systems, Vol. 1, (John Wiley and Sons, 1942),p. 345, Eq. 1.363.

Chapter 7

Doppler Shifts for Mode-Locked Laser Detection

7.1 Introduction

This chapter will deal with the use of the passive Fabry-Perot resonant cavity as a device to measure Doppler shifts of either passive or active vehicles in motion relative to the receiver. First the relativity equations are developed and then applied to the mode-locked laser in motion. We will see that by vernier adjustments of the passive cavity length we can read a large range of approach velocities with a resolution that is independent of velocity v, i.e. $\delta h_o/h_o \approx \delta v/c$ for $v/c \ll 1$. Thus with $\delta h_o/h_o = 3.3 \times 10^{-8}$ we have a resolution of $\delta v = 10 m/s$.

7.2 The Relativity Formulas

Before we discuss the passive cavity as a velocity meter we will consider the transformation equations. Since the wave equation in one dimension for simplicity must be invariant in any coordinate system by Einstein's first postulate, we have the following general equation (Fig. [7-1]).

$$\frac{\partial^2 U}{\partial x_1^2} + \frac{\partial^2 U}{\partial y_1^2} + \frac{\partial^2 U}{\partial z_1^2} - \frac{1}{c^2}\frac{\partial^2 U}{\partial t_1^2} = \frac{\partial^2 U}{\partial x_2^2} + \frac{\partial^2 U}{\partial y_2^2} + \frac{\partial^2 U}{\partial z_2^2} - \frac{1}{c^2}\frac{\partial^2 U}{\partial t_2^2}, \quad (7\text{-}1)$$

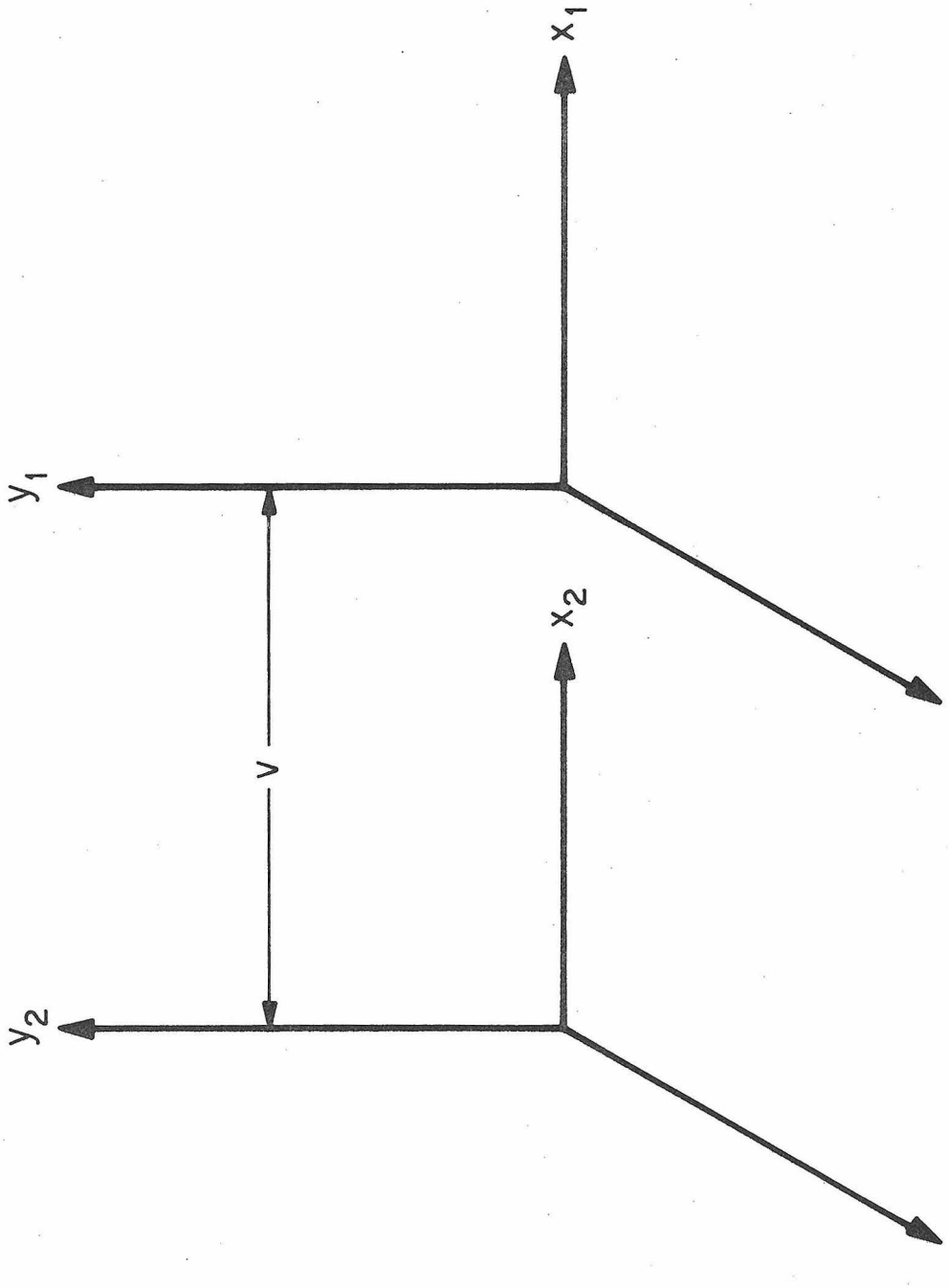

Fig. [7-1]

where c is the speed of light and constant in both systems. Then the transformation equations are

$$x_2 = a_{11}\, x_1 + a_{12}\, t_1 \qquad \frac{\partial x_2}{\partial x_1} = a_{11} \qquad \frac{\partial x_2}{\partial t_1} = a_{12} \tag{7-2a}$$

and

$$t_2 = a_{21}\, x_1 + a_{22}\, t_1 \qquad \frac{\partial t_2}{\partial x_1} = a_{21} \qquad \frac{\partial t_2}{\partial t_1} = a_{22} \tag{7-2b}$$

Then to derive the a coefficients we start with the first partials

$$\frac{\partial U}{\partial x_1} = \frac{\partial U}{\partial x_2}\,\frac{\partial x_2}{\partial x_1} + \frac{\partial U}{\partial t_2}\,\frac{\partial t_2}{\partial x_1}$$

$$\frac{\partial U}{\partial t_1} = \frac{\partial U}{\partial x_2}\,\frac{\partial x_2}{\partial t_1} + \frac{\partial U}{\partial t_2}\,\frac{\partial t_2}{\partial t_1}$$

With these first partial derivatives and Eqs. (7-2a,b) we have

$$\frac{\partial^2 U}{\partial x_1^2} = \frac{\partial}{\partial x_1}\left(a_{11}\,\frac{\partial U}{\partial x_2} + a_{21}\,\frac{\partial U}{\partial t_2}\right) = a_{11}\,\frac{\partial}{\partial x_1}\left(\frac{\partial U}{\partial x_2}\right) + a_{21}\,\frac{\partial}{\partial x_1}\left(\frac{\partial U}{\partial t_2}\right)$$

$$= a_{11}\left(\frac{\partial^2 U}{\partial x_2^2}\,a_{11} + \frac{\partial^2 U}{\partial t_2 \partial x_2}\,a_{21}\right) + a_{21}\left(\frac{\partial^2 U}{\partial x_2 \partial t_2}\,a_{11} + \frac{\partial^2 U}{\partial t_2^2}\,a_{21}\right)$$

$$= a_{11}^2\,\frac{\partial^2 U}{\partial x_2^2} + a_{21}^2\,\frac{\partial^2 U}{\partial t_2^2} + 2a_{11}a_{21}\,\frac{\partial^2 U}{\partial t_2 \partial x_2}$$

In a similar fashion we write

$$\frac{\partial^2 U}{\partial t_1^2} = \frac{\partial}{\partial t_1}\left(a_{12}\frac{\partial U}{\partial x_2} + a_{22}\frac{\partial U}{\partial t_2}\right) = a_{12}\frac{\partial}{\partial t_1}\left(\frac{\partial U}{\partial x_2}\right) + a_{22}\frac{\partial}{\partial t_1}\left(\frac{\partial U}{\partial t_2}\right)$$

$$= a_{12}\left(\frac{\partial^2 U}{\partial x_2^2}a_{12} + \frac{\partial^2 U}{\partial t_2 \partial x_2}a_{22}\right) + a_{22}\left(\frac{\partial^2 U}{\partial t_2 \partial x_2}a_{12} + \frac{\partial^2 U}{\partial t_2^2}a_{22}\right)$$

$$= a_{12}^2\frac{\partial^2 U}{\partial x_2^2} + a_{22}^2\frac{\partial^2 U}{\partial t_2^2} + 2a_{12}a_{22}\frac{\partial^2 U}{\partial t_2 \partial x_2}$$

Thus equating coefficients of Eq. (7-1) we obtain from the above

$$\frac{\partial^2 U}{\partial x_1^2} - \frac{1}{c^2}\frac{\partial^2 U}{\partial t_1^2} = \left(a_{11}^2 - \frac{1}{c^2}a_{12}^2\right)\frac{\partial^2 U}{\partial x_2^2} + \left(a_{21}^2 - \frac{1}{c^2}a_{22}^2\right)\frac{\partial^2 U}{\partial t_2^2}$$

$$+ 2\left(a_{11}a_{21} - \frac{1}{c^2}a_{12}a_{22}\right)\frac{\partial^2 U}{\partial t_2 \partial x_2} = \frac{\partial^2 U}{\partial x_2^2} - \frac{1}{c^2}\frac{\partial^2 U}{\partial t_2^2}$$

Thus the equations relating the coefficients of Eq. (7-2a,b) are

$$a_{11}^2 - \frac{1}{c^2}a_{12}^2 = 1 \tag{7-3}$$

$$a_{21}^2 - \frac{1}{c^2}a_{22}^2 = -\frac{1}{c^2} \tag{7-4}$$

$$a_{11}a_{21} - \frac{1}{c^2}a_{12}a_{22} = 0 \tag{7-5}$$

Now if we include the condition that $x_2 = 0 \rightarrow x_1 = - vt_1$ so from Eq. (7-2a)

$0 = a_{11}(- vt_1) + a_{12}t_1$ or $a_{12} = + a_{11}v$ so from Eq. (7-3)

$$a_{11}^2\left(1 - \frac{v^2}{c^2}\right) = 1$$

$$a_{11} = \frac{1}{\sqrt{1 - \frac{v^2}{c^2}}}$$

so

$$a_{12} = + \frac{v}{\sqrt{1 - \frac{v^2}{c^2}}}$$

Eq. (7-5) indicates that

$$a_{21} = + \frac{v}{c^2} a_{22}$$

or

$$\frac{v^2}{c^4} a_{22}^2 - \frac{1}{c^2} a_{22}^2 = - \frac{1}{c^2}$$

thus

$$a_{22} = \frac{1}{\sqrt{1 - \frac{v^2}{c^2}}}$$

and

$$a_{21} = + \frac{v}{c^2} \frac{1}{\sqrt{1 - \frac{v^2}{c^2}}}$$

Thus Eqs. (7-2) become

$$x_2 = \gamma(x_1 + vt_1)$$

$$t_2 = \gamma(t_1 + \frac{v}{c^2} x_1) \quad , \qquad \gamma = \frac{1}{\sqrt{1 - \frac{v^2}{c^2}}} \qquad (7\text{-}6)$$

$$y_2 = y_1$$

$$z_2 = z_1$$

7.3 The Doppler for Mode-Locked Lasers

Now if we assume we have a plane electromagnetic wave whose space-time dependence may be given by $\exp j(k_2 x_2 + \omega_2 t_2)$ which is a wave traveling in the minus x_2 direction, then from Eq. (7-6) an observer in the sub_1 coordinate system will see

$$\exp j(k_2\gamma(x_1 + vt_1) + \omega_2\gamma(t_1 + \frac{v}{c^2} x_1))$$

$$= \exp j(\gamma(k_2 + \frac{v}{c^2} \omega_2)x_1 + \gamma(k_2 v + \omega_2)t_1)$$

Thus $\exp j(k_1 x_1 + \omega_1 t_1)$

where

$$k_1 = \gamma k_2 (1 + \frac{v}{c^2} \frac{\omega_2}{k_2}) = \gamma k_2 (1 + \frac{v}{c})$$

and

$$\omega_1 = \gamma \omega_2 (1 + \frac{v}{\omega_2} k_2) = \gamma \omega_2 (1 + \frac{v}{c})$$

Thus since $\omega_2 = 2\pi f_2$

$$f_1 = f_2 \frac{(1 + \frac{v}{c})}{\sqrt{1 - \frac{v^2}{c^2}}} = \frac{\sqrt{1 + \frac{v}{c}}}{\sqrt{1 - \frac{v}{c}}} \cong f_2 (1 + \frac{v}{c} - \frac{1}{2} \frac{v^2}{c^2} + \ldots)$$

So if we started with a representation for the mode-locked laser pulses in the x_2 coordinate system (suppressing space dependence) we have from Eq. (B-1)

$$E(t_2) = \sum_{p=-N}^{N} e^{j(\omega_{2o} + p\omega_{2c} t_2)} = e^{j\omega_{2o} t_2} \frac{\sin[(2N+1)\frac{\omega_{2c} t_2}{2}]}{\sin \frac{\omega_{2c} t_2}{2}}$$

Then in the receiving coordinate system we would have

$$E(t_1) = e^{j\omega_{2o}\gamma(1+\frac{v}{c})t_1} \frac{\sin[(2N+1)\omega_{2c}\gamma(1+\frac{v}{c})\frac{t_1}{2}]}{\sin(\frac{\omega_{2c}\gamma(1+\frac{v}{c})t_1}{2})}$$

Thus to detect the mode-locked laser doppler shifted up in frequency we must have the condition,

$$f_{2c} = \frac{c}{2h}$$

$$\omega_{2c} = \frac{\pi c}{h}$$

so

$$h_o = \frac{\pi c}{\omega_{2c}\gamma(1+\frac{v}{c})} = \frac{h}{\gamma(1+\frac{v}{c})} \qquad (7\text{-}7)$$

Similarly if the mode-locked laser and the passive cavity were on a common platform, then the echo from a vehicle moving toward this platform with velocity v would be shifted by $\omega_{1c} = (1+2v/c)\omega_{2c}$ where we have set $\gamma = 1$. So by vernier adjustments (PZT driven mirror) of the passive cavity we can read a large range of approach velocities.

7.4 Resolution of the Passive Cavity

From the expressions above we see that in addition to the selective filtering characteristics of the passive cavity acting as a matched-filter, a readout of the vernier length control, peaking the output, provides for an extremely wide range of velocity measurements

with either an active or a passive vehicle moving relative to the receiver. To derive the resolution of the cavity to measure velocities we see, taking the derivative of Eq. (7-7), that

$$\frac{\partial h_o}{\partial v} = - \frac{h/c}{(1+\frac{v}{c})^2}$$

Thus for $v/c << 1$ we have $\delta h_o/h_o \simeq \delta v/c$. So if $\delta h_o/h_o = 3.3 \times 10^{-8}$ which is very reasonable with a PZT driven end mirror, then the resolution of the passive cavity is given by $\delta v = 10 m/s$. To obtain this resolution in the case where a vehicle is sending a signal to an observer, a local reference tone must be used to establish the zero relative velocity point.

Chapter 8

Experiment

8.1 Introduction

The purpose of this experiment is to demonstrate the degree of improvement which is obtained in the pre-detected signal-to-noise ratio of a self-mode-locked He-Ne laser signal with use of a passive Fabry-Perot resonant cavity which is matched in length to the laser cavity. The pre-detected signal-to-noise ratio is measured for various relative cavity lengths and as a function of passive cavity finesse. Due to the sensitivity of the experiment to variations in temperature, path lengths, and vibration the entire experiment was performed in a controlled acoustical environment which provided isolation from external turbulence and mechanical fluctuations. The design of this environment is considered and the degree of isolation is measured. A detailed discussion of the experiment is given and the results are summarized for various aspects of the signal-to-noise measurement.

8.2 Experimental Set-Up

To demonstrate the sensitivity of this experiment to mechanical fluctuations consider Eq. (5-3) for small variations in h_o around $\lambda/2$. Then for a measured $\sqrt{P} = 156$ the change in h_o on the order of .001μm will reduce the output to 1/2 maximum. For this reason the entire experiment was mounted on an isolation table. The 4' x 8', 4,000 lb. cast iron table was floated by rubber diaphragms and compressed air cylinders at each of the four legs. The isolation from the floor as

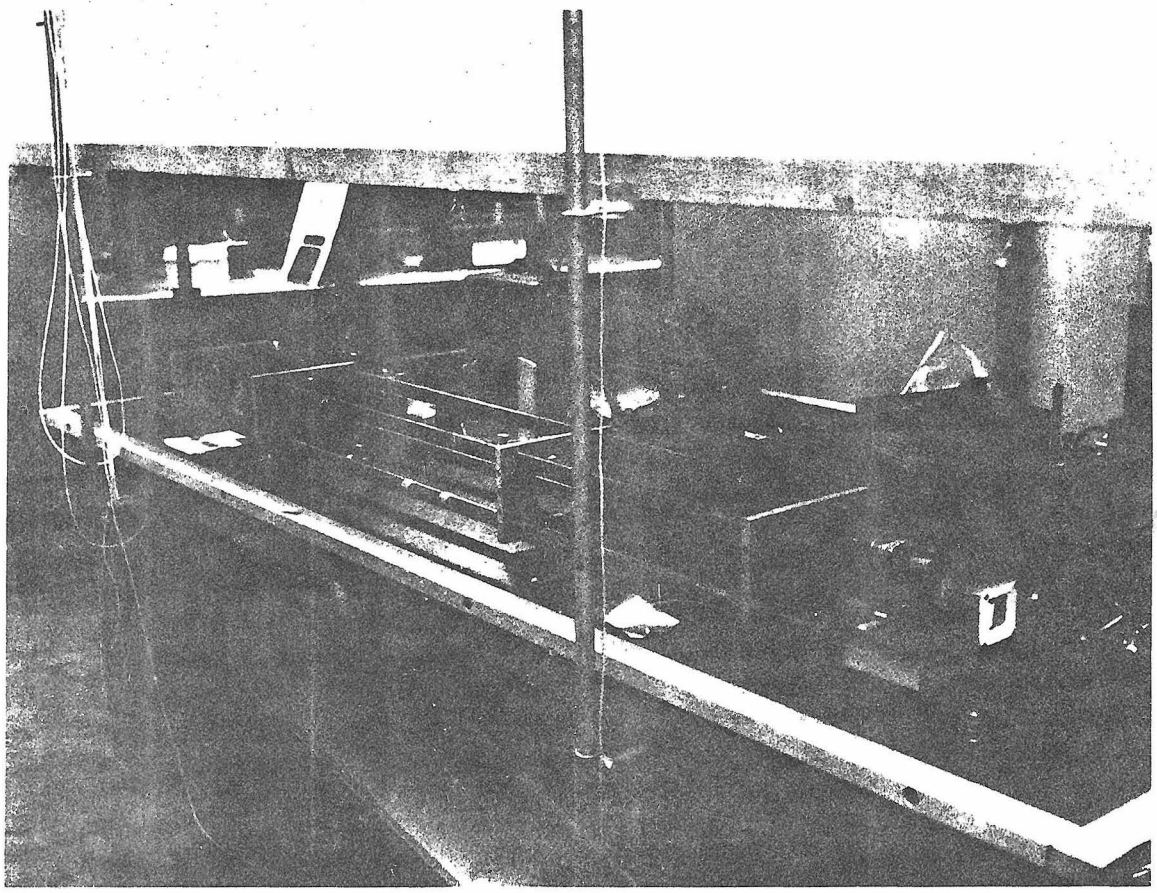

Fig. [8-1]

Fig. [8-2]

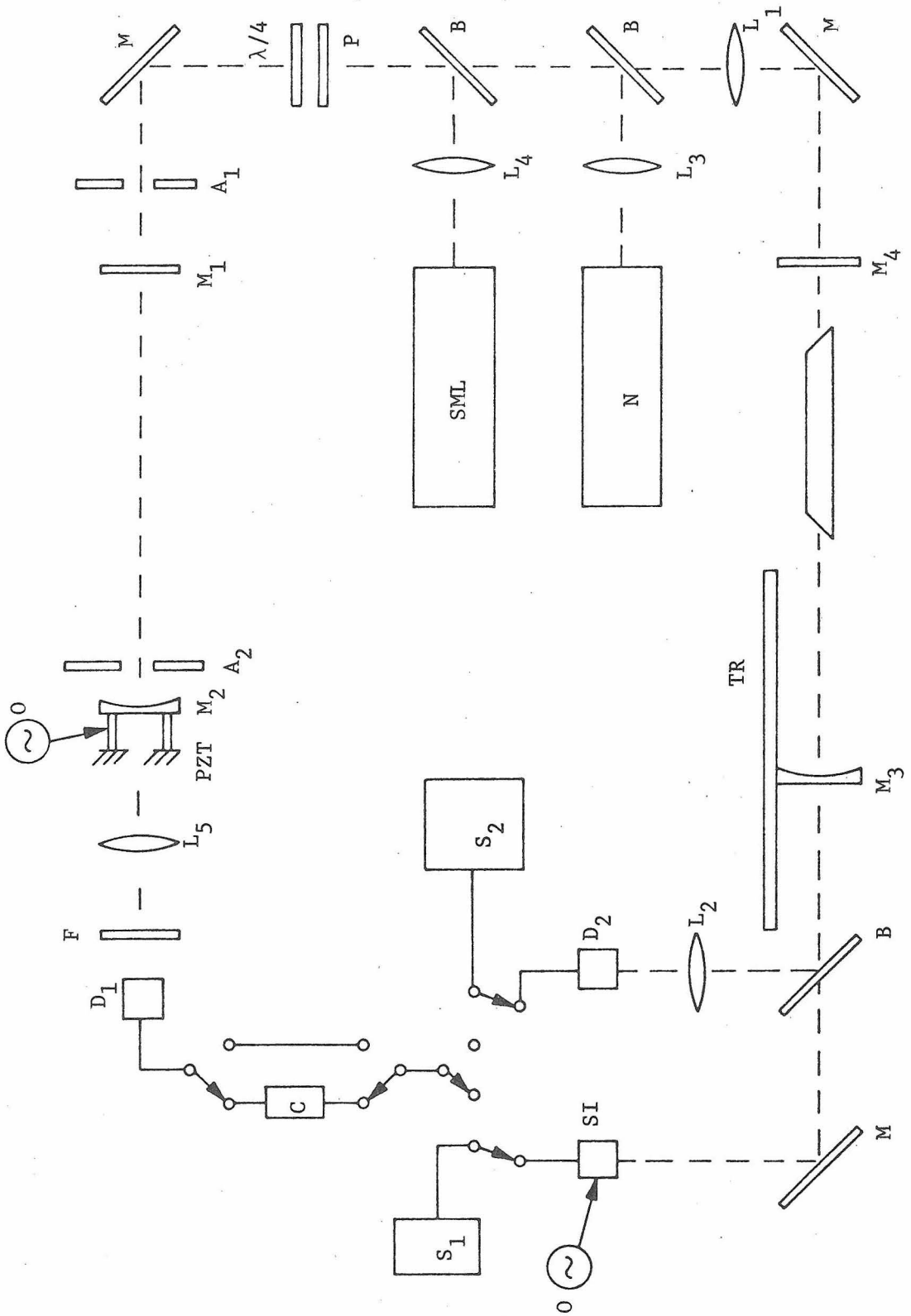
M
λ/4
P
B
B
L1
M
A1
L4
L3
M1
M4
SML
N
A2
TR
M2
PZT
M3
L5
S2
F
D2
L2
B
D1
C
SI
M
S1

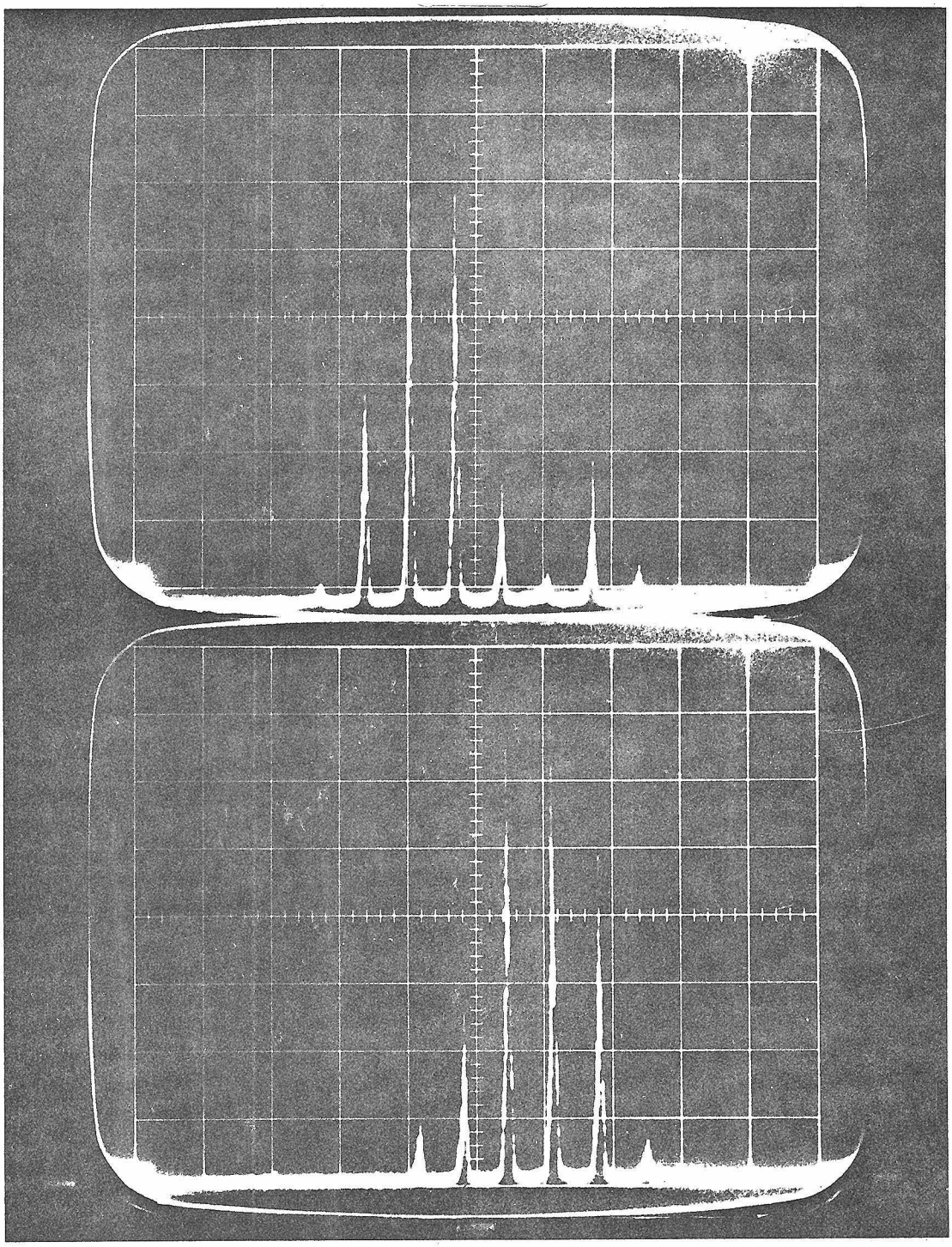

Fig. [8-3]

measured by geophone was better than 70 db for frequencies higher than 100 Hz while the decay time to 1/e was less than one second. To reduce air turbulence and cut down on acoustical fluctuations the entire set-up was enclosed in a double wall acoustical shield which provided ~10 db sound attenuation plus complete reduction in air turbulence which would have normally influenced the effective cavity lengths of the passive and laser cavities. The passive cavity was fabricated with the end mirrors mounted on invar rods to reduce the variations in cavity lengths due to thermal contraction or expansion. These rods as well as the rigid mirror mounts, provided with differential micrometer movements for sensitive alignment of the passive cavity mirrors, are shown in Fig. [8-1].

The total experimental layout is illustrated in Fig. [8-2]. In the experiment it was necessary to change the lengths of the passive and laser cavities. The change in length of the laser h was provided by the motion of mirror M_3 on a teflon runner TR while the fine fractional wavelength control (1μm full scale) of the passive cavity with length h_o was provided by motion of mirror M_2 on a PZT, driven by the oscillator O. The passive cavity was scanned at a 1 Hz rate to eliminate the effect of any remaining acoustical fluctuations. The teflon runner and a rigid mirror mount for M_3 allowed the laser to continue oscillation during large changes in the laser cavity length. The spectrum of the laser was monitored by a scanning interferometer SI controlled by the same oscillator O and then displayed on oscilloscope S_1 which was scanned in synchronism with O. An example of the multi-tone laser spectrum with 6 modes oscillating is shown in Fig. [8-3].

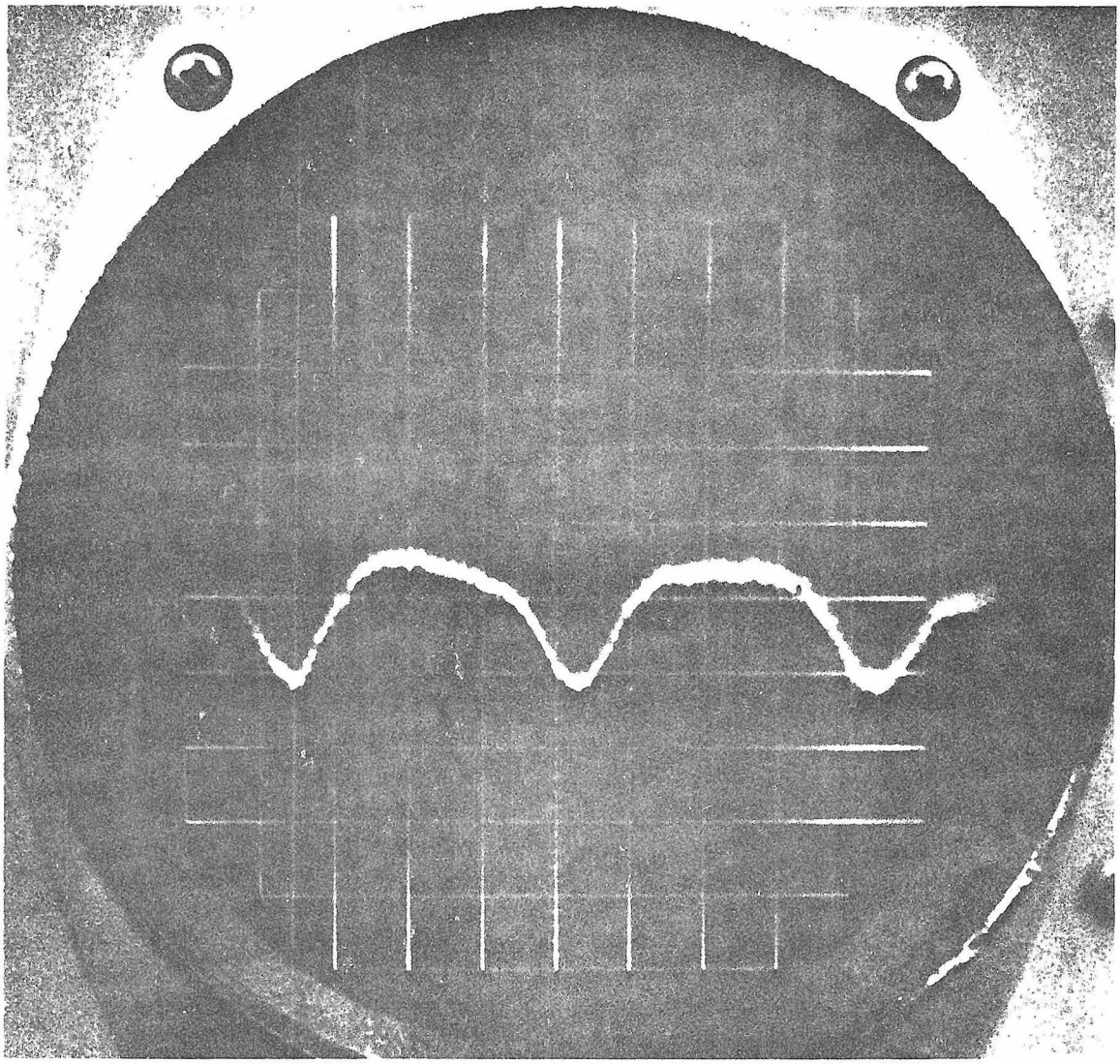

Fig. [8-4]

8.3 Mode-Locked Laser Pulses

The time display was observed using a Philco 4530 PIN diode D_2 with appropriate circuitry to impedance match into the H-P 185B sampling oscilloscope S_2. The inverted output of the self-mode-locked He-Ne laser with 4 modes oscillating is shown in Fig. [8-4] which may be compared with the theoretical results of Eq. (B-1). The optical frequency ω_o is not detected but the envelope of period 8 ns with pulse width 2 ns is observed. The period of the pulses is controlled by the laser cavity length h in that $2h/c$ is the period of the pulse train (for $h = 1.2$m, $2h/c = 8$ ns). The pulse width is controlled by the bandwidth of the total number of modes oscillating $(4c/2h)^{-1} =$ 2 ns).

8.4 Finesse

The finesse of the passive cavity was experimentally measured by first scanning the cavity through one free spectral range with the Spectra-Physics Model 119 single mode laser SML coupled by lens L_4 into the input. The $\lambda/4$ plate and polarizer P were used for isolation of the passive cavity from the single mode laser. The lens L_4 and the aperture A_1 were used to match the curvature and diameter of the input single mode wave to that which would be supported by the passive cavity so that higher order tranverse modes were not excited in the cavity. The output of the cavity is focused on detector D_1 by lens L_5 and displayed on S_1. The scope face is then calibrated to full scale by the free spectral range given by $c/2h_o =$ 150 MHz for $h_o = 1$ m.

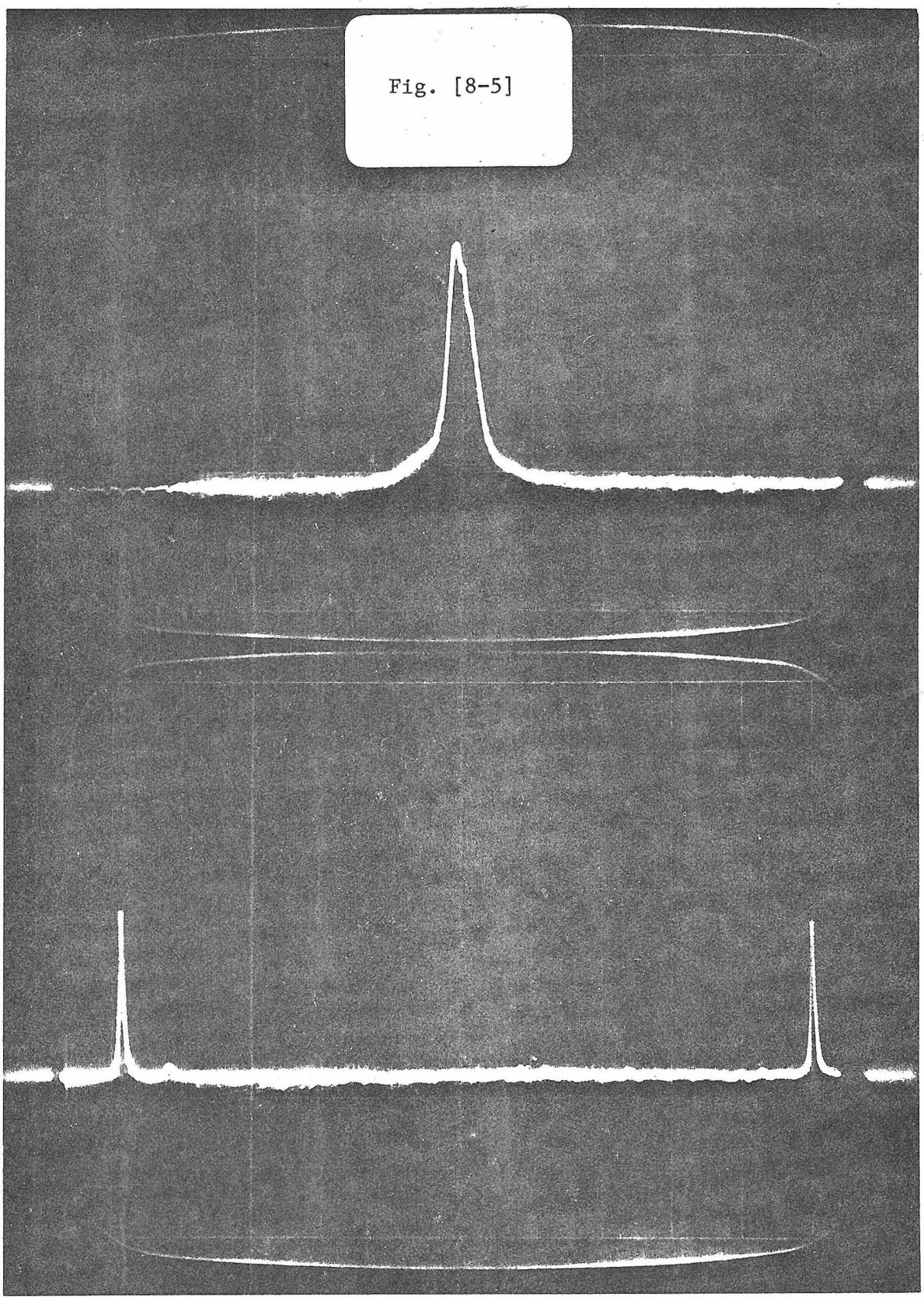
Fig. [8-5]

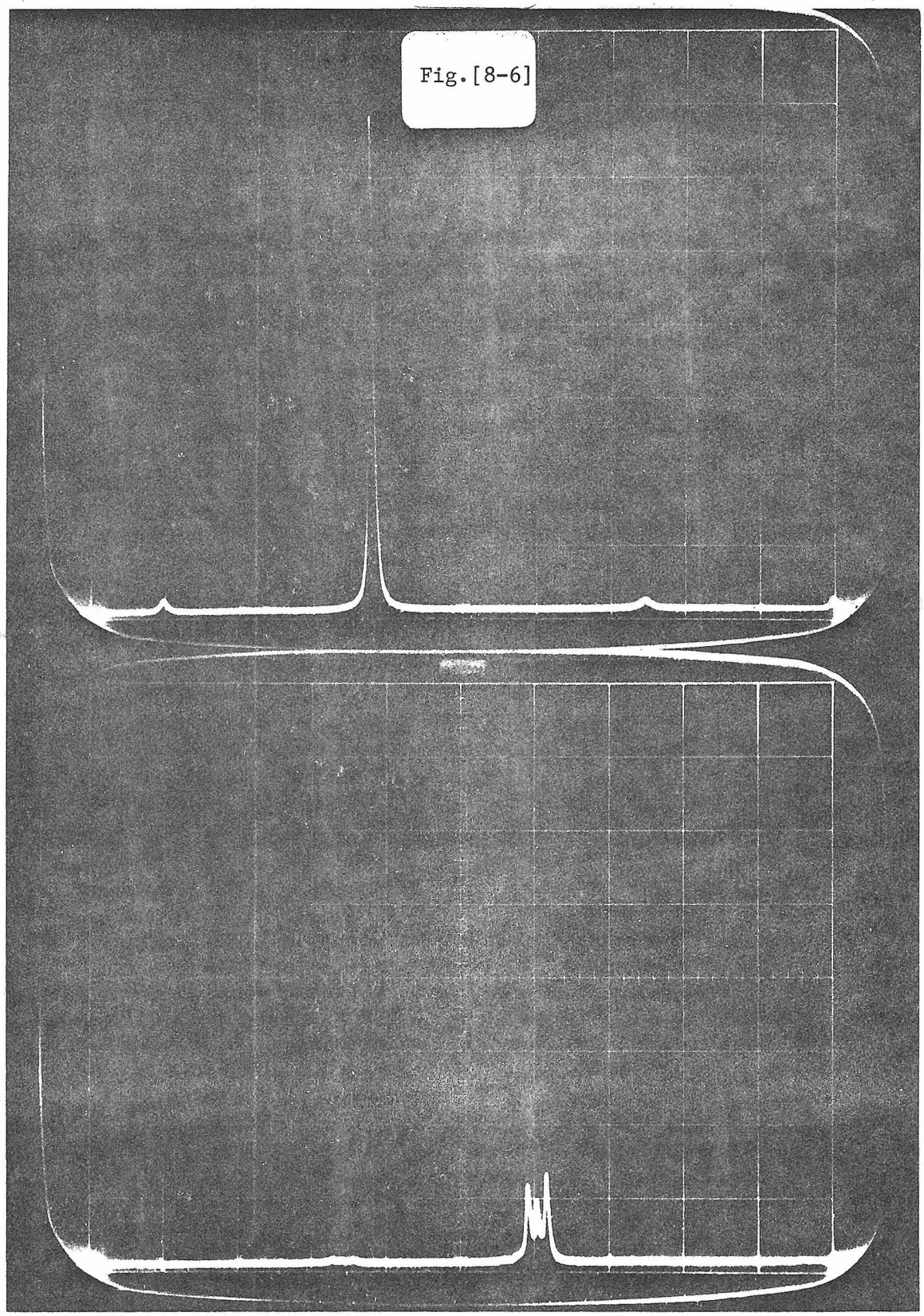
Fig.[8-6]

The horizontal magnification of scope S_1 will then control the dispersion of the display. Thus the resonant width obtained will yield the finesse as per Eq. (4-1). Figure [8-5] illustrates the principle of measuring the experimental passive cavity finesse. The experimental curve of Fig. [4-1] was generated by controlling the diffraction loss of the passive cavity by changing the aperture A_2 and the length h_o. This allowed a variation of the Fresnel number and hence a variation in the diffraction loss at the end mirrors.

8.5 Signal-to-Noise Measurements

In this experiment the signal-to-noise ratio improvement by pre-detection filtering of the mode-locked laser optical input by a passive Fabry-Perot resonant cavity was measured as a function of several parameters: relative cavity lengths and passive cavity finesse. Since the passive cavity is a good approximation to the matched-filter for mode-locked lasers only when the cavity lengths are perfectly matched, the detector D_1 output was monitored for various relative cavity lengths. The mode-locked laser signals were obtained from the self-locking He-Ne laser operating at 0.633μm with a length of 1.2 m and an average power output of 2 mW. As was mentioned earlier the mirror M_3 was translated along the laser axis without disturbing the laser oscillation. Thus continuous monitoring of the passive cavity output while the length of the laser cavity was changed allowed us to exactly match the cavity lengths by peaking the output. The top display of Fig. [8-6] shows the output of the cavity with the cavities equal in length. The bottom display shows the output of the

passive cavity with a mismatch of 4 mm which is analogous to the graph of Fig. [5-2]. Note that all of the modes of the laser are transmitted simultaneously in the matched condition. The peak power output was observed to go as $(2N+1)^2$, i.e., as the square of the number of modes oscillating.

To measure the signal-to-noise ratio improvement, white noise from an a-c driven tungsten lamp N at ~3200°K was introduced axially into the system. The white noise power at the input of the passive cavity was 1.5 W in a 100Å band around 0.633μm. The output of the passive cavity in the noise measurements was focused by L_5 onto a Texas Instrument TIXL55 avalanche diode detector and then passed to the Avantek T 1002 preamp C which provides 14 db of gain in a 5 - 1000 MHz range for display by the H-P sampling oscilloscope S_2. The thermal noise of the TIXL55 detector in a 500 MHz range was three orders of magnitude higher than the shot noise value $(2eI_o\Delta f)^{\frac{1}{2}}$ for operating currents of 0.1μA. Thus for the signal-to-noise measurements the 60 cycle envelope of the white noise source was used as the unwanted signal corresponding to the noise of the signal-to-noise measurement. Mirror M_1 was a standard Spectra-Physics flat laser reflector with reflectivity 0.991. Mirror M_2 was a standard Spectra-Physics laser reflector with radius of curvature 2m and reflectivity of .991 (M_3 is the same as M_2). Both reflectors were chosen to maximize the ideal finesse by minimizing loss; it is given by Eq. (4-8) as 346. In all cases the measured finesse was lower than the ideal finesse due to mirror surface roughness and scattering from occlusions in the mirror multi-layer as was described in Chapter 4. With the cavity set for the

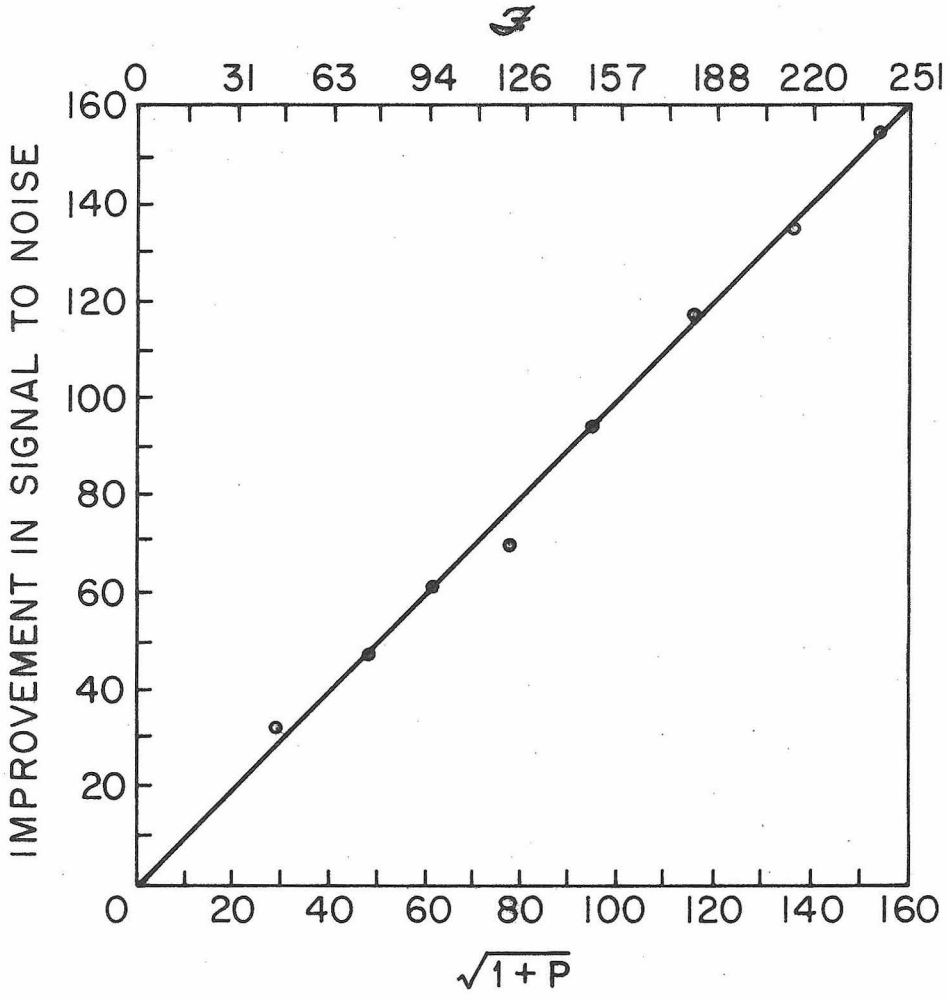
F
0
31
63
94
126
157
188
220
251
160
140
120
100
80
60
40
20
0
IMPROVEMENT IN SIGNAL TO NOISE
20
40
60
80
100
120
140
160
√1+P

Fig. [8-7]

largest Fresnel number (50), i.e., end apertures were limited by the mirror dimensions (15 mm), the signal and noise were measured with M_1 and M_2 aligned to maximize the passive cavity finesse. The finesse was also measured and found to be 245. The mirrors M_1 and M_2 were removed and apertures were introduced to maintain the same exit pupil diameter. The signal and noise were measured again. All measurements of signals and noise were made using neutral density filters which had been calibrated at 0.633 μm to avoid non-linearities in the detector electronics. The ratio of the signal-to-noise with the passive cavity in place to the signal-to-noise without the cavity in place was 156. From Eq. (4-8) we find using the measured finesse that $\sqrt{P} = 156$ which we may compare to the theoretical improvement given by Eq. (5-8). The experiment was repeated for various values of finesse by controlling the aperture size A_2 and the length of both cavities always such that $h = h_o$. The results of these measurements are summarized in Fig. [8-7] along with a plot of Eq. (5-8). It was noted that the improvement occurred also when the laser was not mode-locked. This is a reasonable result since He-Ne is a low gain laser and the mode pulling has a negligible effect on the transmission of the passive cavity.

Chapter 9

Summary and Conclusions

In this work we have shown that the passive Fabry-Perot resonant cavity which is equal in length to the laser cavity is probably as close a physical realization to a matched-filter for multi-toned mode-locked gas laser signals as can be attained in a passive system. This was done by first developing a matrix formalism to describe the fields in a stratified dielectric media. Then the formalism was applied to the analysis of the Fabry-Perot which led to a transmission function. The generalized transmission function Eq. (2-31) was cast in the Laplace transform domain which allowed us to develop a transient analysis in Chapter 6. With this passive cavity characterization we developed the matched-filter condition and showed that the mode-locked laser signal is that for which the Fabry-Perot is a matched-filter.

An important characteristic which influences the performance of the passive cavity as a matched-filter for mode-locked laser signals is the finesse. Chapter 4 dealt with the factors that control the finesse and some interesting physical limitations on the finesse were discussed and experimentally verified. The signal-to-noise improvement of the passive cavity and the departure from the matched-filter condition for mismatches in mode-width and cavity length were considered next. Gain narrowing invariably results in the linewidth of the laser being less than the mode-width of the passive cavity,[1] thereby limiting the observed pre-detection signal-to-noise ratio improvement factor

$\sqrt{1+P}$, Eq. (5-8), from its optimal value, Eq. (5-29). For high gain lasers[2] with cavities of low finesse, the receiver can be made close to ideal, while greater departures are to be expected in the case of low gain. We note, too, that larger bandwidths, $\Delta\omega_p$, are called for with information modulated lasers and cavity-dumped lasers where mode-locking may not have been employed.

The Laplace transform representation of the passive Fabry-Perot resonant cavity which was developed in Chapter 2 was then used to analyze the rise-time of the passive cavity by using two different techniques which led to an identical result Eq. (6-29).

It was shown in Chapter 7 that in addition to the selective multi-tone filtering characteristics of the passive cavity, a readout of the passive cavity's vernier length control, peaking the output, provides for a wide range of velocity measurements with either an active or a passive vehicle moving relative to the receiver.

An experiment was performed to demonstrate the degree of improvement which is obtained in the pre-detected signal-to-noise ratio of a self mode-locked He-Ne laser signal with use of a passive Fabry-Perot resonant cavity. The pre-detected signal-to-noise was measured for various relative cavity lengths and cavity finesse. The results were described and presented in good comparison with the theoretical results.

Further study of the cavity as a matched-filter using some regenerative gain seems interesting; however, the gain media may introduce noise into the detection process sufficient to cancel the resulting benefits of a narrower linewidth. In any event the formalism which was developed for the passive cavity is completely general and may be

directly applied to the analysis of the regenerative active matched-filter for multi-tone gas laser signals.

Chapter 9

References

1. A. Yariv, Quantum Electronics, (John Wiley, New York, 1967), p. 409.

2. L.W. Casperson, Ph.D. Thesis, California Institute of Technology, Pasadena, California, 1971.

Appendix A

The Matched-Filter

The problem of determining a filter which will yield the maximum signal-to-noise ratio when the signal is well defined is a problem of great interest in radar and in optical communication systems. The salient features of this analysis are reviewed in the following paragraphs.[1,2] An understanding of the expressions for the matched-filter $h(t)$ with Fourier transform $H(\omega)$ for an input signal $f(t)$ with Fourier transform $F(\omega)$, Eq. (A-23) and Eq. (A-36), will be assumed in the text of this thesis.

Consider the linear-time-invariant system with impulse response function $h(t)$. If the total input to this system is a signal $f(t)$ in the presence of noise $n(t)$ then the output, from linear system theory, is given by

$$g(t) = (f(t) \circledast h(t)) + (n(t) \circledast h(t)), \qquad \text{(A-1)}$$

where $\circledast$ indicates convolution defined by

$$(f \circledast h) = \int_{-\infty}^{t} h(t-\tau)\, f(\tau)\, d\tau \quad . \qquad \text{(A-2)}$$

We note also that if we assumed that $h(t)$ acted on the input for only a period T then

$$(f \circledast h)_T = \int_{0}^{T} h(\tau)\, f(t-\tau)\, d\tau \quad . \qquad \text{(A-3)}$$

We may consider the power output from Eq. (A-1) as

$$gg^* = |f \circledast h|^2 + (f \circledast h)(n \circledast h)^* + (f \circledast h)^*(n \circledast h) + |n \circledast h|^2 \quad . \qquad \text{(A-4)}$$

And in taking the mean value of Eq. (A-4), defined for a function $q(t)$ by

$$\langle q \rangle \equiv \lim_{T\to\infty} \frac{1}{2T} \int_{-T}^{T} q(t)dt \quad , \qquad \text{(A-5)}$$

we assume $f(t)$ is uncorrelated with $n(t)$ and $\langle n(t) \rangle = 0$ so

$$\langle gg^* \rangle = \langle |f \circledast h|^2 \rangle + \langle |n \circledast h|^2 \rangle \quad . \qquad \text{(A-6)}$$

The problem is to find an $h(t)$ which optimizes the signal-to-noise ratio defined by

$$SNR \equiv \frac{|f \circledast h|^2}{\langle |n \circledast h|^2 \rangle} \quad . \qquad \text{(A-7)}$$

To do this we will review some familiar linear system theory. The auto-correlation function of $q(t)$ is defined by Eq. (A-5) as

$$R_q(t) \equiv \langle q(t+\tau)\, q^*(\tau) \rangle = \lim_{a\to\infty} \frac{1}{2a} \int_{-a}^{o} q(t+\tau)\, q^*(\tau)d\tau + \lim_{b\to\infty} \frac{1}{2b} \int_{o}^{b} q(t+\tau)q^*(\tau)d\tau \qquad \text{(A-8)}$$

where the asterisk denotes the complex conjugate.

Then we define the power spectral density as

$$S_q(\omega) = \int_{-\infty}^{\infty} R_q(t)\ e^{-j\omega t}\ dt$$

$$R_q(t) = \frac{1}{2\pi} \int_{-\infty}^{\infty} S_q(\omega)\ e^{j\omega t}\ d\omega \quad , \qquad \text{(A-9)}$$

and hence $R_q(\tau)$ and $S_q(\omega)$ are Fourier transform pairs. The reason for presenting Eqs. (A-8) and Eqs. (A-9) is to express the mean-squared value of the additive output noise, i.e., the denominator of the signal-to-noise expression Eq. (A-7) since the Fourier transform of n(t) generally does not exist.

Now we recall from linear system theory that if for a function q(t)

$$Q(\omega) = \int_{-\infty}^{\infty} q(t)\ e^{-j\omega t}\ dt \quad , \qquad \text{(A-10)}$$

and

$$q(t) = \frac{1}{2\pi} \int_{-\infty}^{\infty} Q(\omega)\ e^{j\omega t}\ d\omega \quad , \qquad \text{(A-11)}$$

are transform pairs then for g, f, and h satisfying Eqs. (A-10) and (A-11) and if g(t) is related to f and h by Eq. (A-2)

$$g = f \circledast h \quad , \qquad \text{(A-12)}$$

then

$$G(\omega) = F(\omega)\ H(\omega) \quad . \qquad \text{(A-13)}$$

Thus Eq. (A-13) relates the output transform in terms of the input

transform and the transform of the impulse response. In a similar fashion we wish to express the output power spectral density $S_g(\omega)$ in terms of the input power spectral density $S_f(\omega)$. We do this by developing the following theorem.

Theorem I: If $g = h \circledast f$, then $R_g = h \circledast \tilde{h} \circledast R_f$ where $\tilde{h} = h^*(-t)$

Proof: Since $g(t + \tau) = \int h(u)\, f(t + \tau - u)du$

$$g^*(t) = \int h^*(v) f^*(t - v)dv$$

then

$$R_g(\tau) = \int \int h(u)h^*(v) < f(t + \tau - u)f^*(t - v)> dudv$$

and by substitution of $r = -v$

$$R_g(\tau) = \iint h(u)h^*(-r)R_f(\tau - u - r)dudr$$

$$R_g(\tau) = h \circledast \tilde{h} \circledast R_f \qquad \text{(A-14)}$$

Q. E. D.

Thus since the Fourier transform of h is $H^*(\omega)$ we have by transforming Eq. (A-14) and using the result of Eq. (A-13)

$$S_g(\omega) = |H(\omega)|^2 S_f(\omega) \qquad \text{(A-15)}$$

Then from Eq. (A-8) and Eq. (A-9) the mean-squared value of g is

$$R_g(0) = <|g|^2> = \frac{1}{2\pi} \int_{-\infty}^{\infty} S_g(\omega)\, d\omega \geq 0 \qquad \text{(A-16)}$$

since $|g|^2 \geq 0$. Note too that $S_f(\omega) \geq 0$ for if it were not then we could

choose an $H(\omega)$ in a region where $S_f(\omega) < 0$ which would create a $S_g(\omega) < 0$ for all ω by Eq. (A-7). However this $S_g(\omega)$ would violate Eq. (A-16) since $R_f(0) \geq 0$ for f(t) real. Thus if we have a linear time-invariant system with impulse response h(t) then the power spectral density of the input is related to the power spectral density of the output by Eq. (A-15). Now we can proceed with the theory of the matched-filter criterion. The modulus-squared value of the signal portion of the output of the filter is given by

$$|f \circledast h|^2 = \left|\frac{1}{2\pi} \int_{-\infty}^{\infty} e^{j\omega t} H(\omega)F(\omega)d\omega\right|^2 \qquad \text{(A-17)}$$

where

$$F(\omega) = \int_{-\infty}^{\infty} f(t)e^{-j\omega t}dt \text{ exists.}$$

The mean-squared value of the noise portion of the output of the filter is given by

$$N = \lim_{T\to\infty} \frac{1}{2T} \int_{-T}^{T} |n(t) \circledast h(t)|^2 dt = \langle |n(t) \circledast h(t)|^2 \rangle$$

$$= \frac{1}{2\pi} \int_{-\infty}^{\infty} S_n(\omega) |H(\omega)|^2 \, d\omega \qquad \text{(A-18)}$$

where $S_n(\omega)$ is the power spectral density of the noise at the input. Thus we may write Eq. (A-7) using Eq. (A-17) for the numerator and Eq. (A-18) for the denominator

$$SNR = \frac{|f \circledast h|^2}{N} = \frac{\left|\frac{1}{2\pi}\int_{-\infty}^{\infty} H(\omega)F(\omega)e^{j\omega t}d\omega\right|^2}{\frac{1}{2\pi}\int_{-\infty}^{\infty}|H(\omega)|^2 S_n(\omega)d\omega} \qquad \text{(A-19)}$$

Now we review Schwarz's Inequality Theorem.(1)

Theorem II: If $p(t) \geq 0$ for all t and x and y are complex, and if

$$\int_{-\infty}^{\infty}|x|^2 p\,dt \quad \text{and} \quad \int_{-\infty}^{\infty}|y|^2 p\,dt \quad \text{exist,}$$

then

$$\left|\int xy^* p\,dt\right|^2 \leq \int |x|^2 p\,dt \int |y|^2 p\,dt \qquad \text{(A-20)}$$

with equality if and only if $x = Ay$, where A is any non-zero complex constant.

As was mentioned previously, we wish to maximize the ratio of the $|\text{peak signal out}|^2$ to the mean-square value of the noise out by an appropriate choice of the filter h(t) or H(ω). To do this we will first make several assumptions about the system we will consider. First, no realizability constraint will be considered in this development. If we wish to employ a realizability constraint, in most cases a sufficient time delay of a realizable filter may satisfactorily approximate the nonrealizable filter. Second, we will assume the time that the output takes on its peak value is t=0. If the peak occurs at some other time or if the peak occurs periodically with period T then by incorporating

delay or anticipation in the filter, i.e., a linear phase shift in $H(\omega)$, we can observe the peak signal without changing the waveshape since this stochastic process is stationary in the wide sense.[3] Thus using. Eq. (A-20), Eq. (A-17) becomes

$$|f \circledast h|^2 = \left|\frac{1}{2\pi} \int_{-\infty}^{\infty} \underbrace{\frac{F(\omega)}{S_n(\omega)}}_{x} \underbrace{H(\omega)}_{y} \underbrace{S_n(\omega)}_{p} \underbrace{d\omega}_{dt}\right|^2 \qquad \text{(A-21)}$$

and Eq. (A-21) using the inequality of Eq. (A-20) becomes

$$|f \circledast h|^2 \leq \frac{1}{(2\pi)^2} \int_{\infty}^{\infty} \left|\frac{F(\omega)}{S_n(\omega)}\right|^2 S_n(\omega)\,d\omega \int_{-\infty}^{\infty} |H(\omega)|^2 S_n(\omega)\,d\omega \qquad \text{(A-22)}$$

where $S_n(\omega) > 0$ is a weighting function and may be considered the power spectral density of the additive input noise. Thus from the statement of Theorem II the equality of Eq. (A-22) will hold if and only if

$$H_m(\omega) = \frac{A\,F(\omega)^*}{S_n(\omega)} \qquad \text{(A-23)}$$

where A is any non-zero complex constant. $H_m(\omega)$ defined by Eq. (A-23) is called the matched-filter for f(t). Hence the time varying modulus-squared value of the signal to the time average mean-squared value of the noise is given by Eqs. (A-17), (A-18), and (A-23) as

$$\frac{|f(t) \circledast h(t)|^2}{N} = \frac{1}{2\pi} \frac{\left| \int_{-\infty}^{\infty} e^{j\omega t} \frac{|F(\omega)|^2}{S_n(\omega)} d\omega \right|^2}{\int_{-\infty}^{\infty} \frac{|F(\omega)|^2}{S_n(\omega)} d\omega} \tag{A-24}$$

with peak value at t = 0 given by

$$\frac{|f \circledast h|^2}{N} = \frac{1}{2\pi} \int_{-\infty}^{\infty} \frac{|F(\omega)|^2}{S_n(\omega)} d\omega \tag{A-25}$$

In the time domain Eq. (A-23) may be expressed as

$$h_m \circledast R_n = Af^*(-t) \tag{A-26}$$

In the case where the Fourier transform of f(t) does not exist we use the time limited definition of h(t) given in Eq. (A-3) so that

$$(h \circledast f)_T = \int_o^T h(\tau) f(t - \tau) d\tau \tag{A-27}$$

$$(n \circledast h)_T = \int_o^T h(\tau) n(t - \tau) d\tau \tag{A-28}$$

and from Eq. (A-14), (A-16) and (A-18)

$$N = (h \circledast \tilde{h} \circledast R_n(0))_T \tag{A-29}$$

If we assume m is the maximum output SNR we have

$$m \geq \frac{|g(t)|^2}{N} \tag{A-30}$$

and assume some function k which satisfies

$$(k \circledast f)_T = 0 \tag{A-31}$$

then for the correct choice of $h = h_m$ we have putting Eq. (A-29) into Eq. (A-30)

$$m = \frac{|g(0)|^2}{(h_m \circledast \tilde{h}_m \circledast R_n(0))_T} \tag{A-32}$$

and

$$m \geq \frac{|g(0)|^2}{((h_m + ak) \circledast \widetilde{(h_m + ak)} \circledast R_n(0))_T} \tag{A-33}$$

where a is any real number. Then subtracting Eq. (A-32) from Eq. (A-33) and collecting terms we obtain

$$(a^2 k \circledast \tilde{k} \circledast R_n(0))_T + (a[k \circledast \tilde{h}_m \circledast R_n(0) + \tilde{k} \circledast h_m \circledast R_n])_T$$

$$\geq 0 \tag{A-34}$$

Equation (A-34) may be satisfied since a can be any number if and only if

$$(k \circledast \tilde{h}_m \circledast R_n(0))_T + (\tilde{k} \circledast h_m \circledast R_n)_T = 0 \tag{A-35}$$

Both terms will vanish if by Eq. (A-31) we select

$$(h_m \circledast R_n)_T = A\, f^*(-t) \tag{A-36}$$

for A any non-zero complex constant. Thus we have shown that the

existence of the Fourier transform of f(t) is not necessary as long as we put some realizability constraint on h(t).

For a time shifted signal $f(t - \tau)$, Eq. (A-36) becomes

$$(h_m \circledast R_n)_T = A f^*(\tau - t) \tag{A-37}$$

which merely indicates that the peak value of the signal-to-noise is also shifted by τ.

Example 1:

If we assume that the noise is additive white noise, i.e., $S_n(\omega) = N_o$ or $R_n(\tau) = N_o\delta(\tau)$, then Eq. (A-23) becomes

$$H_m(\omega) = \frac{A[F(\omega)]^*}{N_o} \tag{A-38}$$

and the peak signal-to-noise is by Eq. (A-25)

$$\frac{|f \circledast h|^2}{N} = \frac{1}{2\pi N_o} \int_{-\infty}^{\infty} |F(\omega)|^2 \, d\omega \tag{A-39}$$

We note that by Parseval's theorem

$$\frac{1}{2\pi} \int_{-\infty}^{\infty} |F(\omega)|^2 \, d\omega = \int_{-\infty}^{\infty} |f(t)|^2 \, dt \tag{A-40}$$

which is the total energy of the signal.

Example 2:

Suppose $f(t)$ is a sinusoidal function with radian frequency ω_o, $f(t) = e^{j\omega_o t}$, then the signal portion of the output of a matched-filter $h(t) = f^*(-t)$ for $S_n(\omega) = 1$ is.

$$f \circledast h = \int_{-\infty}^{\infty} h(t-\tau)\, f(\tau)\, d\tau = \int_{-\infty}^{\infty} e^{-j\omega_o(-t+\tau)}\, e^{j\omega_o\tau}\, d\tau$$

$$= e^{j\omega_o t} \int_{-\infty}^{t} d\tau \qquad \text{(A-41)}$$

which we see is infinite. There are two ways of handling this situation. First we shall suppose that the filter acts on the input for a certain amount of time T. Then the signal portion of the output may be written,

$$(f \circledast h)_T = \int_{t-T}^{t} h(t-\tau)f(\tau)d\tau = \int_{o}^{T} h(\tau)f(t-\tau)\, d\tau$$

$$= \int_{o}^{T} e^{j\omega_o\tau}\, e^{j\omega_o t - j\omega_o\tau}\, d\tau = T\, e^{j\omega_o t} \qquad \text{(A-42)}$$

The second way is to consider the input as a slowly decaying sinusoidal function given by $f(t) = \exp(i\omega_0 t - at)u(t)$ for which $f(t)$ is down to $1/e$ when $t = 1/a$. The Fourier transform for this signal is

$$F(\omega) = \frac{1}{a - i(\omega-\omega_o)} = \frac{1}{a} \frac{1}{1 - i\left(\frac{\omega-\omega_o}{a}\right)} \tag{A-43}$$

As a check we may take the limit of Eq. (A-43) as $a \to 0$ which is a delta function $\delta(\omega-\omega_o)$.[4] We choose the matched-filter from Eq. (A-23) with $A = 2a$, and $S_n(\omega) = 1$ we have

$$H(\omega) = \frac{2}{1 + i\left(\frac{\omega-\omega_o}{a}\right)} \tag{A-44}$$

The signal portion of the output is then given by

$$f \circledast h = \frac{1}{2\pi} \int_{-\infty}^{\infty} \frac{2}{a} \frac{e^{i\omega t} d\omega}{\left[1 + \left(\frac{\omega-\omega_o}{a}\right)^2\right]} \tag{A-45}$$

And this may be integrated to yield[5]

$$f \circledast h = e^{i\omega_o t - a|t|} \tag{A-46}$$

If we now let $a \to 0$ then Eq. (A-46) becomes

$$f \circledast h = e^{i\omega_o t} \tag{A-47}$$

The matched-filter defined by Eq. (A-44) is reasonable in that it has a finite gain as $a \to 0$. This limits the output, Eq. (A-46), to the finite damped sinusoid. This points out the fact that the shape of the filter spectrum must match the shape of the input spectrum for the matched

condition and any arbitrary gain or loss can be supplied by the A factor.

Example 3:

Suppose that

$$f(t) = \sum_{p=-N}^{N} \exp\, i(\omega_o + p\omega_c)t \qquad \text{(A-48)}$$

where $f(t)$ may be considered the output of a mode-locked laser with $(2N+1)$ modes oscillating spaced by ω_c around ω_o. We will develop the matched-filter signal output by again approximating the input signal transform of Eq. (A-48) by

$$F(\omega)_A = \sum_{p=-N}^{N} \frac{1}{a} \frac{1}{1 + i\left(\frac{\omega - (\omega_o + p\omega_c)}{a}\right)} \qquad \text{(A-49)}$$

Then the matched-filter for $S_n = 1$ and $A = 2a$ is given by Eq. (A-23)

$$H(\omega) = \sum_{p=-N}^{N} \frac{2}{1 - i\left(\frac{\omega - (\omega_o + p\omega_c)}{a}\right)} \qquad \text{(A-50)}$$

Then the output of a linear system with transfer function $H(\omega)$ and input $F(\omega)$ is

$$f \circledast h = \frac{1}{2\pi} \int_{\infty}^{\infty} e^{i\omega t}\, F(\omega)\, H(\omega)\, d\omega \qquad \text{(A-51)}$$

and using the method of residues we obtain an output

$$f \circledast h = e^{-a|t|} \sum_{p=-N}^{N} e^{i(\omega_o + p\omega_c)t}$$

$$+ i2a\, e^{-a|t|} \sum_{\substack{p,q=-N \\ p \neq q}}^{N} \frac{e^{i(\omega_o + p\omega_c)t} + e^{i(\omega_o + q\omega_c)t}}{2a + i\omega_c(q - p)} \qquad \text{(A-52)}$$

and if $a \to 0$

$$f \circledast h = \sum_{p=-N}^{N} e^{i(\omega_o + p\omega_c)t} \qquad \text{(A-53)}$$

Appendix A

References

1. William M. Brown, Analysis of Linear Time-Invariant Systems, (McGraw-Hill, 1963), Chapter 8.

2. Davenport and Root, Random Signals and Noise, (McGraw-Hill, 1968).

3. A. Papoulis, Probability, Random Variables, and Stochastic Processes, (McGraw-Hill, 1965), p. 302.

4. A. Messiah, Quantum Mechanics, Vol. 1, (John Wiley & Sons, 1966), p. 469, Eq. (A.15c).

5. I.S. Gradshteyn, I.M. Ryzhik, Tables of Integrals Series and Products, (Academic Press, 1965), p. 312, Eq. (3.354-5).

Appendix B

The Mode-Locked Laser

B.1. A Source of Optical Pulses

The mode-locked helium-neon laser is a source of short duration optical pulses. A detailed analysis of the helium-neon laser is beyond the scope of this work; however, a brief description of its operation will be given in the following sections. In the experiment, the mode-locked laser is used as a source of short duration optical pulses to be detected by a sensitive mode-locked laser radiation receiver. It is therefore necessary to understand the basic assumption made concerning the mode-locked helium-neon laser before the analysis of the optical detection system may be considered.

B.2. Basic Components of the Helium-Neon Laser

The basic operation of the He-Ne laser may be described by considering the function of its two components: the active gain media which amplifies an electromagnetic field, and a resonant cavity which provides positive feedback to the system to allow oscillation of the electromagnetic fields. The active gain media is provided in the form of a long glass tube filled at low pressures with a mixture of helium and neon gases. When these gases are excited by some energy source (typically a d.c. discharge), they are capable of providing amplification to the waves in the media. The feedback system is provided by two uniaxial mirrors aligned to produce a

passive cavity similar to a Fabry-Perot interferometer. The components are allowed to interact when the gain tube is positioned along the axis of the passive cavity. When an electromagnetic field of the proper frequency interacts with the gas media, photons of the proper phase and direction are emitted by the stimulated transitions of atoms in the upper states of the neon to provide amplification to the field undergoing the interaction.[1,2] Oscillation will occur when the gain that the electromagnetic field in the cavity receives is greater than the losses in the system.

There are three main transitions in neon which are commonly used in lasers. These transitions correspond to optical wavelengths of 6328Å, 1.15μ and 3.39μ. The experiments to be described in Chapter 8 will make use of the 6328Å transition which while relatively low in gain is advantageous in the experiments being described herein since it oscillates in many modes and it is relatively simple to mode-lock.

While the 3.39μm laser has a much higher gain it has a relatively narrow Doppler broadened gain curve, 20MHz/60MHz,[3] and thus it is not feasible to obtain 6 to 8 independently oscillating modes. The 1.15μm transition, the first gas laser oscillation to be observed,[4] was not used mainly because its gain is only about that of the 0.6328μm line (low) and hence it offers no advantage. Then too, since it is not visible, the experimental detail would be unduly complicated.

B.3 Characterization of the Mode-Locked Laser

In general the operation of a laser may be characterized by a sequence of independent oscillators with random phase and amplitude. However, under certain circumstances the phases of the laser modes may be

locked together creating a "mode-locked" condition. We will assume throughout this work that this condition may be represented by the idealized field amplitude at the output of the mode-locked laser with 2N+1 modes as

$$E_1(t) = \sum_{p=-N}^{N} \exp i(\omega_o + p\omega_c)t = \exp(i\omega_o t)\, \frac{\sin\left[(2N+1)\frac{\omega_c}{2}t\right]}{\sin\left[\frac{\omega_c}{2}t\right]} \qquad (B\text{-}1)$$

where ω_o is the center frequency of the laser output, $\omega_c = 2\pi f_c$, $f_c = c/2h$ is the spacing between modes, and h is the effective cavity length. We note that the mode-locked laser generates a pulsed monochromatic field whose envelope has a period $T_p = 2\pi/\omega_c$. Thus we see the equivalence of the following two statements: A mode-locked laser generates 2N+1 monochromatic tones equally spaced by ω_c in frequency and no phase ambiguities. A mode-locked laser generates a monochromatic frequency ω_o with an envelope sin Mx/sinx.[5,6]

There are basically two methods to mode-lock a He-Ne laser. These methods correspond to self-mode-locking or feedback controlled mode-locking. Self-mode-locking, unlike the feedback controlled mode-locking, is obtained without any intercavity modulation or device. The control of the locking is accomplished by long laser cavities and careful adjustment of the mirrors and gain. With argon self-mode-locking is not readily obtained.[7,8] However, this laser is readily mode-locked using an intercavity modulator which establishes both coherence and stabilization of its modes. Such devices are available on a commercial basis (e.g.

Spectra-Physics Model 361 Acousto-Optical Mode-Locker). Since the natural linewidth of argon is much less than the Doppler broadened line, the detection technique described in this thesis is also appropriate for this laser. In fact, the much higher effective temperatures in this discharge give a Doppler line-width of 5,000 MHz. Thus for a one meter cavity length we would have 5000/c/2h = 33 modes.

The experiments in this work have been conducted only with He-Ne for reasons of economy.

Appendix B

References

1. A. E. Seigman, An Introduction to Lasers and Masers, (McGraw-Hill, 1971).
2. A. Yariv, Introduction to Optical Electronics, (Holt, Rinehart and Winston, 1971).
3. A. Yariv, Quantum Electronics, (John Wiley and Sons, 1967), p. 457.
4. A. Javan, W. R. Bennett, Jr., D. R. Herriott, Phys. Rev. Letters 6, p. 106 (1961).
5. C. C. Cutler, Proc. IRE 43, p. 140, February (1955).
6. L. E. Hargrove, R. L. Fork, M. A. Pollack, Appl. Phys. Lett. 5, p. 4 (1964).
7. O. L. Gaddy, E. M. Schaeffer, Appl. Phys. Lett. 9, p. 281 (1966).
8. S. U. Heising, S. M. Jarrett, IEEE J. Quantum Electron. QE-7, p. 205, May (1971).

Appendix C

Matrix Formalism Applied to Dielectric Media

Maxwell's equations in the Laplace transform domain for a linear, isotropic media, i.e., μ, ε, and σ are scalars and independent of time, for an electric field vector $\underline{E}(\underline{r},s)$ polarized in the x direction, i.e. $\underline{E}$ $(E_x,0,0)$ and H $(0,H_y,H_z)$, reduce to

$$(\nabla^2 - (s^2\mu\varepsilon + s\mu\sigma))\ E_x = 0 \qquad \text{(C-1.1)}$$

and

$$H_y = -\frac{1}{s\mu}\ \frac{\partial E_x}{\partial z} \qquad \text{(C-1.2)}$$

The solution follows using separation of variables as

$$E_x = Y(y)\ U(z) \qquad \text{(C-2)}$$

So substituting into Eq. (C-1.1) we obtain

$$\frac{Y''}{Y} + \frac{U''}{U} - (s^2\mu\varepsilon + s\mu\sigma) = 0 \qquad \text{(C-3)}$$

and if we let

$$\frac{U''}{U} = -\beta^2 \quad \text{and} \quad \frac{Y''}{Y} = -k_o^2\ a^2 \qquad \text{(C-4)}$$

where

$$\beta^2 + k_o^2\ a^2 + s^2\mu\varepsilon + s\mu\sigma = 0 \qquad \text{(C-5)}$$

then the solutions to Eqs. (C-4) are

$$U(z) = a_1 \sin \beta z + a_2 \cos \beta z \qquad \text{(C-6)}$$

$$Y(y) = c_1 \sin k_o\ ay + c_2 \cos k_o\ ay \qquad \text{(C-7)}$$

Thus Eq. (C-2) becomes

$$E_x(x,y,z) = (a_1 \sin \beta z + a_2 \cos \beta z)(c_1 \sin k_o ay + c_2 \cos k_o ay) \qquad \text{(C-8)}$$

Now since from Eq. (C-1.2)

$$\frac{\partial E_x}{\partial z} = -s\mu H_y = \beta(a_1 \cos \beta z - a_2 \sin \beta z)Y(y) \qquad \text{(C-9)}$$

then we can write as a matrix

$$\begin{bmatrix} E_x \\ H_y \end{bmatrix} = \begin{bmatrix} \cos \beta z & -\frac{s\mu}{\beta} \sin \beta z \\ \frac{\beta}{s\mu} \sin \beta z & \cos \beta z \end{bmatrix} \begin{bmatrix} a_2 Y(y) \\ -\frac{\beta}{s\mu} a_1 Y(y) \end{bmatrix} \qquad \text{(C-10)}$$

Now if we assume normal incidence, y variation may be neglected and for the boundary condition at z = 0

$$\begin{bmatrix} E_x \\ H_y \end{bmatrix}_{out} = \begin{bmatrix} 1 & 0 \\ 0 & 1 \end{bmatrix} \begin{bmatrix} E_x \\ H_y \end{bmatrix}_{in} \qquad \text{(C-11)}$$

or

$$E_x|_{z=0} = a_2 Y(y) , \quad H_y|_{z=0} = -\frac{\beta}{s\mu} a_1 Y(y) \qquad \text{(C-12)}$$

So the output electromagnetic field (on the left side of the output interface) of a dielectric slab of length z is related to the input field by the matrix

$$\begin{bmatrix} E_x \\ H_y \end{bmatrix}_{out} = \underbrace{\begin{bmatrix} \cos \beta z & -\frac{s\mu}{\beta} \sin \beta z \\ \frac{\beta}{s\mu} \sin \beta z & \cos \beta z \end{bmatrix}}_{\bar{Q}(z)} \begin{bmatrix} E_x \\ H_y \end{bmatrix}_{in} \qquad \text{(C-13)}$$

Consider two adjacent media, the first one extending from $z = 0$ to $z = z_1$ and the second from $z = z_1$ to $z = z_2$. Then if $\bar{Q}_1(z)$ and $\bar{Q}_2(z)$ are the characteristic matrices for the media then the output wave of the first medium is related to input wave of the first media by

$$\begin{bmatrix} E_x \\ Hy \end{bmatrix}_{z=z_1} = \bar{Q}_1(z_1) \begin{bmatrix} E_x \\ Hy \end{bmatrix}_{z=o}$$

and then similarly

$$\begin{bmatrix} E_x \\ Hy \end{bmatrix}_{z=z_2} = \bar{Q}_2(z_2 - z_1)\bar{Q}_1(z_1) \begin{bmatrix} E_x \\ Hy \end{bmatrix}_{z=0} \qquad \text{(C-14)}$$

Then to express the input fields in terms of the output fields we pre-multiply Eq. (C-14) with the inverse of $\bar{Q}_2$ and $\bar{Q}_1$.

Thus for an N-layer multilayer, denoting the input field components by

$$\begin{bmatrix} E_{x1} \\ H_{y1} \end{bmatrix}$$ and the output by $$\begin{bmatrix} E_{x2} \\ H_{y2} \end{bmatrix},$$

we can write

$$\begin{bmatrix} E_{x_1} \\ H_{y_1} \end{bmatrix} = \bar{Q}_1^{-1}\,\bar{Q}_2^{-1} \cdots \bar{Q}_N^{-1} \begin{bmatrix} E_{x_2} \\ E_{y_2} \end{bmatrix} . \qquad \text{(C-15)}$$

The matrix product is customarily denoted by the A,B,C,D, parameters.

Thus, specifically, we define the A,B,C,D matrix by

$$\begin{bmatrix} E_{x1} \\ H_{y1} \end{bmatrix} = \begin{bmatrix} A & B \\ C & D \end{bmatrix} \begin{bmatrix} E_{x2} \\ H_{y2} \end{bmatrix} \tag{C-16}$$

where by Eq. (C-15), we have $\begin{bmatrix} A & B \\ C & D \end{bmatrix} = \bar{\bar{Q}}_1^{-1}\bar{\bar{Q}}_2^{-1} \cdots \bar{\bar{Q}}_N^{-1}$

The chain matrix of Eq. (C-16) is given by

$$\begin{bmatrix} A & B \\ C & D \end{bmatrix} = \prod_{k=1}^{N} \begin{bmatrix} \cos \beta_k h_k & + \frac{s\mu_k}{\beta_k} \sin \beta_k h_k \\ -\frac{\beta_k}{s\mu_k} \sin \beta_k h_k & \cos \beta_k h_k \end{bmatrix} \tag{C-17}$$

where N is the number of layers; $\beta_k^2 = -s^2\mu_k\varepsilon_k - s\mu_k\sigma_k$ and h_k, μ_k and ε_k are the thickness, permeability and dielectric constant for the k^{th} layer, respectively. The steady state form for $e^{i\omega t}$ time dependence, e.g., see Born and Wolf, Sec. 1.6.5, follows by replacing the Laplace transform variable s with $i\omega$.

Now if we consider a plane wave incident upon a periodically stratified medium that is bounded on each side by a homogeneous, semi-infinite medium, then we shall derive expressions for the amplitude and intensity of the reflected and transmitted waves. We may write Eq. (C-10) as

$$E_{x1} = (a_1 e^{-j\beta_1 z} + b_1 e^{+j\beta_1 z}) Y_1(y) \qquad \text{(C-18.1)}$$

and since

$$-s\mu H_{y1} = \frac{\partial E_{x1}}{\partial z}$$

$$H_{y1} = g_1(a_1 e^{-j\beta_1 z} - b_1 e^{j\beta_1 z}) Y_1(y) \qquad \text{(C-18.2)}$$

where

$$g_1 = \frac{j\beta_1}{s\mu}$$

Similarly for output waves propagating from Eq. (C-16) we have

$$E_{x2} = (a_2 e^{-j\beta_2 z} + b_2 e^{+j\beta_2 z}) Y_2(y) \qquad \text{(C-19.1)}$$

$$H_{y2} = g_2(a_2 e^{-j\beta_2 z} - b_2 e^{+j\beta_2 z}) Y_2(y) \qquad \text{(C-19.2)}$$

where

$$g_2 = \frac{j\beta_2}{s\mu}$$

Now since the tangential component of the electric and magnetic fields are continuous across the boundary of a dielectric interface

and since we assume no fields incident from the right, i.e., $b_2 = 0$ then for transmission from $1 \rightarrow 2$, input fields

$$\begin{bmatrix} E_{x1} \\ H_{y1} \end{bmatrix} = \begin{bmatrix} a_1 + b_1 \\ g_1(a_1 - b_1) \end{bmatrix} \quad \text{and output fields} \quad \begin{bmatrix} E_{x2} \\ H_{y2} \end{bmatrix} = \begin{bmatrix} a_2 \\ g_2 a_2 \end{bmatrix} \tag{C-20}$$

are assumed. Note that these fields are obtained from Eqs. (C-18.1), (C-18.2), (C-19.1), and (C-19.2) by setting $z = 0$ at each interface.

So from Eqs. (C-16) and (C-20) we have

$$\begin{aligned} a_1 + b_1 &= (A + g_2 B) a_2 \\ a_1 - b_1 &= (C + g_2 D) \frac{a_2}{g_1} \end{aligned} \tag{C-21}$$

The amplitude transmission function, defined by the ratio of the amplitude of the field propagated into region 2 to the amplitude of the field incident in region 1, is given by

$$T_{12} \equiv \left. \frac{a_2}{a_1} \right|_{b_2 = 0} \tag{C-22}$$

and is found from Eq. (C-21) to be

$$T_{12} = \frac{2}{(A + \frac{g_2}{g_1} D) + (g_2 B + \frac{C}{g_1})} \tag{C-23}$$

The amplitude reflection function from the input surface defined by the ratio of the amplitude of the field propagated back from that surface to the amplitude of the field incident in region 1, is given by

$$R_1 \equiv \left. \frac{b_1}{a_1} \right|_{b_2 = 0} \tag{C-24}$$

and is found from Eq. (C-21) to be

$$R_1 = \frac{(A - \frac{g_2}{g_1} D) + (g_2 B - \frac{C}{g_1})}{(A + \frac{g_2}{g_1} D) + (g_2 B + \frac{C}{g_1})} \tag{C-25}$$

Since we are concerned with how the energy of the incident field is divided into the two secondary fields, one transmitted into region 2 and one reflected back into region 1, we define the following energy relationships:

$$R \equiv |R_1|^2 \quad , \qquad T \equiv |T_{12}|^2 \tag{C-26}$$

called the reflectivity and transmissivity respectively.

Appendix D

The Periodically Stratified Media and Chebyshev Representation For Unimodular Matrices

If we consider the case where the first m layers of Equation (2-29) are periodically stratified as shown in Figure [2-1] then the first two layers of the multilayer may be represented by the following matrix:

$$M = \begin{bmatrix} \cos \beta_{11}h_{11} & \frac{s\mu}{\beta_{11}} \sin \beta_{11}h_{11} \\ -\frac{\beta_{11}}{s\mu} \sin \beta_{11}h_{11} & \cos \beta_{11}h_{11} \end{bmatrix} \cdot \begin{bmatrix} \cos \beta_{12}h_{12} & \frac{s\mu}{\beta_{12}} \sin \beta_{12}h_{12} \\ -\frac{\beta_{12}}{s\mu} \sin \beta_{12}h_{12} & \cos \beta_{12}h_{12} \end{bmatrix}$$

$$= \begin{bmatrix} \cos^2\beta h - \frac{n_2}{n_1} \sin^2 \beta h & -\frac{i}{g_o}\left[\frac{1}{n_2} + \frac{1}{n_1}\right] \cos\beta h \sin\beta h \\ -ig_o(n_1+n_2)\cos\beta h \sin\beta h & \cos^2\beta h - \frac{n_1}{n_2} \sin^2\beta h \end{bmatrix} \qquad (D\text{-}1)$$

where we have assumed $\beta_{11}h_{11} = \beta_{12}h_{12} = \beta h$ and

$$\frac{\beta_{11}}{s\mu} = in_1g_o \quad \text{and} \quad \frac{\beta_{12}}{s\mu} = in_2g_o. \qquad (D\text{-}2)$$

Now if

$$M = \begin{bmatrix} m_{11} & m_{12} \\ m_{21} & m_{22} \end{bmatrix} \tag{D-3.1}$$

then

$$M^N = \begin{bmatrix} \hat{m}_{11} & \hat{m}_{12} \\ \hat{m}_{21} & \hat{m}_{22} \end{bmatrix} \tag{D-3.2}$$

Then we have from matrix theory according to which the $N^{\underline{th}}$ power of a unimodular matrix M is given by

$$M^N = \begin{bmatrix} m_{11}U_{N-1}(a) - U_{N-2}(a) & m_{12}U_{N-1}(a) \\ m_{21}U_{N-1}(a) & m_{22}U_{N-1}(a) - U_{N-2}(a) \end{bmatrix} \tag{D-4}$$

where U_N are the Chebyshev Polynomials of the second kind and $a = \frac{1}{2}(m_{11} + m_{22})$.

So we have for Eq. (D-3.2) using Eq. (D-4)

$$\hat{m}_{11} = [\cos^2\beta h - \frac{n_2}{n_1}\sin^2\beta h]U_{N-1}(a) - U_{N-2}(a)$$

$$\hat{m}_{12} = -\frac{i}{g_o}[\frac{1}{n_1} + \frac{1}{n_2}]\cos\beta h \sin\beta h\, U_{N-1}(a) \tag{D-5}$$

$$\hat{m}_{21} = -ig_o[n_2 + n_1]\cos\beta h \sin\beta h\, U_{N-1}(a)$$

$$\hat{m}_{22} = [\cos^2\beta h - \frac{n_1}{n_2}\sin^2\beta h]\, U_{N-1}(a) - U_{N-2}(a)$$

where

$$a = \frac{m_{11} + m_{22}}{2} = \cos^2\beta h - \frac{1}{2}[\frac{n_2}{n_1} + \frac{n_1}{n_2}]\sin^2\beta h \qquad \text{(D-6)}$$

and

$$\begin{aligned} U_o(a) &= 1 & U_3(a) &= 8a^3 - 4a \\ U_1(a) &= 2a & U_4(a) &= 16a^4 - 12a^2 + 1 \\ U_2(a) &= 4a^2 - 1 & U_5(a) &= 32a^5 - 32a^3 + 6a \end{aligned} \qquad \text{(D-7)}$$

$$U_j(a) = 2aU_{j-1}(a) - U_{j-2}(a)$$

Now if we consider the special case of the periodically stratified multilayer in which

$$\beta_{11}h_{11} = \beta_{12}h_{12} = \beta_{13}h_{13} \cdots = \beta h = \frac{2\pi}{\lambda_o} n_{1p}h_{1p} \qquad \text{(D-8)}$$

and we have quarter wave films such that

$$n_{1p}h_{1p} = \frac{\lambda_o}{4} \qquad \text{(D-9)}$$

then Eq. (D-3.2) reduces to

$$M^N = \begin{bmatrix} \left(-\frac{n_2}{n_1}\right)^N & 0 \\ 0 & \left(-\frac{n_1}{n_2}\right)^N \end{bmatrix} \tag{D-10}$$

Then we see that Equation (2-13) reduces to

$$t_1 = T_{12}\big|_{\lambda=\lambda_o} = \frac{2}{(-\frac{n_2}{n_1})^N + (-\frac{n_1}{n_2})^N} \tag{D-11}$$

where $g_o = g_1 = g_2$.

Thus we see that t_1, t_2, r_{12}, r_{21} may be considered constant for a region of frequencies around λ_o. Now we can derive Equation (2-31) for the passive laser cavity by considering the following matrix multiplication:

$$M_{TOTAL} = M^N \cdot \begin{bmatrix} \cos \beta_o h_o & \frac{s\mu}{\beta_o} \sin \beta_o h_o \\ -\frac{\beta_o}{s\mu} \sin \beta_o h_o & \cos \beta_o h_o \end{bmatrix} \cdot M^N$$

$$= \begin{bmatrix} (-\frac{n_2}{n_1})^{2N} \cos \beta_o h_o & \frac{s\mu}{\beta_o} \sin \beta_o h_o \\ -\frac{\beta_o}{s\mu} \sin \beta_o h_o & (-\frac{n_1}{n_2})^{2N} \cos \beta_o h_o \end{bmatrix} \tag{D-12}$$